Deltares

Final Report

WAGENINGEN UNIVERSITY & RESEARCH

Seaward

VATTENFALL

De Rijke Noordzee

Deltares

Final Report

Author(s)
Birte Leutelt
Christiaan van Sluis
Francesca Di Paola
Frank Jacobs
Iris Menger
Isaac de Boer Ferrier
Joop W.P. Coolen
Leandra Kornau
Marjolijn Mascini
Natalia Strigin
Niek Bruinsma
Renate Olie
Samah Assafadi
Tim Wilms

Partners
Vattenfall N.V., Amsterdam
Seaward, Oegstgeest
Stichting De Noordzee, Utrecht
Wageningen Marine Research, Den Helder

Final Report

Client	Topsector Offshore Energie
Contact	Stefanie W. Westerik
Project reference	TKITOE_WOZ_2410
Keywords	Replenishment holes, offshore wind, ecology, marine growth

Document control	
Version	1.0
Date	20-04-2026
Project nr.	11211298-000
Document ID	11211298-000-HYE-0003
Pages	80
Classification	
Status	Final

Author(s)		
	Birte Leutelt Christiaan van Sluis Francesca Di Paola Frank Jacobs Iris Menger Isaac de Boer Ferrier Joop W.P. Coolen Leandra Kornau Marjolijn Mascini Natalia Strigin Niek Bruinsma Renate Olie Tim Wilms	

The allowed use of this table is limited to check the correct order-performance by Deltares. Any other client-internal-use and any external distribution is not allowed.

Doc. version	Author	Reviewer	Approver
1.0	Natalia Strigin	Luca van Duren	Helena van der Vegt

Summary

The Joint Industry Project entitled Nature incLusive water replenishment desIgn For offshorE wind (JIP-LIFE) project investigated whether water replenishment holes (WRHs) in offshore wind monopiles allows for the interior of monopile foundations to develop into a viable ecological habitat. As offshore wind farm (OWF) development rapidly expands in the North Sea, monopiles (MPs) create large areas of hard substrate that can host biological communities, yet most ecological assessments have focused solely on exterior surfaces. With the design of WRHs for corrosion prevention, hard substrate surfaces become accessible inside OWF monopiles. Recent insights suggest that monopile interiors—with WRHs facilitating the exchange of seawater—may form a distinct, sheltered habitat. Because these interiors are dark and physically more isolated, their ecological potential depends on the balance between biological consumption of oxygen and food, and their replenishment driven by hydrodynamic forcing through the WRHs. The JIP-LIFE project combined offshore monitoring, detailed ecological analysis, and coupled hydrodynamic–water quality modelling to understand how WRH design parameters may affect the ecological developments inside the monopiles and how interior water quality conditions evolve over the course of one season

The JIP-LIFE project assessed two of the monopiles installed at Hollandse Kust Zuid (HKZ), while also analysing data that had been obtained through a separate project, led by Waardenburg Ecology, at additional monopiles in HKZ. In total, five monopiles - E5, D1, D6, F1 and F4 - were analysed across all work packages (WP). However, the individual WPs focused on fewer monopiles for analysis, depending on data availability.

Monitoring of the monopiles included abiotic measurements, environmental DNA (eDNA) and nutrient sampling as well as video footage collection. The timing of the monitoring was defined as T3, occurring 2 years after the baseline data collection (T0). Operational challenges such as equipment failures and weather constraints caused some data gaps, yet sufficient information was collected to characterise interior conditions.

Video data analysis showed clear ecological contrasts between the exterior and the interior surfaces of the monopiles. The exterior part of the monopiles was densely covered by mussels, amphipods, anemones and other typical North Sea hard substrate epifauna. Meanwhile, the interiors showed lower epifaunal biomass and lacked the strong vertical zonation typical of exterior surfaces. Inside, communities were more heterogeneous and dominated by sponges, sea squirts, anemones, brittle stars, and tube-building polychaetes. The development of such unique communities highlights the need for continued monitoring to track the long-term development of the communities and to assess the risk of non-indigenous species settling in these new habitats. In some monopiles, microbial mats and fine organic matter deposits were observed on the seabed, suggesting possible localised oxygen stress due to organic matter accumulation and microbial decomposition.

The eDNA analysis confirmed the presence of many fish species, though the mixing of water between MP interior and exterior meant that eDNA could not reliably indicate which of the detected species were exclusively present inside or outside the monopile.

Nutrient measurements showed that the insides of the monopiles display unique vertical concentration profiles, differing from the outside concentrations. Overall, ammonium, phosphate, nitrite, and silicate were more concentrated inside the monopiles compared to outside, likely due to mineralisation processes and the absence of phytoplankton uptake in the dark water column.

The hydrodynamic modelling reproduced key features of replenishment processes, underpinning that the internal environment is strongly shaped by external water level fluctuations and wave driven pressures at the WRHs. Concentrations of oxygen and particulate organic carbon (POC) remained broadly near ambient for much of the water column, but distinct vertical gradients occurred. Conditions above the upper WRH and below the lower WRH were most prone to reduced replenishment, the latter aligning with field observations of microbial mat formation near the seabed.

A sensitivity analysis on key parameters (WRH size/total open area, horizontal layout/orientation (angular position), vertical position, wave and current forcing direction relative to the WRHs) confirmed that the total open area of WRHs is a dominant factor influencing internal water quality. Larger total area of WRHs improved oxygen and food availability, while reductions in opening size led to lower minimum concentrations. The horizontal layout also plays a role: symmetric cross-shaped configurations of WRH enhanced hydraulic efficiency, whereas distributing the same total area among a greater number of smaller holes increased hydraulic losses and reduced exchange. Vertical placement influences local conditions above and below the WRH openings, particularly under low-replenishment scenarios. The WRH's orientation had only limited effect, with slight improvements when aligned with dominant tidal currents and negligible influence from wave direction.

Taken together, the monitoring and modelling results showed that monopile interiors represent a distinct ecological habitat. While biomass remains lower inside relative to outside the MP, presumably due to limited oxygen and food supply, the environment supports a unique assemblage of species. WRHs, when appropriately sized and configured, can maintain internal oxygen and food conditions at levels suitable for these communities. Suboptimal WRH designs, however, may create zones of low oxygen, particularly near the seabed.

Overall, the project concluded that WRHs represents a low-cost, structurally embedded (rather than add-on) design feature that is easily scalable across entire wind farms. Underpinning design choices by site-specific modelling can support successful application in offshore wind development.

Contents

1 Introduction

1.1 Research Motivation

Offshore wind infrastructure in the North Sea is expanding rapidly as part of the energy transition. These hard-substrate structures can function as novel habitat for biological communities on submerged foundation surfaces and associated scour protection. At the same time, the net ecological effect of these new habitats (e.g., biodiversity gain, stepping-stone effects, and broader food-web interactions) remains an active area of research.

Most ecological assessments of offshore wind foundations have so far focused on the monopile exterior. More recently, attention has shifted to the monopile interior as a potentially distinct habitat, particularly when water replenishment holes (WRHs) are present in the wetted part of the foundation. These openings are introduced primarily from an engineering perspective, following developments in internal corrosion protection that leads to designs using WRHs to refresh the internal water volume and mitigate undesirable side effects of certain corrosion protection approaches (e.g., pH changes and internal gas formation such as chlorine and bromine).

At wind farm “Hollandse Kust Zuid” (HKZ), the monopiles are designed without an active internal impressed current cathodic protection (ICCP) system; internal corrosion protection is provided by a protective coating system instead, while WRHs are installed as a backup in case ICCP may be needed to support the coating. Notably, creating openings in the monopile also enables marine organisms to enter the foundation. Early monitoring has shown that multiple local species (e.g., fish, crabs and other invertebrates) can establish themselves inside monopiles within months after installation.

A key uncertainty is that the monopile interior is dark and relatively isolated compared to the exterior. Essential resources such as dissolved oxygen and food must be transported into the monopile through the WRHs. Whether the interior can support life therefore depends on a balance between (i) food and oxygen consumption by the developing community and (ii) replenishment driven by external hydrodynamic conditions and WRH design (size, elevation, orientation).

Prior modelling indicated that oxygen and food availability inside monopiles can be limiting, with strong sensitivity to sea state and WRH sizes, highlighting the need for improved process representation and validation data from the field. Deltares has developed and applied a coupled hydrodynamic–water-quality modelling framework for monopile interiors, originally for internal corrosion-protection purposes and extended towards oxygen/food dynamics; however, further development and validation are required to robustly assess habitat suitability and translate results into design guidance.

JIP LIFE brings together industry, non-governmental organisations and research partners to combine offshore monitoring, measurement analysis, and validated modelling to understand how WRH design and environmental forcing govern internal water quality and ecological potential. A baseline (“T0” measured before installation) measurement shortly after installation and prior to significant colonisation by biota, provides context on initial conditions, while the main dataset and analysis in this project are based on the follow-up monitoring (“T3” measured three years after installation). The motivation is to enable evidence-based recommendations for WRH systems in monopile foundations that are practical for industry application and defensible from an ecological perspective.

1.2 Objectives and research questions

Overall objective

The overall objective of JIP LIFE is to assess the potential of using water replenishment holes (WRHs) while ensuring the development of viable communities inside monopiles for offshore wind.

Specific research objectives

To achieve the overall objective, JIP LIFE integrates offshore monitoring, data analysis, and coupled hydrodynamic–water-quality modelling to:

- **Collect and curate a structured offshore monitoring dataset** describing abiotic conditions inside monopiles with WRHs (with emphasis on dissolved oxygen and supporting water-quality variables), alongside relevant external forcing data (waves, water levels, currents where available).
- **Quantify internal abiotic variability and replenishment behaviour** by analysing how dissolved oxygen and related indicators respond to external forcing and WRH characteristics (e.g., size, elevation and horizontal orientation), and by identifying the dominant controls on oxygen/food availability.
- **Characterise ecological communities inside monopiles** through analysis of biotic observations (attached and mobile fauna), in terms of species composition, and functional/ecological interpretation of observed communities.
- **Place interior observations in context of the monopile exterior**, by comparing interior biotic observations with exterior communities and available reference information, to assess whether the interior functions as a distinct habitat and to identify likely drivers of differences.
- **Improve, calibrate, and validate the coupled hydrodynamic–water-quality modelling framework** using the monitoring observations, and quantify achievable model skill and uncertainty given the available data.
- **Use the validated model to assess design sensitivities and transferability**, including scenario evaluation of alternative WRH configurations and the use of buoy/metocean data to support application at other sites.

Deliverables and outcomes

This report consolidates the project outcomes into (i) a structured dataset of offshore observations describing biotic and abiotic conditions inside monopiles with WRHs (including a baseline context from T0 and the main follow-up dataset from T3); (ii) an improved and validated modelling framework for water exchange and internal water quality; and (iii) a synthesis of the dominant controls and sensitivities linking external forcing and replenishment-hole design to habitat suitability. Together, these outputs provide an evidence base for practical Nature Inclusive Design recommendations for water replenishment holes that are technically feasible for monopile implementation and ecologically meaningful, and that support transfer of the developed approach to other offshore wind sites.

1.3 Research consortium

JIP LIFE is a project in which industry, non-governmental organisations and research partners collaborate to develop a shared evidence base on the effect of WRHs on the local epifaunal communities. Partners contribute expertise, data, and in-kind resources across offshore monitoring, ecological interpretation, and model development. The results are jointly discussed and consolidated into this technical report, reflecting a shared set of methods, assumptions, and conclusions developed within the consortium.

Consortium partners and roles:

- **Deltares** – Project coordination and integration; development and application of the coupled hydrodynamic–water quality modelling framework; synthesis across work packages; lead of technical reporting.
- **Natuur & Milieu + Stichting De Noordzee = programme De Rijke Noordzee (DRN)** – supporting monitoring campaign and analysis, stakeholder perspective; supports translation of findings towards nature-inclusive practice and communication.
- **Seaward** – Offshore operations and monitoring support; execution support for offshore measurement campaigns (deployment/retrieval and data acquisition).
- **Vattenfall** – Wind farm owner/operator and industrial end-user; provides site access and relevant site/design/context information; supports offshore planning and practical applicability of recommendations.
- **Wageningen Marine Research (WMR)** – Ecological monitoring and analysis; species identification and ecological interpretation; quantitative analysis of biotic data and link to habitat suitability.

1.4 Project approach

JIP LIFE follows an integrated approach that combines offshore monitoring, desktop literature study, targeted data analysis, and numerical modelling to understand and predict the abiotic conditions inside monopiles with water replenishment holes (WRHs), and to translate this understanding into practical design guidance. The work is organised as a sequence of connected steps: (i) establishing the relevant system understanding and hypotheses, (ii) collecting and processing field observations that describe both the internal water quality and ecological development, (iii) improving and validating a coupled hydrodynamic–water quality modelling framework against the measurements, and (iv) using the validated model to explore sensitivities and evaluate alternative WRH configurations.

Offshore monitoring provides the empirical basis for the project, including both abiotic measurements inside the monopile (with emphasis on dissolved oxygen as a key indicator of habitat suitability) and observations of biotic development. A T0 campaign shortly after installation provides a baseline snapshot of early conditions, while the monitoring and analyses in this report primarily build on the follow-up T3 campaign conducted approximately two years later. Monitoring is complemented by analysis of external forcing (e.g., waves, water levels, and currents, as available) to relate internal conditions to the hydrodynamic drivers that govern exchange through the WRHs.

The modelling component builds on an existing coupled framework for internal water exchange and water-quality processes. Model development focuses on representing the dominant mechanisms controlling oxygen and food availability inside the monopile, including exchange through WRHs and internal consumption processes. Calibration and validation are performed using the offshore observations, with the aim to reproduce both the magnitude and variability of internal abiotic conditions under realistic forcing. Once validated, the model is applied in a sensitivity and scenario mode to evaluate the influence of WRH design parameters (e.g., size, elevation, and horizontal orientation). The combined monitoring–modelling evidence is then synthesised into actionable recommendations for WRH configurations that are robust across relevant environmental conditions and practical for implementation in monopile design.

1.5 Site and system description

1.5.1 HKZ offshore windfarm

Hollandse Kust Zuid (HKZ) is an offshore wind farm in the Dutch sector of the North Sea, located off the west coast of the Netherlands (see the wind farm zone indicated in yellow in Figure 1-1). The monopiles were installed in July–August 2021. Offshore monitoring was carried out in two campaigns: a baseline T0 campaign in November 2021–January 2022, and a follow-up T3 campaign in October–November 2024. In this report, T0 is primarily used as baseline context, while the main analyses and modelling validation are based on T3.

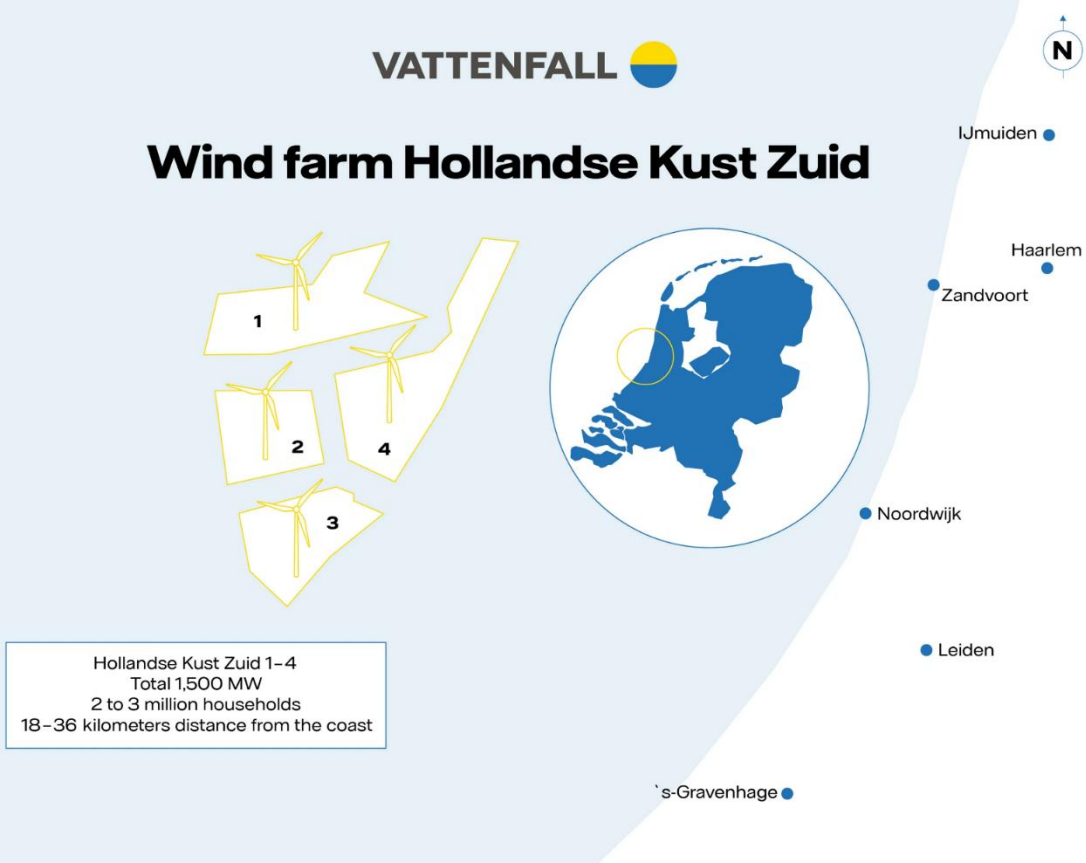

Figure 1-1 Location of HKZ OWF near the Dutch west coast

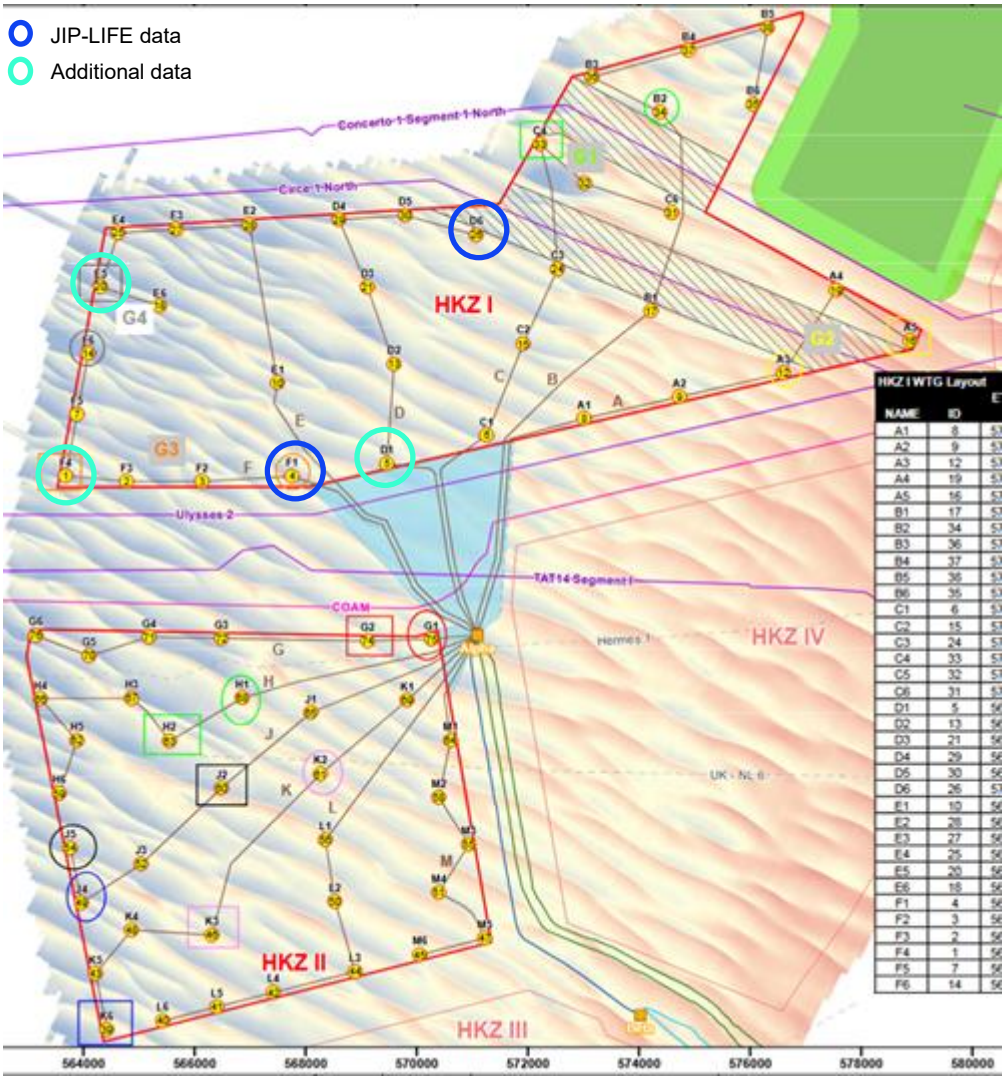

Figure 1-2 Location of individual monopiles and specification of data sourcing as part of JIP-LIFE or outside of the project

1.5.2 Monopile designs

The offshore monitoring in JIP LIFE focuses on two HKZ monopile foundations: F1, D6. In addition, D1, E5 and F4 data was obtained through a separate project which was made available to the JIP-LIFE project. Across HKZ, the foundations share the same overall geometry (Figure 1-3): a tapered steel monopile with an 8 m diameter in the lower section (from mudline down to −10.6 mLAT) transitioning to a 7 m diameter in the upper section (from −3.0 mLAT up to the airtight platform at about +16.2 mLAT).

Water exchange between the monopile interior and the surrounding seawater is enabled by two vertical levels of water replenishment holes (WRHs). The upper WRHs are located at approximately −1.0 mLAT and have a fixed horizontal orientation of 191° and 255° (degN). The WRHs are elliptical with a minor axis of 320 mm and major axis of 960 mm (represented in the modelling by area-equivalent circular openings). In addition, air ventilation holes (approximately +14.1 mLAT, 150 × 450 mm and orientation of 191° and 255° (degN)) provide pressure equalisation for the enclosed air volume above the internal water surface.

The main geometric differences between the monopiles relevant to this study are the water depth and the elevation and horizontal orientation of the lower WRHs, which are positioned near the seabed (approximately 4.35 m above the mudline). These parameters are summarised in Table 1-1 and are used throughout this report to interpret differences between monitored monopiles and to define the modelling cases and design-sensitivity analyses.

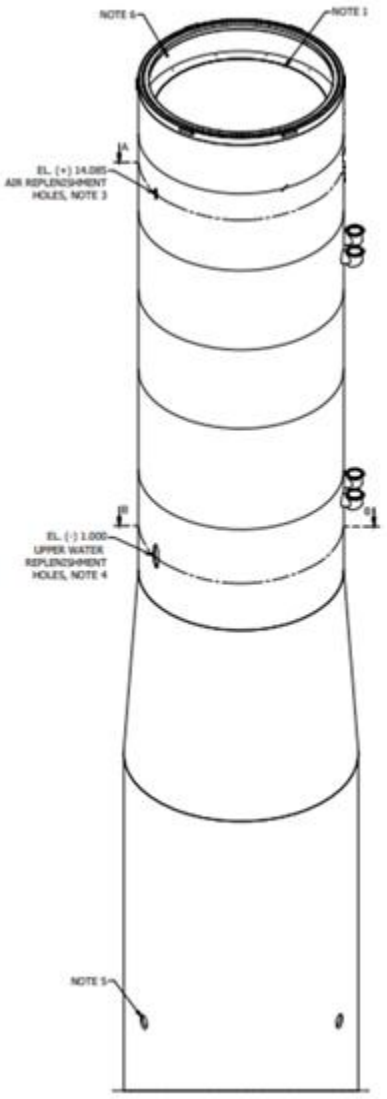

Figure 1-3 Monopile design for HKZ OWF.

Table 1-1 Angular and vertical position of the lower water replenishment holes in the monopiles.

WTG name	Water depth [mLAT]	Lower WRH elevation [mLAT]	Lower WRH orientation [degN]
F1	-24.53	-20.18	191 and 25
F4	-24.97	-20.62	191 and 258
E5	-25.24	-20.89	191 and 258
D1	-23.26	-18.91	191 and 258
D6	-23.93	-19.58	191 and 50

1.6 Report structure

This report is structured as follows.

Chapter 1 introduces the motivation, objectives, consortium, approach, and the HKZ case study and monopile system description.

Chapter 2 describes the offshore monitoring programme and measurement methods for the abiotic and biotic observations inside the monopiles.

Chapter 3 presents the monitoring results and data analysis.

Chapter 4 describes the numerical modelling framework, including setup, calibration, and validation against the monitoring data.

Chapter 5 synthesises the findings and translates them into conclusions and recommendations for water replenishment hole design, including considerations for transfer of the approach to other offshore wind sites.

2 Offshore monitoring

2.1 Offshore monitoring method, limitations and output

As research into water replenishment holes and their effects on water quality and the local communities is limited, the JIP-LIFE monitoring campaign added valuable information to the existing T0 monitoring which had been conducted by DRN and Vattenfall in 2021-2022. The JIP-LIFE project's T3 monitoring gives important insights in the situation after a few years, in 2024.

The T3 offshore monitoring campaign of this project took place during four days between October 16th -17th and November 4th -5th 2024. Works have been carried out on the monopile exterior from a Crew Transfer Vessel (CTV) and simultaneously from the Air Tight Platform (ATP) at the interior, as to have as much overlap in monitoring conditions for the data acquisition conditions as well as post processing.

Following standard procedures for offshore monitoring campaigns, the following safety measured and documentation were arranged prior to the campaign to measure the possible species and biodiversity growth inside the monopiles of HKZ:

- Project Plan
- Responsibility Matrix
- Method Statement
- Hazard Identification and Risk Assessment (HIRA) / Risk Assessment Matrix
- Mandatory Certifications (Global Wind Organisation (GWO) basic safety training, VCA (Veiligheid, Gezondheid en Milieu Checklist Aannemers checklist), offshore medical)
- Personal Protective Equipment (PPE)
- Daily Progress Reports (DPRs)

Various specifically designed equipment and methodologies for monitoring were used in order to obtain the best possible dataset based on the inputs needs for the JIP-LIFE project. Specifically, the project obtained:

- eDNA: insight in biodiversity of species
- Abiotic monitoring: Dissolved Oxygen (DO), Turbidity (TURB), Temperature (TEMP), Conductivity (COND), and pH. Salinity (SAL) and Total Dissolved Solids (TDS) are automatically calculated from the Conductivity and Temperature readings: insights into the physical conditions inside compared to outside of the monopile.
- Biotic (chlorophyll-a): insights in the food availability
- Video and photo: insights in biodiversity and species between inside and outside

Monitoring included long term and spot monitoring at two monopiles, namely F1 and D6. Long term monitoring was undertaken by placing a frame on the seabed inside the F1 monopile from 17 October until 4 November. The spot monitoring was undertaken at three different depths – the Upper Water Replenishment Hole (UWRH), the middle of the monopile (MID), and the Lower Water Replenishment Hole (LWRH). Both methods (long term and spot) took videos and (timelapse) photos inside and outside of the monopile (F1 and D6), though the focus for this project was on the inside of the monopile.

The Manta 35+ (one battery and one cable powered multiparameter water quality probe manufactured by Eureka Water Probes) was used for the abiotic parameters. For the long-term monitoring, an additional Aquatroll 600 probe was mounted on the tripod frame for higher frequency monitoring (same parameters as the Manta). Moreover, using the fluorometer

options Chlorophyll-a (CHLA) was measured. Finally, eDNA samples (see chapter 3) were taken. In addition to these monitoring methodologies, several other equipment and data sources were tried, however due to availability of other source material some of this monitoring data was not used. Monitored but not used data includes several GoPro videos and timelapses with underwater video lights, local wave buoy data and nutrient water sample data.

2.2 Outputs/Result

The below Table 2-1 shows the data obtained through the monitoring campaign. Throughout the campaign, several issues occurred which limited the retrieved information from being suitable to use for further analysis, as the explanations are provided through the colour coding of the table and the notes section in the table.

Table 2-1 - Data Availability Overview (DAO) from the monitoring campaign

	Locations	**F1 - 16-10**	**F1 - 16-10**	**F1 17-10**	**F1 4-11**	**F1 4-11**	**D6 5-11**	**D6 5-11**
Scope	Scope	spot and frame deployed		put Aqua Troll on	spot and frame retrieved		spot	
	Monitoring locations	ATP inside	CTV outside	ATP inside	ATP inside	CTV outside	ATP inside	CTV outside
Monitoring Scope	3x depths 10min			-	5		8	
	2x vertical transect up			-	6			
	2x vertical transect down			-	7			
	eDNA UWRH	1		-				
	eDNA MID			-				
	eDNA LWRH			-				
	Nutrient samples	2		-				
Monitoring Equipment	Battery Manta		-	10min				
	Wired Manta	-		-	-	-	-	-
	Aqua Troll	-	-	1min	-	-	-	-
	GoPro video			3				9
	GoPro timelapse	-	-	4	-	-	-	-

Notes

Red: data could not be used, yellow: data could only partially be used, green: full data set could be used
1. Only one eDNA sample at UWRH; broken Niskin
2. No 1m nutrient samples; F1-1-10m-B missing
3. Lamp malfunction/dead battery
4. Timelapse made but settings not optimal
5. Missing ATP spot UWRH
6. Missing ATP vertical transects
7. No eDNA sample at UWRH; broken Niskin
8. Only ATP spot UWRH and part of MID is available, rest corrupted
9. No GoPro available due to time restrictions on site

eDNA 1500ml filtered unless otherwise stated in DPR
Manta settings 0.5Hz unless otherwise stated

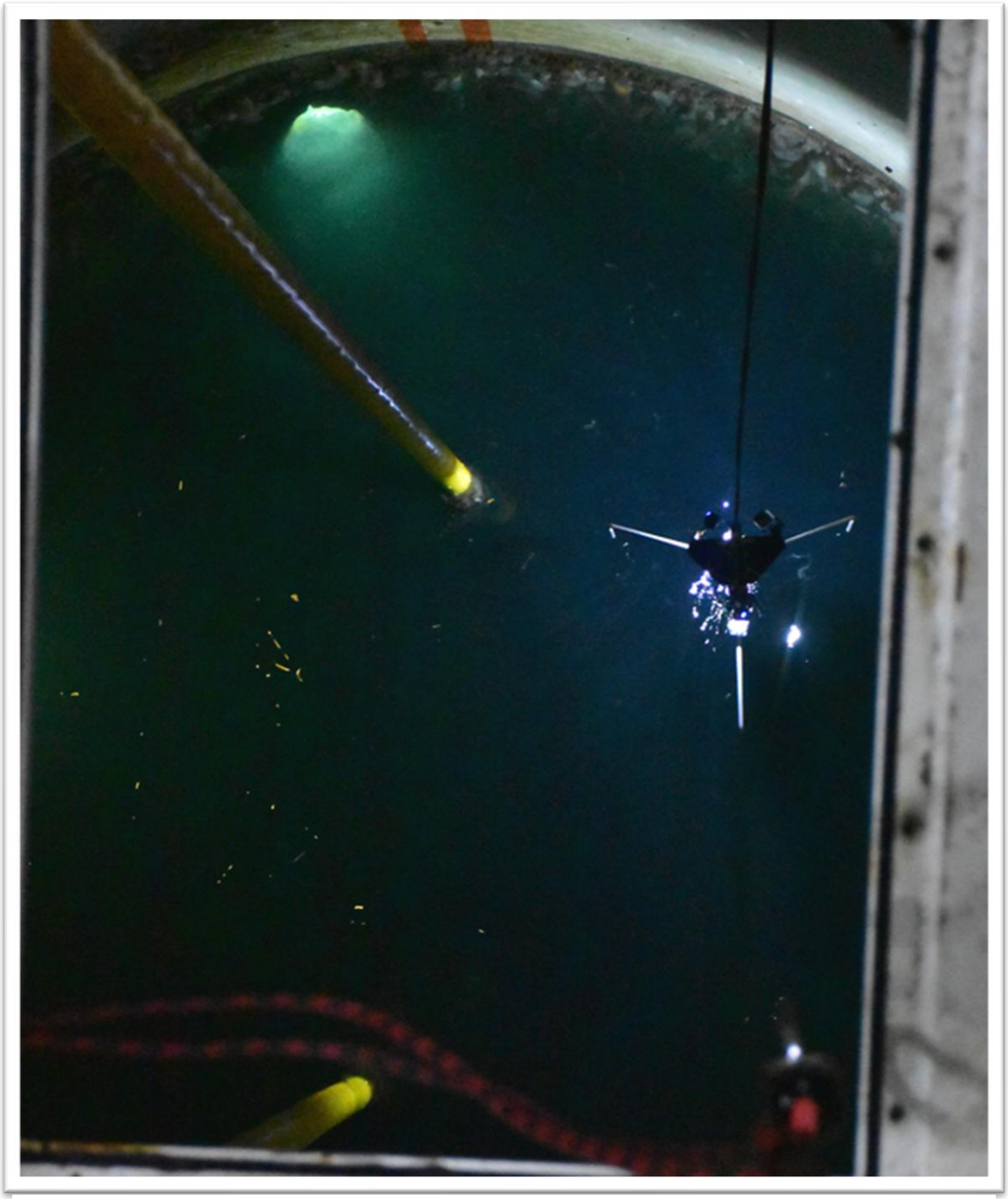

Figure 2-1 Specialised frame with multiprobe, diving lights and GoPro cameras being lowered at the inside of turbine F1. Clearly visible in the top of the picture is the UWRH (source: De Rijke Noordzee)

Figure 2-2 Picture of the tripod frame on the Air Tight Platform upper ring in turbine F1. Clearly visible is the Eureke multiprobe (left cylinder), Aquatroll multiprobe (right cylinder) and various GoPro cameras and underwater video lights (source: De Rijke Noord)

In addition, the project was able to access additional video footage taken by Waardenburg Ecology as part of a separate project undertaken together with Vattenfall. The additional video footage was collected between May and September 2024 at monopiles D1, E5, F1, and F4. The quality was better suited for species community analysis (see section 3), which led to the decision to utilize this footage instead. Footage was collected using a GoPro mounted on a small ROV. At each monopile, between 2 and 5 vertical transects were recorded on both the inside and outside surfaces, along with horizontal video transects of the seabed on both sides, resulting in a total of 15 vertical inside transects and 9 vertical outside transects, as well as 4 horizontal inside transects and 9 horizontal outside transects Table 2-2.

Table 2-2 - Video footage and abiotic data obtained through Vattenfall and Waardenburg Ecology.

Monopile		**D1**		**E5**		**F1**		**F4**	
Video orientation	Location	n transects	Date	n transects	Date	n transects	Date	n transects	Date
horizontal	Inside	1	09.05.2024	1	09.09.2024	1	09.06.2024	1	09.07.2024
vertical	Inside	4	09.05.2024	4	09.09.2024	4	09.06.2024	4	09.07.2024
horizontal	Outside	2	03.09.2024	3	01.09.2024	2	03.09.2024	2	30.08.2024
vertical	Outside	2	03.09.2024	2	01.09.2024	2	03.09.2024	3	30.08.2024

2.3 Lessons learned and recommendations for future offshore monitoring

The offshore monitoring campaigns was affected by a number of issues resulting in data gaps. Some of these issues are general risks while others provide valuable lessons learned for future operations. One major issue encountered was a broken Niskin bottle, which affected eDNA sample collection. Moreover, complicated operational conditions added further complexity, with high time pressure, bad weather, and even a broken vessel generator (genset) impacting schedules and performance. Flexibility also proved essential; the ability to adapt and agree on changes to the plan ensured that the campaign could continue despite setbacks.

The application of different monitoring setups demonstrated that the video acquisition technique is a key factor determining the success of video analysis of epifaunal community composition. Footage collected with GoPros by JIP LIFE and Waardenburg was of higher quality than recordings obtained with the ROV used in the Waardenburg Ecology monitoring campaign. In addition, adequate lighting and controlled, stable camera movement were essential for obtaining usable footage. GoPros mounted on the Waardenburg Ecology ROV produced more stable images than those mounted on the hand-suspended frame described in Figure 2-2. Equipment reliability was another challenge, as there were battery malfunctions in both video lights and the Manta system, resulting in some data gaps.

A key takeaway is the importance of having spare monitoring equipment available to mitigate the impact of failures. Regarding current speed monitoring, the Aquadopp system was not used because previous trials in 2021–2022 showed that data accuracy could not be guaranteed due to signal interference from the metal inside the monopile. Consequently, the tilt sensor, previously used to calibrate Aquadopp data, was omitted as well.

3 Monitoring data analysis & results

3.1 eDNA Data

3.1.1 eDNA Analysis Method

Samples for eDNA analysis were collected in triplicates at 1 m, 10 m, and 20 m water depth. Approximately 1.5 L of water were filtered across a cellulose nitrate membrane filter (pore size: 1.2 µm), which was stored in 400 µl DNA/RNA shield at -18°C. DNA isolation was performed using the DNeasy Blood & Tissue Kit (Qiagen). MiFish primers, targeting fish and mammal species, were modified to include unique barcodes attached to each primer (Miya, et al. 2015). One barcoded primer set was used per sample to enable pooled sequencing and distinguish sequencing data per sample in bioinformatic processing. PCR amplification was performed using 35 cycles. One sequencing library was prepared using the SQK-LSK114 kit and sequenced on a MinION device using an R10.4.1 flow cell (Oxford Nanopore Technologies (ONT)). Raw data was SUP basecalled and demultiplexed using Dorado (ONT) and further processed using the Decona pipeline (Oosterbroek 2024). Decona output was further analysed using RStudio.

Data was filtered to remove birds, which were not of interest for the habitat use inside the monopile, and terrestrial mammals, as these were likely contaminations. Thus, only fish and marine mammals were included in the data analysis. For each sample, the relative read count of each species was calculated by dividing the species' read count by the total read count of the sample. Relative read counts were then averaged across all samples collected at the same monopile, either inside or outside, regardless of sampling depth.

A heatmap showing the relative read counts was generated using the ggplot2 package v. 3.5.2 in R (Wickham 2016).

3.1.2 eDNA results

The results from the eDNA analysis are plotted the heatmap plot in Figure 3-1.

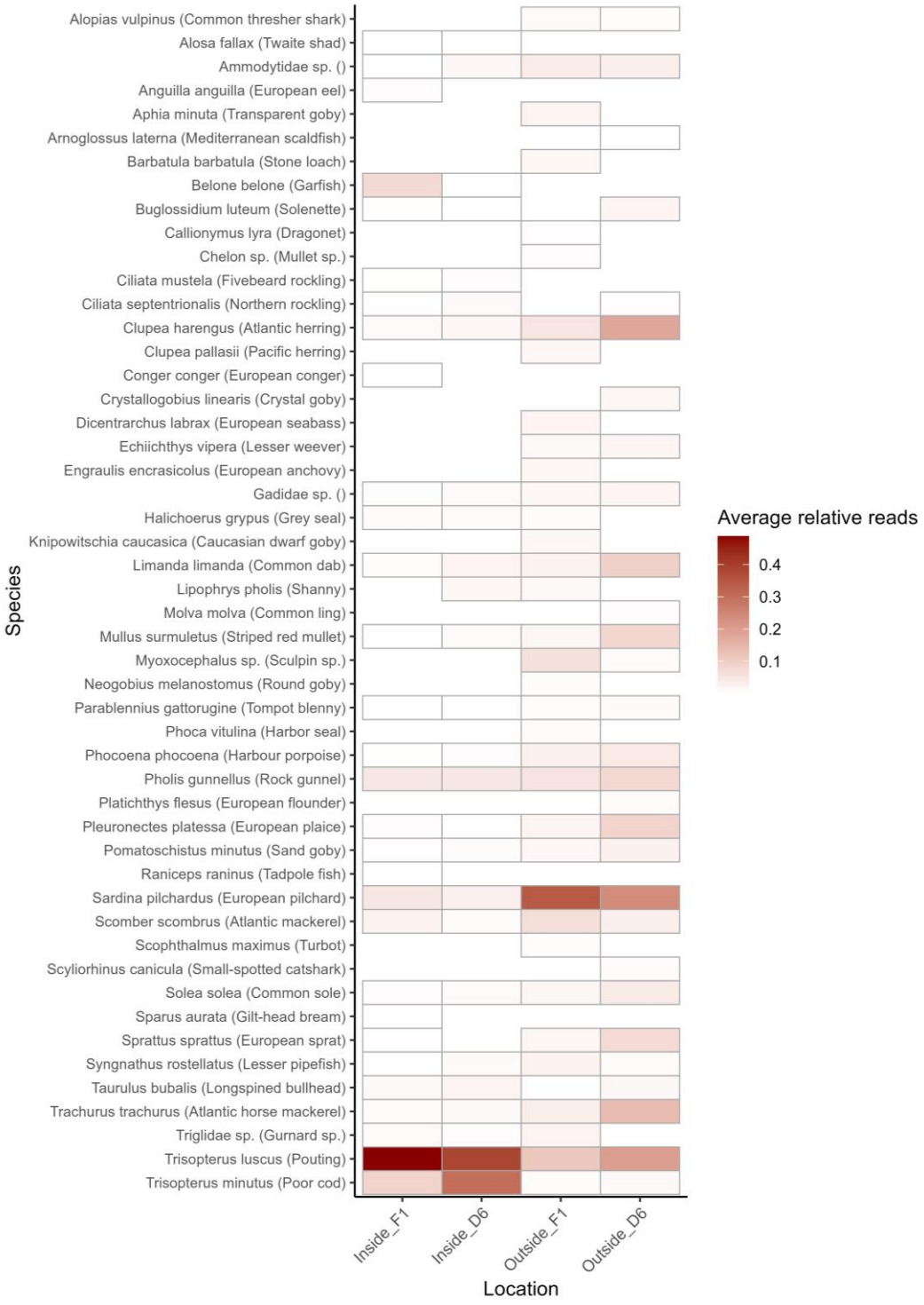

Figure 3-1 Average relative read counts for fish and marine mammal species detected using the MiFish primers in eDNA samples taken inside and outside of monopiles F1 and D6. Clupea pallasii (Pacific herring) likely is a wrongly matched Atlantic herring and is excluded in the numbers below.

The heatmap in Figure 3-1 shows that a total of 30 species were detected in the DNA material collected inside the monopiles, of which seven were unique to the inside. Outside the monopiles, 42 species were detected, of which 17 were uniquely occurring outside. Among these outside occurring species was *Alopias vulpinus* (Thresher shark), which was detected at

both monopiles. At F1, more species were recorded both inside (30) and outside (35) when compared to D6 (26 and 29 respectively).

The presence of harbour porpoise DNA inside the monopile suggests that genetic material is exchanged between the inside and outside as water refreshes, as it is less likely that these animals accessed the interior through the WRHs due to their size (although a grey seal has been recorded in T0 measurements to have entered the monopile via the WRH). Consequently, the eDNA profile cannot be interpreted as guaranteed physical presence of a species inside or outside the monopile.

Nevertheless, *Trisopterus luscus* and *Trisopterus minutus* (pouting and poor cod) are commonly known to be strongly associated with hard structures and at least one of the species was also observed in video recordings, making them likely users of this new habitat. Although not observed in the videos, several species detected only inside the monopiles, including *Anguilla anguilla* (European eel), *Conger conger* (European conger), *Raniceps raninu*s (Tadpole fish) which rarely occur offshore, and *Ciliata mustela* (Fivebeard rockling), could indeed benefit from this habitat as they are sheltering species (Avant 2007, Dye, et al. 2024, Kerckhof, F.; Rumes, B.; Degraer 2018, Reeve 2007). The use of eDNA enables the detection of non-indigenous species (NIS), and several detections in this study initially suggested the presence of non-native fish. However, these likely represent false positives. For instance, the Pacific herring (*Clupea pallasii*) is almost certainly a mismatch of the native Atlantic herring (*Clupea harengus*). Similarly, the Caucasian dwarf goby (*Knipowitschia caucasica*) is native to the Black and Caspian Sea and is not known to occur in the North Sea, suggesting a genetic mismatch with a closely related native goby. Furthermore, the detection of the stone loach (*Barbatula barbatula*), a freshwater species, likely stems from riverine eDNA input from nearby deltas rather than local presence. Overall, the current data does not suggest that non-indigenous fish species are established at the sampling sites.

3.1.3 Recommendations

Due to the mixing of water inside and outside the monopile, eDNA appears to have limited suitability for assessing whether specific species actively use the monopile as habitat for shelter or foraging. For future monitoring efforts aimed at understanding species presence, baited camera traps or high-resolution video monitoring are recommended, as these methods allow direct observation of species presence and behaviour.

Nevertheless, eDNA sampling remains valuable at a broader scale and may be effectively used to detect the presence of non-native species in the surrounding area, as these may benefit from the introduction of the novel habitat type. Especially the application of primers targeting the detection of invertebrates may be of use, since we hypothesize that this is where major difference in communities may occur.

The eDNA data was therefore not further utilized within the context of the JIP-LIFE project specifically and the focus put on the video analysis, as this dataset provided relevant inputs for the different modelling exercises as well.

3.2 Video data analysis

3.2.1 Methods for community analysis and biomass determination

To analyse species communities on the monopile hard substrate, additional video footage collected by Waardenburg Ecology between May and September 2024 at monopiles D1, E5, F1, and F4. Videos were analysed using the TransectMeasure software (SeaGIS, Australia). On vertical transects, roughly every 1 meter, a suitably sharp frame was selected. On horizontal transects, non-overlapping frames were chosen manually. The depth and orientation of the camera were noted and the frames size was estimated. A grid of 200 points/m^2 was overlayed

in which each point was manually assigned a value that was either the lowest identifiable taxonomic group, “not colonised” if the point was assigned to a location without growth or only biofilm or labelled “blurry” if a specific point could not be assessed due to footage quality. Points assigned to "blurry” (11.6% of all points scored) were later removed from the dataset and are thus not considered in the coverage percentages. From each of the 559 analysed frames, a coverage percentage was calculated for each taxonomic group based on the assigned number of points.

Biomass over depth was estimated for all transects of the monopile, resulting in ash free dry weight (AFDW) data for the inside and outside of the monopile. Firstly, for each vertical and horizontal transect, all analysed frames were visually ranked from highest to lowest biomass. The highest- and lowest-ranked frames from each transect were then compared across all transects and monopiles to establish an overall ranking of frames from 1 to 10. Secondly, the estimation of the actual biomass was done using two methods. Whenever possible, the highest and lowest biomass video frames were linked to footage from other projects in which video and biomass data was collected for the community. Footage was linked by looking for frames with similar species composition and comparable biomass. As these datasets are very limited, for the remaining frames, organisms were counted individually and biomass estimated on average specific-specific biomass.

Most frames were linked to reference videos from a HKZ sampling campaign conducted with the marine growth sampling tool in November 2023 (Coolen, van der Weide, et al. 2025). During this campaign, both videos and scrape samples were collected. The scrape samples were processed for AFDW, thereby directly allowing linking visual with AFDW data. Particularly for frames from the mussel layer, videos and biomass data from platform L10-AD (October 2015) were used. For this location, only the species’ wet weights were available. To convert this data to AFDW data, species-specific conversion factors from wet weight to AFDW were calculated from a large dataset of scrape samples collected in the Dutch North Sea or Wadden Sea, by calculating the average species-specific ratio of wet weight to AFDW.

On the inner side of monopiles, species composition differed substantially from the outer side, and biomass was often estimated to be much lower than ever recorded in the above-mentioned datasets. Therefore, individuals in frames with the highest and lowest biomass were counted manually and converted to total ash free dry weight using average species-specific ash free dry weight values.

Through this, ash free dry weight per m² values were obtained for all frames with the highest and lowest biomass in each transect. Based on the initial ranking, interpolation was then applied to assign ash free dry weight values to all remaining frames, assuming a linear distribution of weight between the highest and lowest value.

The coverage data from the video analysis of vertical transects in combination with depth, estimated distance from the nearest water replenishment hole and observed area in view, were used to assess community patterns. For this purpose, generalised linear latent variable models (GLLVMs) were created using the gllvm package (Niku, et al. 2019, van der Veen 2025). These models allow for statistical testing of relations between multiple environmental variables and multiple species simultaneously. Model preparation was performed using methods from (Zuur and Ieno 2025)) and (van der Veen 2025). Sample ID (video frame grab) nested in transect, nested in turbine ID were included as a random effect to compensate for repeated sampling of the same turbine. Since large numbers of zero observations were present in the data, it was assumed to be zero inflated, and a beta hurdle distribution (betaH) was used (P. Korhonen, et al. 2024), while applying extended variational approximations using method=“EVA” (Korhonen, et al. 2025, P. Korhonen, et al. 2023). The need to include latent variables (LVs) was tested to account for relations with unknown environmental variables not included in the model. Models with 0, 1 and 2 LVs were created and compared using AIC (Akaike 1973). The model with the

lowest AIC was selected for further interpretation. Model validation was performed by plotting residuals against fitted values as well as variables included in the model, and fitted versus observed values. These plots were visually inspected to confirm that assumptions of homogeneity of variance and normality were met.

Generalised species pattern plots to visualise differences between the inside and outside of turbine foundations along the depth range were generated using the GLLVM predict.gllvm function. For prediction purposes, the estimated sampled area and distance to the nearest water replenishment hole were set to the average in the dataset.

3.2.2 Video analysis results

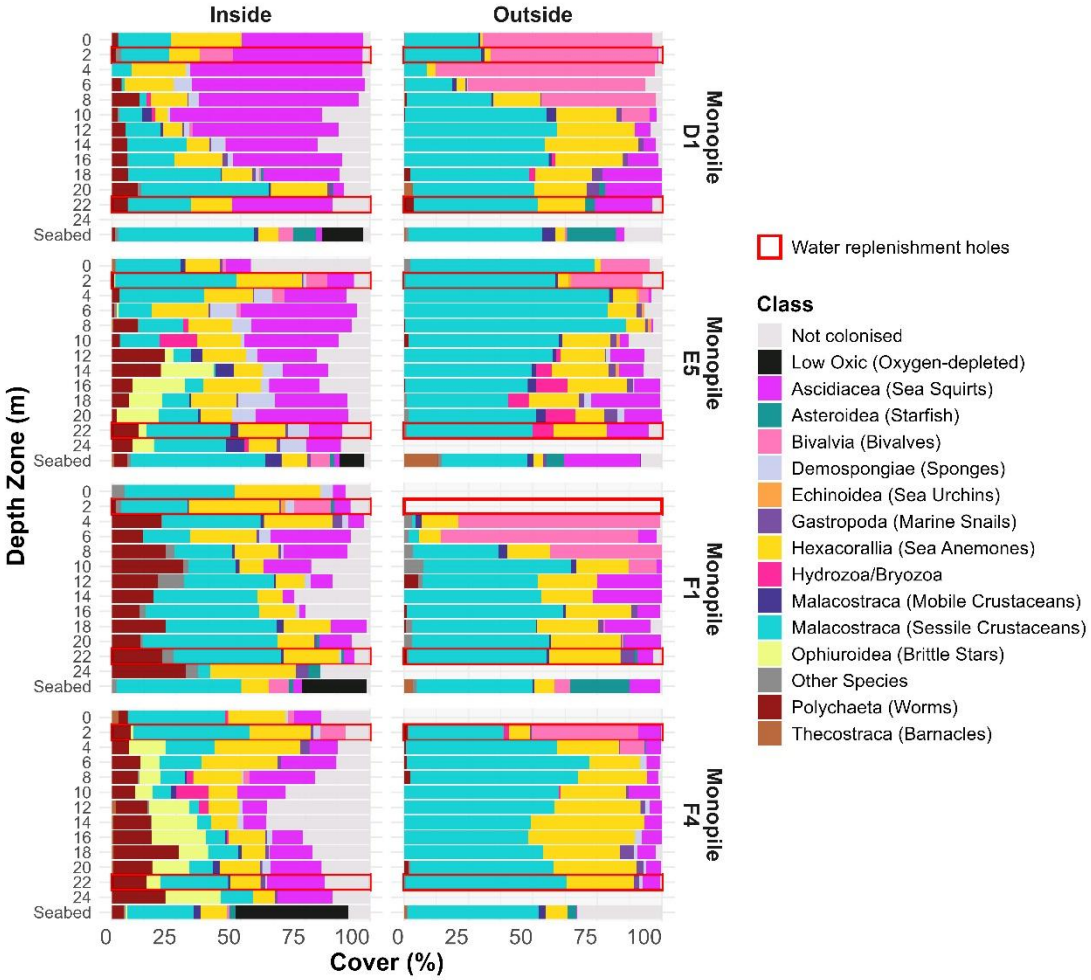

Figure 3-2 - Average relative cover of the different taxonomic groups per depth zone inside and outside the four analysed monopiles. Depth zones are in 2 m intervals.

The overview of the relative cover of species groups across depth and between the inside and outside of monopiles (Figure 3-2) reveals several ecological patterns in the fouling communities. Generally, the outer surfaces of the monopiles are largely covered by epifauna, with relatively little uncovered substrate. Macroalgae were observed sparsely and only close to the water surface. On the outside of the monopiles, benthic communities are comparable to those reported from similar offshore structures (De Mesel, et al. 2015). Three species groups dominate these communities: bivalves, anemones, and amphipods (crustaceans). Community composition varies with depth, shifting from bivalve-dominated assemblages (primarily *Mytilus edulis*) near the surface to anemone and amphipod-dominated communities closer to the

seafloor. For the analysed videos, the deeper layers were also partially covered with sea squirts.

Some variation exists between monopiles. monopiles F4 and E5 show a reduced presence of bivalves near the sea surface. While the bivalve zone on the outside of the other monopiles is solely dominated by *Mytilus edulis*, in F4 the sparse bivalve layer differs between sides of the monopile: one side is dominated by *Mytilus edulis*, whereas the other side is dominated by *Magallana gigas*. Additionally, the outside of E5 differs from other monopiles as sponges and sea urchins are present, although these groups remain minor contributors relative to the three dominant taxa. Sponges are also present on the outside of F4.

In contrast to these typical epifauna patterns on the outside, the insides of the monopiles support more heterogenous communities, characterized by a more even distribution among species groups and a substantially higher proportion of uncovered surface. Visual estimates indicate that overall biomass (also in terms of thickness of the epifauna) inside the monopiles is considerably lower than on the outside. The depths with the lowest surface coverage occur roughly between 10 and 17 m, corresponding approximately to the area in the middle of the two WHRs. Environmental conditions might limit biomass, through decreased flow velocities or decreased amounts of available food or oxygen.

Furthermore, the vertical zonation commonly observed on offshore structures is largely absent inside the monopiles. Blue mussels were rarely observed and, when present, were typically restricted to the edges of the WRHs. Amphipod mats were less common and thinner than those observed on the outside. Anemones occurred throughout the entire depth range inside the monopiles. Notably, Urticina anemones were commonly found near the WRHs. Sponges and sea squirts covered a larger area inside the structures compared to the outside, and calcareous tube-building worms (Serpulidae) seemed more abundant internally.

Differences were also observed between individual monopiles. Inside monopiles F4 and E5, large clusters of brittle stars were recorded, a feature not observed this strongly in the other monopiles. Species groups such as sponges, sea squirts, and brittle stars are known to frequently occur in sheltered microhabitats, including crevices and the interior of shipwrecks in the North Sea. These taxa may benefit from the more sheltered conditions in such environments, either through reduced competition with epifaunal species that are less tolerant of these conditions (e.g. lower current velocities and reduced food availability), or due to an intrinsic preference for these sheltered habitats. Although not counted specifically, mobile species such as *Cancer pagurus* and small gadoids, likely pouting, were observed inside the monopile. We are not aware of other wind farms in the North Sea displaying epifaunal communities similar to those observed inside the monopiles.

The creation of novel habitat carries the risk of facilitating the spread or settlement of epifaunal non-indigenous species (NIS). While video-based identification to the species level was limited, several observations confirmed or showed a high potential for NIS presence. The slipper limpet (*Crepidula fornicata*) and Pacific oyster (*Magallana gigas*) are non-native species in the North Sea and were observed in this study. There was no indication that the interior of the monopiles specifically promotes the occurrence of these species.

The observed colonial ascidians may include non-indigenous species, although identification to species level was not possible. Colonial ascidians showed higher coverage percentages inside the monopiles, thus this group may represent a potential risk in terms of NIS establishment. Other groups that are difficult to identify from video frames, but are known to harbour NIS, include polychaetes and barnacles. Future monitoring using molecular techniques, such as targeted DNA or scrape sampling, would be necessary to identify these taxa and accurately assess the NIS risk.

On the seafloor inside the monopiles we locally observed spots of what looks like microbial mats. These mats are e.g. known from the Grevelingen Lake, a saltwater body where the limited exchange with the North Sea, strong stratification in summer and a high amount of organic material leads to oxygen-depleted conditions near the sediment (Lipsewers, et al. 2016). Under these conditions, certain bacteria can proliferate, forming characteristic grey mats on the sediment surface, often accompanied by a decline or absence of other benthic macrofauna. Similar microbial mats have also been widely reported from hypoxic and anoxic regions of the Baltic Sea, where restricted water exchange, strong stratification, and eutrophication create comparable environmental conditions (Kulinski, et al. 2022). When looking at the modelling results for oxygen near the sediment-water interface inside the monopiles and considering the high likelihood of high organic matter input coming from (pseudo)faeces of the epifauna above and Particulate Organic Carbon (POC) settling inside the monopile, similar hypoxic conditions may develop locally within the monopiles. The accumulation of sediment or organic matter is also visible when comparing the inside seabed from this monitoring campaign with the T0 data, as the scour protection layer has largely been covered by a brown layer. These conditions could support microbial communities comparable to those observed in the Grevelingen Lake.

The GLLVM with two latent variables showed the best model fit and is presented here. The model output confirms the strong differences between the inside and outside communities along a depth gradient (Figure 3-3). In particular, strong differences exist between modelled cover percentages inside and outside for Amphipoda, Ascidiacea, *Metridium senile*, *Mytilus edulis* and Serpulidae, which is in line with the initial interpretation of the video data.

Together, the observations and model outcomes suggest that the interior of monopiles represents a distinct ecological habitat, differing fundamentally from the exterior in terms of community structure, biomass, and depth-related zonation.

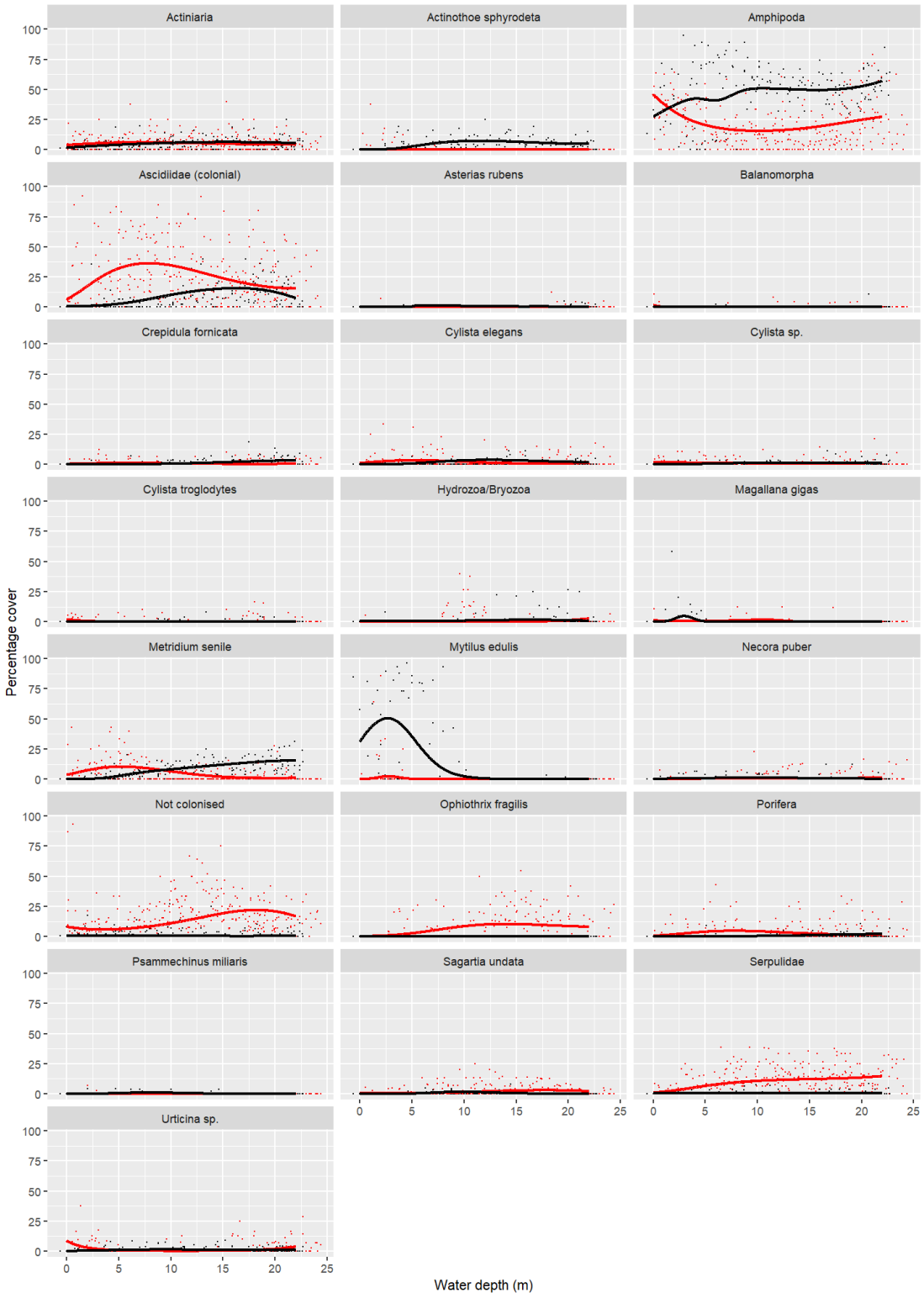

Figure 3-3 - observed (dots) and modelled (line) relation generalised for all turbine foundations, between species and depth, for communities inside (red) and outside (black) the monopile foundations.

3.2.3 Recommendations

Physical sampling is preferable for data analyses as presented here, due to its higher taxonomic resolution, increased likelihood of detecting non-indigenous species, and ability to quantify biomass. If this approach is not possible, video-based monitoring should employ using high-resolution cameras. When using this method appropriate lighting, standardised viewing

angles, fixed distances from the steel of the monopile and video overlay information on date, time, water depth, heading, monopile ID and transect ID should be ensured. Given the observed differences in community composition inside the different monopiles, further monitoring of ecological outcomes is strongly recommended. The long-term development of biological communities inside these structures remains unclear and likely differs from the successional patterns typically observed in comparable environments. In particular, the potential presence of microbial mats should be considered a priority in future monitoring efforts, as the effects likely become stronger as organic matter further accumulates at the bottom of the monopiles.

3.3 Nutrient sample analysis

3.3.1 Nutrient sample analysis method & limitations

During the water sampling at monopiles D6 and F1, some water was set aside in a cool environment for nutrient sample collection. These water samples were filtered over a 0.8/0.2 µm syringe filter (Pall Acropak) and collected in three-times rinsed 4.5 mL vials, that were stored at -20°C. Phosphate, nitrate, nitrite, ammonium, total nitrogen, and silicate concentrations were determined at the nutrient laboratory of NIOZ (Yerseke). A Type II three-way factorial ANOVA was performed for each nutrient, treating Position (Inside vs. Outside), Depth, and Monopile as fixed factors. An interaction term (Position x Depth) was included to determine whether the vertical nutrient profile differed significantly between the interior and exterior of the structures. Significance was defined as $p < 0.05$.

3.3.2 Nutrient sampling results

Nutrient concentrations as a function of depth were plotted for the inside and outside of each monopile (Figure 3-4).

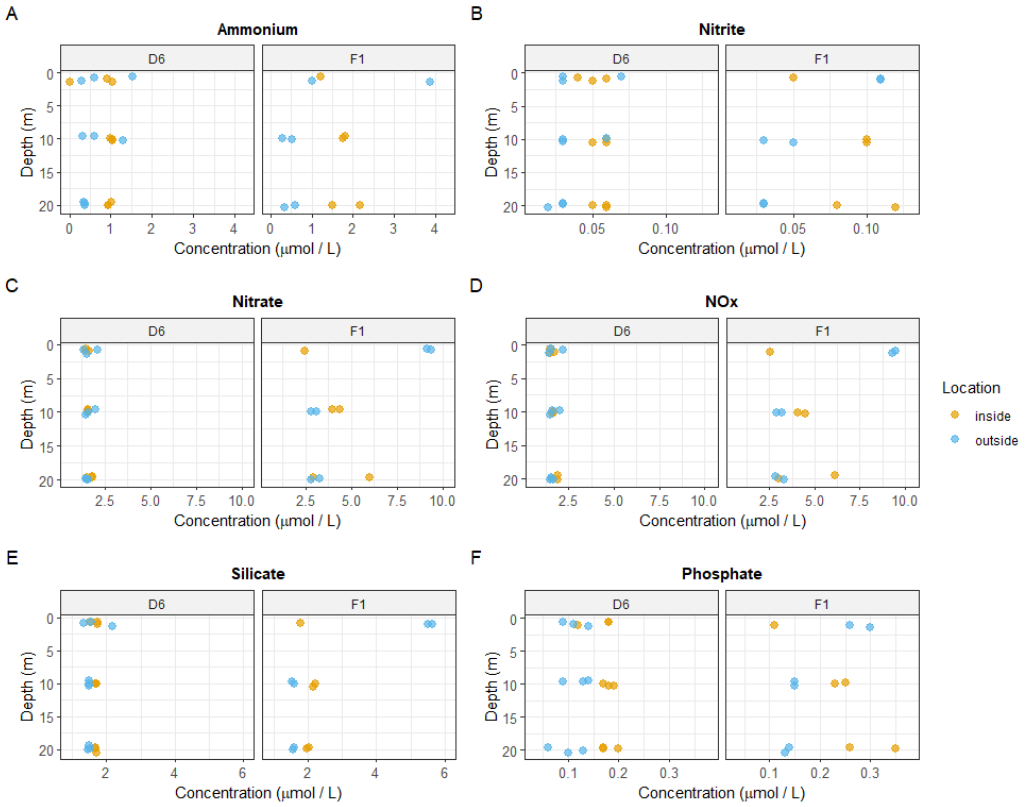

Figure 3-4 Concentrations of different inorganic nutrients and silicate over the depth gradient for monopile D6 and F1. Colours represent inside (orange) vs. outside (blue).

Overall, concentrations of ammonium, nitrite, phosphate, and silicate tended to be higher inside the monopiles compared to outside, and in some cases increased with depth. The ANOVA revealed a significant interaction between Depth and Position for all nutrients. This suggests that nutrient concentrations are not uniformly affected by the structure; instead, the "Inside" effect is amplified over the vertical gradient. For example, in Figure 3-4 B, nitrate concentrations increase with depth inside the structure, while remaining relatively uniform outside. In marine systems vertical gradients in nutrient concentrations can be present, as nitrate, phosphate, and silicate are depleted by phytoplankton growth in surface waters where light is available and organic matter decomposition near the seabed releases additional inorganic nutrients (Loebl, et al. 2009, Siems, et al. 2024). The strength of these gradients depends on mixing and light conditions and is more common in deeper regions of the North Sea. In the present dataset, such depth-related gradients were not consistently observed outside the monopiles. It is currently unclear which processes are driving the depth gradient patterns inside the monopiles. One possibility is that organic matter accumulating and decomposing within the monopiles, along with excretion from fouling communities on vertical surfaces, contributes nutrients at rates higher than can be balanced with the water entering from the surroundings. Simultaneously, limited light inside the monopiles may constrain phytoplankton growth, thereby reducing overall nutrient uptake and enhancing internal nutrient accumulation. Finally, the ANOVA also showed a significant effect of the sampled monopile.

Recommendations

Although nutrient data may be valuable for inclusion in future water quality assessments, the current data resolution is insufficient to describe what biogeochemical processes are driving the observed patterns. Future sampling campaigns should prioritise standardised collection and processing of water samples to minimise degradation and variability due to temporal variation, as well as the collection of sufficient replicates. Increasing vertical resolution by subdividing depth intervals would likely allow clearer trends to emerge. Furthermore, based on the modelled POC and oxygen concentrations, as well as the observation of potential microbial mats, biogeochemical processes at the seafloor within monopiles could be altered. Targeted sampling for inorganic nutrient concentrations very close to the seafloor inside monopiles may yield valuable insights into these modified biogeochemical dynamics.

3.3.3 Species Traits

For the species composition of the inside of F1 monopile, additional trait information was assessed. The taxa found inside monopile F1 include predominantly Arthropoda, Chordata, Cnidaria, Echinodermata and Mollusca, as well as Porifera, Bryozoa, Annelida, and Chlorophyta, though with fewer species or classes identified. The traits describe (Mavraki, Want, et al. 2026 under review)

- Body shape: the physical shape of seafloor organisms (e.g. growing upright, flat lying, or building tubes) which influences their interactions with currents, sediments, and other species.
- Feeding: how organisms obtain food (e.g. by filtering particles from the water, eating material in the sediment, scavenging, or preying on other animals) which shapes their role in energy flow of marine ecosystems.
- Larval development: how offspring develop and disperse, ranging from larvae that drift and feed in the water column to those that rely on yolk or develop directly on the seafloor, which determines how far a species can spread.
- Habitat: where an organism lives on or in the seafloor (e.g. attached to hard surfaces, burrowed into sediments, or tucked into crevices) influencing coping strategies with environmental conditions and disturbance.
- Longevity: how long a species typically lives (less than a year to over a decade), influencing how quickly populations turn over and their resilience to environmental change.

- Productivity: how quickly a species converts resources into new biomass, indicating slow or fast growth and reproduction and its energy contribution to the ecosystem.

In the following Table 3-1 the different species and their traits are visualized based on the classification in (Mavraki, Want, et al. 2026 under review). The trait abbreviations and definitions can be found in the Annex section (Annex 6A).

The trait classification is fuzzy coded, with values within one trait totalling to 1 across all modalities. A score of 1 means the species is fully 'associated' with that one modality within the specific trait. A score below 1 means that the species is associated with multiple different modalities within the specific trait. The closer the score is to 1, the stronger the species is associated with that modality.

Table 3-1 - Trait description of taxa found in monopile F1 (source (Mavraki, Want, et al. 2026 under review))

Traits/ Taxa	Body Shape						Feeding					Larval Development			Habitat						Longevity				Productivity				
	PmErfle	PmErNfle	PmTube	PmEnfle	PmEnNfle	PmNone	fSuspension	fDeposit	fScavenger/ Opportunist	fPredator	fParasite	ldPla	ldLec	ldDir	lhTube	lhBurrow	lhFree	lhCrevice	lhEpi	lhAttach	l<1	l1-3	l3-10	l>10	pb1	pb2	pb3	pb4	pb5
Actiniaria	0,00	0,00	0,00	0,00	0,00	1,00	1,00	0,00	0,00	0,00	0,00	0,57	0,36	0,07	0,00	0,13	0,00	0,01	0,24	0,62	0,00	0,02	0,22	0,76	1,00	0,00	0,00	0,00	0,00
Actinothoe sphyrodeta	0,00	0,00	0,00	0,00	0,00	1,00	1,00	0,00	0,00	0,00	0,00	0,00	0,00	0,00	0,00	0,00	0,00	0,00	0,50	0,50	0,00	0,00	0,00	0,00	1,00	0,00	0,00	0,00	0,00
Alcyonium digitatum	0,20	0,80	0,00	0,00	0,00	0,00	1,00	0,00	0,00	0,00	0,00	1,00	0,00	0,00	0,00	0,00	0,00	0,00	0,00	1,00	0,00	0,00	0,00	1,00	1,00	0,00	0,00	0,00	0,00
Amphipoda	0,00	0,00	0,21	0,00	0,00	0,79	0,24	0,44	0,15	0,13	0,04	0,00	0,00	1,00	0,33	0,07	0,45	0,08	0,06	0,00	0,56	0,42	0,00	0,00	0,00	0,00	0,00	0,00	1,00
Jassa herdmani	0,00	0,00	1,00	0,00	0,00	0,00	1,00	0,00	0,00	0,00	0,00	0,00	0,00	1,00	1,00	0,00	0,00	0,00	0,00	0,00	0,50	0,50	0,00	0,00	0,00	0,00	0,00	0,00	1,00
Ascidiacea	0,00	0,00	0,00	0,03	0,00	0,97	1,00	0,00	0,00	0,00	0,00	0,00	1,00	0,00	0,00	0,00	0,00	0,11	0,44	0,44	0,36	0,36	0,29	0,00	1,00	0,00	0,00	0,00	0,00
Asterias rubens	0,00	0,00	0,00	0,00	0,00	1,00	0,00	0,00	0,50	0,50	0,00	1,00	0,00	0,00	0,00	0,00	1,00	0,00	0,00	0,00	0,00	0,00	1,00	0,00	1,00	0,00	0,00	0,00	0,00
Balanomorpha	0,00	0,13	0,00	0,00	0,87	0,00	1,00	0,00	0,00	0,00	0,00	1,00	0,00	0,00	0,00	0,00	0,00	0,00	0,22	0,78	0,00	0,25	0,75	0,00	0,00	1,00	0,00	0,00	0,00
Botrylloides sp.																													
Cancer pagurus	0,00	0,00	0,00	0,00	0,00	1,00	0,00	0,00	0,00	1,00	0,00	1,00	0,00	0,00	0,00	0,00	0,50	0,50	0,00	0,00	0,00	0,00	0,00	1,00	0,00	0,00	0,00	1,00	0,00
Crepidula fornicata	0,00	0,40	0,00	0,00	0,60	0,00	1,00	0,00	0,00	0,00	0,00	1,00	0,00	0,00	0,00	0,00	0,00	0,00	0,00	1,00	0,00	0,00	1,00	0,00	1,00	0,00	0,00	0,00	0,00
Cylista elegans	0,00	0,00	0,00	0,00	0,00	1,00	1,00	0,00	0,00	0,00	0,00	0,50	0,50	0,00	0,00	0,00	0,00	0,00	0,00	1,00	0,00	0,00	0,00	1,00	1,00	0,00	0,00	0,00	0,00
Cylista	0,00	0,00	0,00	0,00	0,00	1,00	1,00	0,00	0,00	0,00	0,00	0,50	0,50	0,00	0,00	0,00	0,00	0,00	0,00	1,00	0,00	0,00	0,00	1,00	1,00	0,00	0,00	0,00	0,00
Cylista troglodytes	0,00	0,00	0,00	0,00	0,00	1,00	1,00	0,00	0,00	0,00	0,00	0,50	0,50	0,00	0,00	0,00	0,00	0,00	0,00	1,00	0,00	0,00	0,00	1,00	1,00	0,00	0,00	0,00	0,00
Diadumene cincta	0,00	0,00	0,00	0,00	0,00	1,00	1,00	0,00	0,00	0,00	0,00	0,00	0,00	0,00	0,00	0,00	0,00	0,00	0,50	0,50	0,00	0,00	0,00	0,00	0,00	1,00	0,00	0,00	0,00
Didemnidae	N/A																												
Didemnum vexillum	N/A																												
Diplosoma listerianum	0,00	0,00	0,00	0,00	0,00	1,00	1,00	0,00	0,00	0,00	0,00	0,00	1,00	0,00	0,00	0,00	0,00	0,00	0,50	0,50	1,00	0,00	0,00	0,00	0,00	1,00	0,00	0,00	0,00
Halichondria (Halichondria) panicea	0,00	0,00	0,00	0,20	0,20	0,60	1,00	0,00	0,00	0,00	0,00	0,00	0,50	0,50	0,00	0,00	0,00	0,00	0,00	1,00	0,00	0,00	1,00	0,00	1,00	0,00	0,00	0,00	0,00
Homarus gammarus																													
Hydrozoa	0,63	0,03	0,00	0,17	0,02	0,13	0,92	0,00	0,00	0,08	0,00	0,84	0,08	0,08	0,00	0,00	0,00	0,00	0,35	0,65	0,28	0,02	0,61	0,00	0,00	1,00	0,00	0,00	0,00
Bryozoa	0,19	0,13	0,00	0,39	0,29	0,00	1,00	0,00	0,00	0,00	0,00	0,10	0,90	0,00	0,00	0,00	0,00	0,00	0,63	0,37	0,41	0,32	0,23	0,07	1,00	0,00	0,00	0,00	0,00
Liocarcinus	0,00	0,00	0,00	0,00	0,00	1,00	0,00	0,00	0,50	0,50	0,00	1,00	0,00	0,00	0,00	0,00	1,00	0,00	0,00	0,00	0,00	0,00	1,00	0,00	0,00	0,00	0,00	1,00	0,00
Magallana gigas	0,00	1,00	0,00	0,00	0,00	0,00	1,00	0,00	0,00	0,00	0,00	1,00	0,00	0,00	0,00	0,00	0,00	0,00	0,00	1,00	0,00	0,00	0,00	1,00	1,00	0,00	0,00	0,00	0,00
Metridium senile	0,00	0,00	0,00	0,00	0,00	1,00	1,00	0,00	0,00	0,00	0,00	1,00	0,00	0,00	0,00	0,00	0,00	0,00	0,50	0,50	0,00	0,00	0,00	1,00	1,00	0,00	0,00	0,00	0,00
Modiolus																													
Mytilus edulis	0,00	1,00	0,00	0,00	0,00	0,00	1,00	0,00	0,00	0,00	0,00	1,00	0,00	0,00	0,00	0,00	0,00	0,00	0,00	1,00	0,00	0,00	0,00	1,00	0,00	0,00	1,00	0,00	0,00
Necora puber	0,00	0,00	0,00	0,00	0,00	1,00	0,00	0,00	0,50	0,50	0,00	1,00	0,00	0,00	0,00	0,00	1,00	0,00	0,00	0,00	0,00	0,00	1,00	0,00	1,00	0,00	0,00	0,00	0,00
Ophiothrix fragilis	0,00	0,00	0,00	0,00	0,00	1,00	0,70	0,30	0,00	0,00	0,00	1,00	0,00	0,00	0,00	0,00	0,50	0,50	0,00	0,00	0,00	0,00	1,00	0,00	1,00	0,00	0,00	0,00	0,00
Ophiura	0,00	0,00	0,00	0,00	0,00	1,00	0,00	0,00	0,50	0,50	0,00	1,00	0,00	0,00	0,00	0,00	1,00	0,00	0,00	0,00	0,00	0,00	1,00	0,00	1,00	0,00	0,00	0,00	0,00
Porifera	0,01	0,06	0,00	0,11	0,23	0,59	1,00	0,00	0,00	0,00	0,00	0,00	0,88	0,13	0,00	0,00	0,00	0,00	0,29	0,71	0,00	0,07	0,89	0,04	1,00	0,00	0,00	0,00	0,00
Psammechinus miliaris	0,00	0,00	0,00	0,00	0,00	1,00	0,00	0,00	0,00	1,00	0,00	1,00	0,00	0,00	0,00	0,00	1,00	0,00	0,00	0,00	0,00	0,00	1,00	0,00	1,00	0,00	0,00	0,00	0,00
Sagartiidae	0,00	0,00	0,00	0,00	0,00	1,00	1,00	0,00	0,00	0,00	0,00	0,50	0,50	0,00	0,00	0,00	0,00	0,03	0,13	0,84	0,00	0,00	0,00	1,00	1,00	0,00	0,00	0,00	0,00
Serpulidae	0,00	0,00	0,64	0,00	0,36	0,00	1,00	0,00	0,00	0,00	0,00	0,80	0,20	0,00	0,60	0,00	0,00	0,00	0,10	0,30	0,20	0,50	0,30	0,00	0,00	0,00	0,00	0,00	1,00
Spirobranchus	0,00	0,00	0,40	0,00	0,60	0,00	1,00	0,00	0,00	0,00	0,00	1,00	0,00	0,00	0,50	0,00	0,00	0,00	0,00	0,50	0,00	0,50	0,50	0,00	0,00	0,00	0,00	1,00	0,00
Taurulus bubalis	N/A																												
Ulva	N/A																												
Urticina felina	0,00	0,00	0,00	0,00	0,00	1,00	1,00	0,00	0,00	0,00	0,00	0,00	1,00	0,00	0,00	0,00	0,00	0,00	0,00	1,00	0,00	0,00	1,00	0,00	1,00	0,00	0,00	0,00	0,00

In Figure 3-5, the mean scores per modality in each trait across all species occurring in monopile F1 is being displayed to provide a sense of which modalities dominate the current community assemblage.

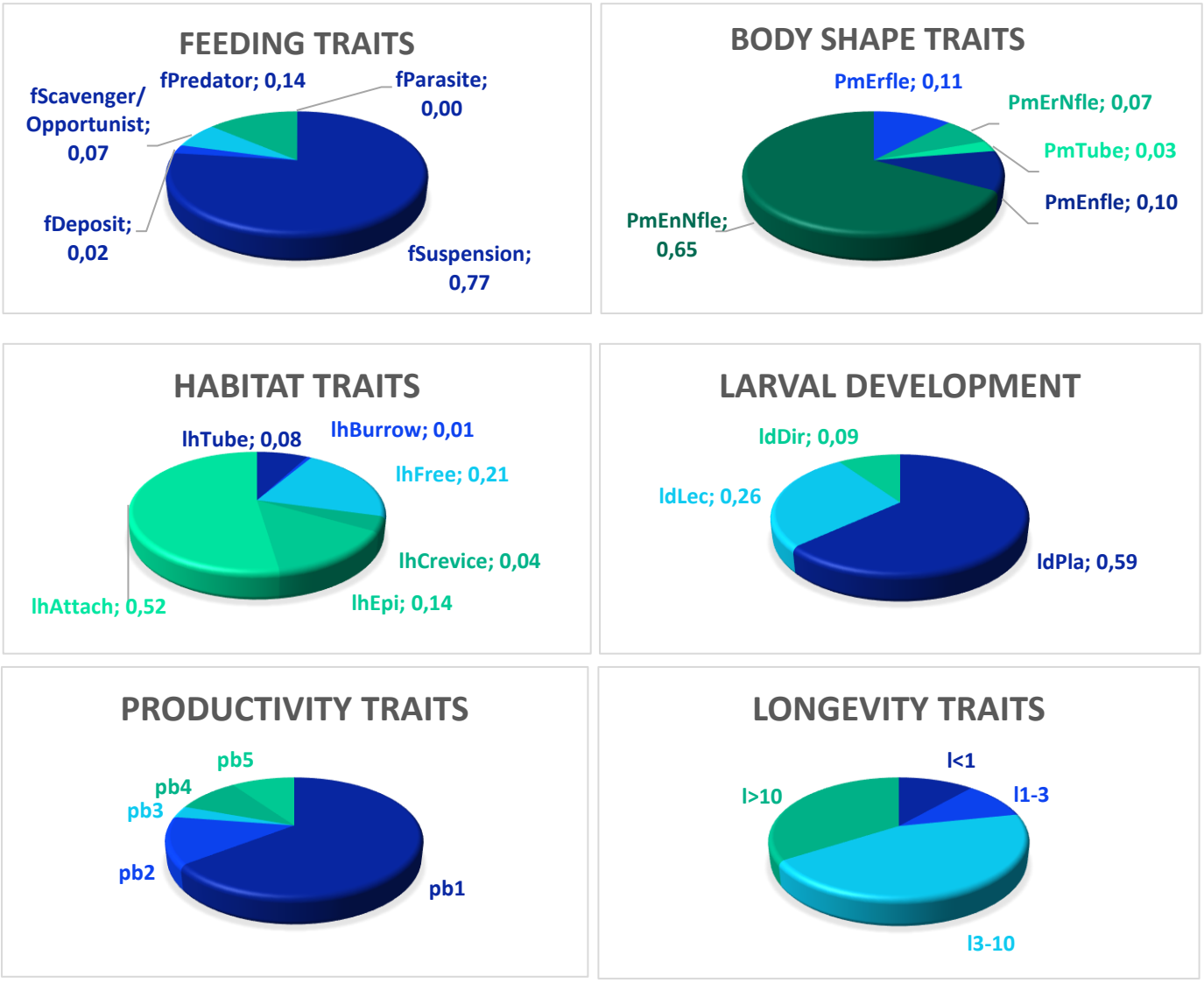

Figure 3-5 Mean score per modality across all occurring species inside monopile F1 (for definitions see Species Traits Definitions

The trait composition of the analysed community reveals a functionally diverse assemblage shaped by hard-substrate habitat conditions.

Feeding traits show a dominance of suspension feeders, such as hydrozoans and mussels in terms of presence/absence (we refrained from biomass weighing as the biomass determination for the video analysis encountered significant limitations). Suspension feeders play a critical role in pelagic–benthic coupling by removing particles from the water column and transferring energy to the benthic realm (Gili and Coma 1998) and can contribute to increased food web complexity through biodeposition (N. Mavraki 2020b). Alongside suspension feeders, predators such as sea stars and crabs as well as opportunists are feeding modalities that occur, adding to the complexity of trophic interactions. Meanwhile, deposit feeders traits are almost not at all expressed in the F1 monopile assemblage.

The body shape of encrusting non-flexible species, including barnacles and sponges, is the dominant modality of this trait. Secondly, species with encrusting flexible body shapes are characterizing the F1 monopile while tube-building species are limited. Therefore, the habitat for the present species is provided by the organisms themselves (e.g. shells, byssus threads, and colonies) rather than by constructed tubes or mounds. These introduce physical complexity and additional surface for attachment or refuge that can contribute to increased biodiversity (Gutiérrez, et al. 2003).

Living habitat traits confirm strong substrate attachment as the prevailing habitat modality among the present assemblage. In addition, species habitat modalities of living on or in other organisms (epi-endozoic/epi-endophytic) are present, contributing to overgrowth and colonization of e.g. ascidians, sponges or tunicates or creating mixed mats. Low mobility for most occurring species implies limited capacity to escape physical stressors but reinforces habitat fidelity and structural integrity (Degen and Faulwetter 2019). A mean score of 21 also indicates several species that are free living on and/or within the sediment.

In terms of larval development modalities, most species exhibit pelagic planktotrophic or lecithotrophic development. Enabling extended planktonic phases and broad colonisation capacity, suggests resilience to local disturbances and a strong ability to disperse (Lewin, et al. 1987). Non-pelagic development is rare, occurring only in a few encrusting taxa, which are limited in their spatial spread but contribute to local persistence (Chust, et al. 2016, de Juan, et al. 2022).

Productivity modalities show species with predominantly low productivity levels which aligns with the longevity patterns observed (Strong, et al. 2015). The prevalence of low-P/B (pb1-pb2) species means a lot of the ecosystem's energy is accumulated in stable biomass (and thus nutrients) in these species' bodies or structures persisting over several years in a stable biomass and thus contributing to habitat complexity but relatively less to short-term productivity.

Longevity patterns suggest that many taxa are medium- to long-lived, such as mussels and sea stars, reflecting K-strategist characteristics. These species invest in somatic growth and delayed reproduction, which enhances population stability but increases vulnerability to disturbances (Degen and Faulwetter 2019, Pearson and Rosenberg 1978, Pianka 1970).

Overall, the trait profile depicts a community that is structurally complex, dominated by suspension feeders, and characterised by high dispersal potential and moderate longevity. Functional roles include efficient energy transfer, habitat engineering, and biodiversity support. These features align with patterns observed on artificial structures such as offshore wind farms, where tube-builders and encrusting taxa thrive, creating heterogeneous habitats that differ from natural rock beds. The interplay of feeding strategies, dispersal traits, and habitat-forming modalities positions this assemblage as a contributor to ecosystem functioning in hard-substrate environments, as demonstrated by studies on artificial structures by (Boutin, et al. 2023, Coolen, Van Der Weide, et al. 2020).

4 Modelling

This chapter describes the modelling framework used to quantify abiotic habitat conditions inside the monitored monopiles and to assess how these conditions respond to changes in WRH design. The approach combines a hydrodynamic replenishment model that translates external forcing into internal water exchange with a coupled DELWAQ water-quality model that simulates the resulting oxygen dynamics and food availability proxies inside the monopile. Section 4.1 first summarises the overall modelling concept, coupling strategy, and key outputs. Sections 4.2 and 4.3 then describe the setup of the hydrodynamic and DELWAQ components, including their specific forcing, boundary conditions, parameterisation choices, and associated uncertainties and limitations. Section 4.4 defines the simulated base cases and WRH design sensitivity scenarios, after which Section 4.5 presents the model results and synthesises their implications for internal habitat suitability and potential design optimisation.

4.1 Modelling framework

The internal environment of an offshore wind monopile is controlled by an enclosed air pocket above an internal water column and a number of openings to the ambient sea. Figure 4-1 schematises the system considered here, with an air-tight platform above the waterline, air replenishment holes in the upper section, and upper water replenishment holes (UWRHs) and lower water replenishment holes (LWRHs) in the wetted part of the monopile. Although WRHs may become partially obstructed by marine growth, no such obstruction was observed at the monitored monopiles during the study period of 3 years. External tide and wave forcing cause fluctuations in the outside water level and pressure field, which generate a time-varying pressure difference across the WRHs and drive internal water exchange.

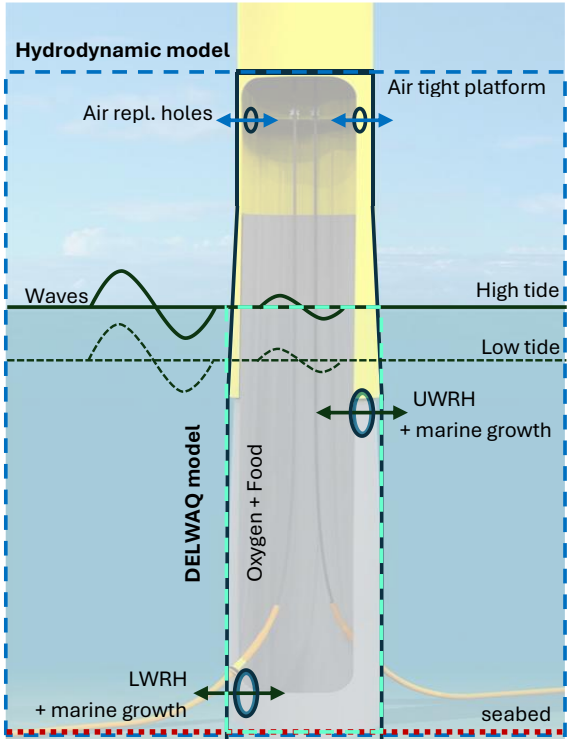

Figure 4-1 Schematic of the monopile system and dominant drivers of internal water exchange (hydrodynamic model) and internal water quality (DELWAQ model) (background image reference www.seaproof.com).

The combined water replenishment and water quality within a monopile foundation are modelled in a two-step coupled modelling approach. First, the exchange of water between the surroundings and the monopile is calculated with a hydrodynamic replenishment model, which converts the external forcing and WRH characteristics into time series of exchange through the WRHs (volume fluxes and associated replenishment behaviour). Second, these replenishment rates are used as input to a 1DV water quality model in DELWAQ (Postma, et al. 2003), which simulates dissolved oxygen dynamics and a proxy for food availability (particulate organic carbon, POC), accounting for internal sinks and transformations such as oxygen consumption and particulate organic matter settling and decay. Sections 4.2 and 4.3 describe the hydrodynamic and DELWAQ model components and setups in more detail, while full model formulations and implementation details are provided in Appendix A and Appendix C.

4.2 Hydrodynamic water replenishment model

4.2.1 Model concept

Water exchange between the ambient sea and the monopile interior is simulated with a one-dimensional vertical (1DV) hydrodynamic model that predicts the internal free-surface elevation and the resulting flow through the replenishment openings. The model represents the monopile as a control volume containing an internal water column overlain by a compressible air pocket beneath the airtight platform. Time-varying external hydrodynamic loading (waves, water level and currents) induces pressure fluctuations at the replenishment holes, which drive inflow and outflow. The excess air pressure resulting from compression/expansion of the enclosed air volume is included in the pressure balance and provides an important restoring mechanism for internal water-level motion. A conceptual sketch of the control volume and openings is shown in Figure 4-2. Full model formulation and implementation details are provided in Appendix B.1.

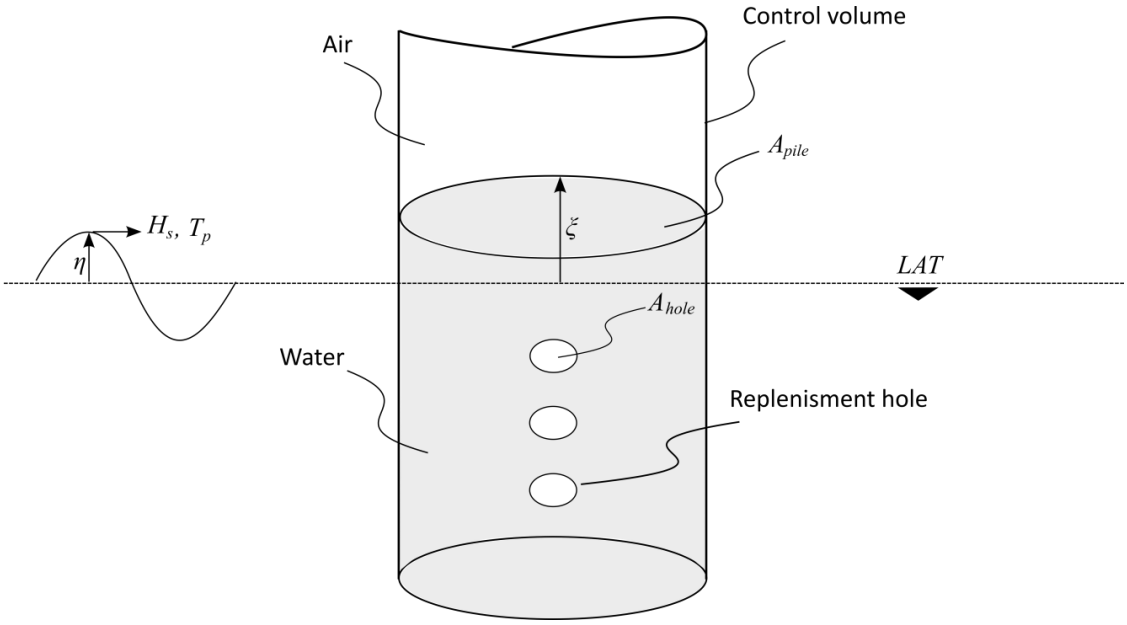

Figure 4-2 Conceptual sketch of the control volume used in the hydrodynamic replenishment model, including the internal water column, compressible air pocket, airtight platform, and replenishment openings.

The 1DV water exchange model is calibrated against laboratory wave tests performed at Deltares, where the prototype wave conditions cover a range of spectral wave heights of 1.5 m to 9.8 m and peak wave periods of 5.5 s to 14.2 s. The laboratory experiments are considered scale-independent, because the Reynolds number for the flow in the holes is between 1,000-10,000 and the loss coefficient for flow through a circular hole is independent of viscous effects

for Reynolds numbers in that range (Idelchik 2008). In general, a good agreement was obtained with an error in the order of 10% between the measured and computed internal wave motion.

4.2.2 Monopile schematisation and replenishment holes

The hydrodynamic model is applied to two of the monitored monopiles (F1 and E5), whose geometry and opening configurations are described in Section 1.5. In the 1DV schematisation, the internal water and air volumes are represented as functions of elevation using cross-sectional area fractions that are consistent with the tapered monopile geometry. This ensures that the internal volume (and therefore the dynamic response to forcing) reflects the transition from the larger lower diameter to the smaller upper diameter.

Exchange with the ambient sea is represented by discrete WRHs located at the as-built elevations for each monopile. For each simulated case, the WRH elevations, total open area and orientation are prescribed following the configurations reported in Section 1.5. Potential obstruction of the holes due to marine growth is normally considered with an effective reduction in opening area; however, since no obstruction was observed at the monitored monopiles during the study period, the base simulations assume unobstructed openings and WRH open area is varied only in the dedicated sensitivity scenarios (Section 4.5.2.1).

4.2.3 Metocean forcing data

The hydrodynamic replenishment model is forced with time-varying wave, water level and current conditions representative for the monitoring period. For this study, metocean forcing was extracted at the monopile locations from Deltares in-house operational/hindcast models using an hourly time step.

Waves

Spectral wave conditions are taken from the Deltares unstructured SWAN model and include the spectral significant wave height H_{m0}(m), peak period T_p(s), and mean wave direction (coming from, °N). These parameters are used to define the hourly sea state in the replenishment model.

Water levels and currents

Water level η (m+NAP) and depth-averaged tidal current components $U$and V(eastward and northward, m/s) are obtained from the Deltares Dutch Continental Shelf Model (DCSM) (Deltares 2022). For convenience in subsequent processing, the current components can be converted to current magnitude and direction where needed; however, the replenishment model uses the component form as input.

The primary forcing period considered in this research is calendar year 2024, which covers the T3 offshore monitoring campaign in October–November 2024. To enable consistent comparison across WRH design variants, all sensitivity simulations are performed for November 2024, which is a month with a good variability in hydrodynamic conditions to illustrate potential effect of these changes on the replenishment and resulting internal water quality. An overview of the 2024 forcing time series, including a zoom for November 2024, is provided in Figure 4-3. The wind and wave directional information is presented in the rose data in Figure 4-4.

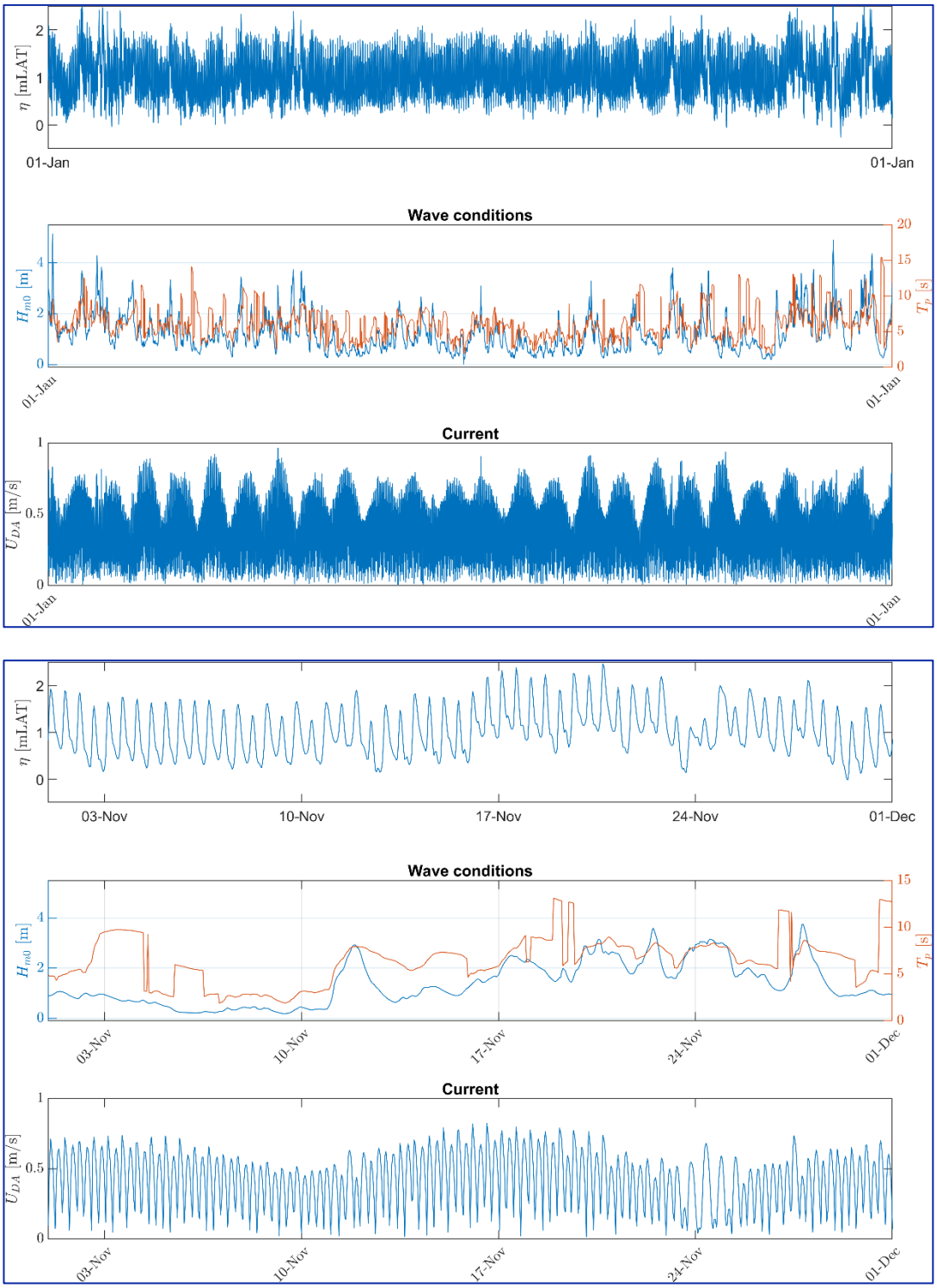

Figure 4-3 Hourly metocean forcing used for the hydrodynamic replenishment model in 2024 (top) with zoom for November 2024 (bottom): water level η , H_{m0}, T_p, , and depth-averaged current.

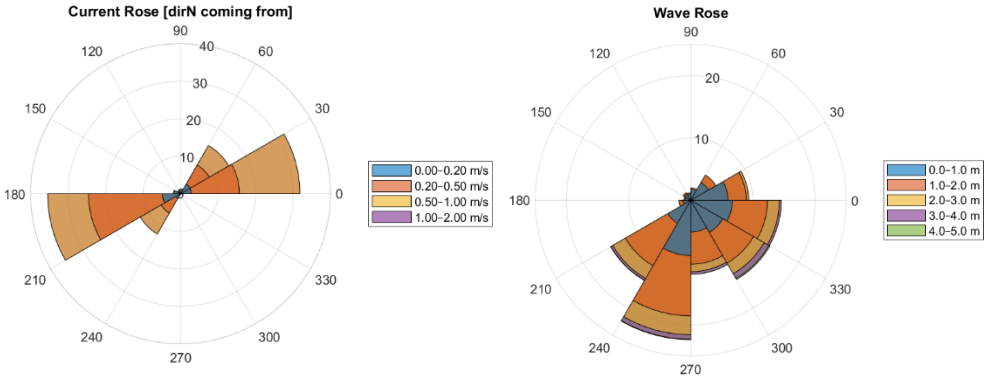

Figure 4-4 Current rose (left panel) and wave rose (right panel) based on data of the full year 2024 at the HKZ OWF.

4.2.4 Translation from metocean conditions to replenishment fluxes

The hydrodynamic replenishment model is driven by pressure fluctuations at the replenishment openings resulting from the combined action of water level variation, tidal currents and waves. These contributions are combined through linear superposition of the corresponding pressure terms at the monopile wall (see Appendix B.1 for the governing formulation and Appendix B.1.1–B.1.2 for the individual forcing components). Water level is treated as a continuous signal, while wave conditions are assumed stationary within each hourly bin defined by the SWAN sea-state parameters.

4.2.4.1 Wave-induced pressures.

For each hour, a realisation of the free-surface elevation is generated from a JONSWAP spectrum using the hourly H_{m0} and T_p (with $\gamma = 3.3$) to represent the stochastic nature of irregular waves. This surface elevation signal is translated into a time-varying dynamic pressure at the elevations of the replenishment holes following linear wave theory, which provides the wave-driven component of the pressure difference across each opening. For an extensive description of how this is derived, the reader is referred to Appendix B.1.

4.2.4.2 Water level and current-induced pressures.

The water level time series provides the low-frequency (tidal) component of the external pressure signal. Depth-averaged tidal currents from DCSM are translated to representative current magnitudes at the elevations of the replenishment holes using a power-law profile with a 1/7th exponent (DNV 2021). The resulting current-induced pressures are calculated using steady flow (no separation effects) and are added to the total external pressure forcing at each opening.

The resulting combined pressure forcing yields a deterministic time series of internal water-level variation and corresponding fluxes through the individual openings. Figure 4-5 illustrates the transformation from the metocean forcing (H_{m0}, T_p, water level and currents) to the internal free-surface elevation and the flux through representative upper and lower replenishment holes. Internal water-level variations are primarily controlled by the tidal water level signal, while the magnitude of exchange through the WRHs is strongly modulated by wave conditions.

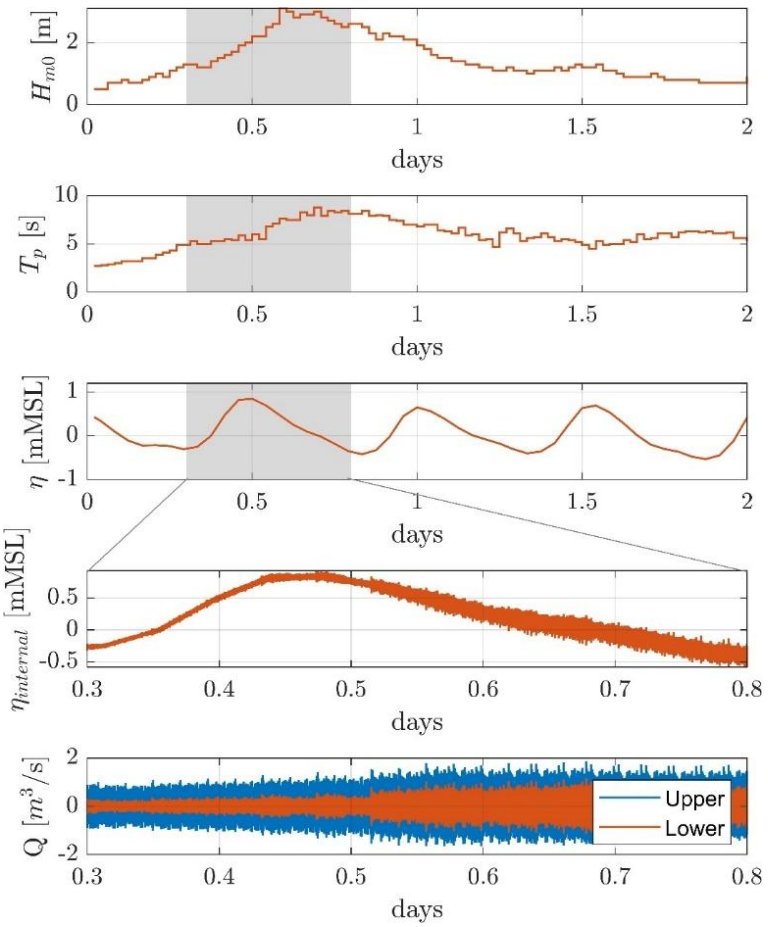

Figure 4-5 Example of the transformation of spectral wave height (H_{m0}), peak wave period (T_p), water level (η), and current speed and direction (not shown) into the water level in the monopile ($\eta_{internal}$) and a flux through the upper and lower water replenishment holes (Q). The grey boxes show the location of the zoom in the lower panel.

4.2.5 Uncertainties and model limitations

The hydrodynamic replenishment model provides an efficient representation of internal water-level response and exchange through the WRHs, but several assumptions introduce uncertainty that should be considered when interpreting the results:

- **1DV representation and mixing.** The model is one-dimensional in the vertical and assumes that horizontal cross-sections are well mixed. As a result, lateral circulation, local jets near openings, and 3D mixing processes inside the monopile are not resolved explicitly. CFD simulations of the WRH exchange indicate that such three-dimensional mixing is primarily localised near the openings, while velocities and turbulence levels in the interior away from the WRHs are relatively low. Given that the dominant exchange processes are vertically organised, a one-dimensional vertical representation provides an appropriate first-order description of the interior water column for the purposes of this study.
- **Idealised representation of openings.** Flow through the WRHs is represented using parameterised loss coefficients. Uncertainty in the effective discharge coefficients (and in the as-built/open area) directly propagates to uncertainty in predicted exchange fluxes.
- **Stationary hourly sea states.** Wave forcing is represented by sea states that are constant within each hourly bin, while the internal response is computed from a stochastic JONSWAP realisation for that hour. Intra-hour variability in spectral parameters is not represented.

- **Current profile at opening elevation.** Currents at WRH elevation are derived from depth-averaged currents using a 1/7th power-law profile. Deviations from this assumed profile, particularly under strongly sheared or stratified conditions, may affect the current-induced pressure contribution.
- **Forcing model uncertainty.** The metocean inputs are derived from numerical models (SWAN and DCSM). Any bias in these hindcasts (e.g., in wave height, water level, or current magnitude/direction) will affect the computed pressure forcing and hence the exchange estimates.
- **Linear wave theory.** The translation of the metocean wave-conditions to the pressures at the water replenishment holes is calculated with linear wave theory. This will result in an conservative estimation of the replenishment, because higher order terms will result in an additional pressure gradient, which increases the flow.
- **Obstruction by marine growth**. Partial obstruction of WRHs by marine growth can reduce effective opening area and alter loss characteristics. This effect is not included in the base simulations because no obstruction was observed at the monitored monopiles during the study period; it is only explored indirectly where WRH area is varied in sensitivity scenarios.
- **Neglected processes**. The model focuses on exchange driven by external hydrodynamics and air compression. Processes such as density-driven stratification, internal resonance (sloshing) modes are beyond the represented dynamics, and small-scale turbulence induced by internal structures are not represented explicitly.

These limitations primarily affect absolute exchange magnitudes, while the model is expected to robustly capture the relative influence of external forcing variability and WRH configuration on internal replenishment behaviour.

4.3 Water quality model (DELWAQ)

4.3.1 Model concept

The water quality modelling is performed with the open-source model DELWAQ (Postma, et al. 2003) developed by Deltares. This advection-diffusion-reaction solver is used for simulating the reactions and transport of water quality substances within the monopile. Due to the slenderness of the monopile the horizontal cross-sections are considered well mixed and a 1DV model setup is used with 61 vertical segments. Here a summary of the model setup is discussed, a more detailed description of the DELWAQ model is given in Appendix B.2.

The output of the hydrodynamic water replenishment model is used as input for the water quality modelling. The calculated volume fluxes are used to describe the water transport inside the 1DV DELWAQ model, see Figure 4-6 for a sketch representing the conceptual model and the internal distribution of the fluxes. Vertical mixing of the enclosed water and the water quality substances will take place due to diffusion and forced convection caused by the inflow of water through the water replenishment holes. All layers above the lowermost replenishment hole experience advection based on the sum of volume flux from holes below this layer. The layers above the uppermost hole function as breathing layers to account for the changing water volume inside the model, where the fluxes distribute evenly over the cells. Below the lower water replenishment hole the volume cannot change, the distribution of the water exchange therefor based on the in- and outflow through a circular hole. This is further detailed in Appendix C. It is noted that although the proposed parameterisation of the internal fluxes is deemed realistic, it has not been validated with experimental data.

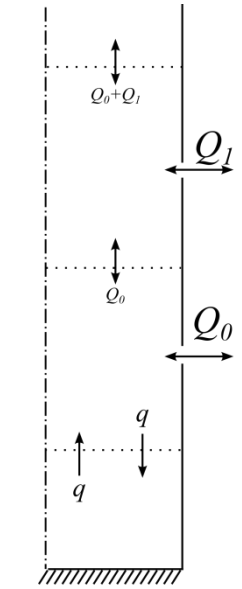

Figure 4-6 Sketch of the vertical exchange inside the monopile in the DELWAQ model.

The water exchange introduces seawater of ambient water quality to the internal of the monopile, where dissolved oxygen and food are the key determinants of habitat suitability. Inside the monopile, the presence of biomass of certain species leads to a local reduction of the concentrations of oxygen and food. DELWAQ can compute the consumption of oxygen and food (in the form of particulate organic material) by the ecological. Normally at sea along the water column, organic material will consist of living algae and detritus (or dead organic material). The circumstances inside the monopile prevent any photosynthesis to happen, therefore the relevant processes are:

- Vertical diffusion represents turbulent mixing in the vertical direction, expressed as a diffusion coefficient (VertDisper m²/s). This parameter ensures that dissolved substances such as oxygen and POC are redistributed between layers.
- Sedimentation of particulate organic carbon. This process transfers organic carbon from the pelagic environment to the benthic compartment, where it becomes subject to slower mineralization.
- Decomposition of detritus: The material that has settled onto the bottom is subject to microbial decay causing particulate organic material to be converted into dissolved carbon and nutrients.
- Biotic consumption processes: negative waste loads for oxygen and POC based on mean community biomass consumption rates.

The listed processes happening in the water and the sediment are taken care of by the process library in DELWAQ. As the lowest replenishment hole in the monopile is several meters above the bottom, there is a distinct possibility that organic material sinks to the bottom and forms a layer that induces a benthic oxygen demand, i.e. the decay of the organic material on the bottom of the monopile causes a nett (diffusive) flux of oxygen, thereby extracting oxygen from the water in the bottom part.

Compared to the earlier approach, an implementation to the process library was made to account for the assimilation of organic material and oxygen by the ecological community inside the monopile. These are now represented through two dedicated processes: fConsumeOXY and fConsumePOC. These processes operate similarly to diffusive and atmospheric loads in DELWAQ. For this application, a variable flux was derived (Section 4.3.2) that depends on the

biomass present on the monopile rather than assuming a constant consumption rate. Instead of introducing a discharge term that could lead to negative concentrations, these processes directly affect the concentrations of dissolved oxygen and particulate organic carbon in the water column. The approach does not explicitly model biomass growth but quantifies the associated “negative waste load” imposed by the organisms. This dynamic representation ensures that the impact of the community on water quality is captured without leading to unrealistic negative concentrations of OXY and POC.

4.3.1.1 Ecophysiology of hard substrate species present

The video analysis provided a list of species found in the different monopiles surveyed as described in Section 2. The focus of the subsequent literature review was narrowed down to the species found in the F1 monopile, as these results were available in time to proceed with the modelling and it covered most of the species found and was thus considered representative. The species found in monopile F1 are show in Table 4-1.

Table 4-1 Species list found inside all monopiles surveyed. Species listed in column ‘Present in monopile F1’ listed in brackets were used as representative species occurring in the North Sea, to complete data for higher order taxonomic groups identified .

	Taxa	WORMS Aphia ID	Present inside monopile F1
1	Actiniaria	103731	X (*Actinia equina*)
2	*Actinothoe sphyrodeta*	107915	X
3	*Alcyonium digitatum*	1354	
4	Amphipoda	106979	X (*Jassa herdmani*)
5	Ascidiidae (colonial)	140003	X
6	*Asterias rubens*	100999	X
7	Balanomorpha	138220	
8	Botrylloides sp.	140480	X
9	*Cancer pagurus*	107285	
10	*Crepidula fornicata*	124988	X
11	*Cylista elegans*	123789	X
12	*Cylista* sp.	164	X
13	*Cylista troglodytes*	124087	X
14	*Diadumene cincta*	101001	X
15	Didemnidae	1045	X
16	*Didemnum vexillum*	131097	X
17	*Diplosoma listerianum*	127165	X
18	*Homarus gammarus*	145897	
19	Hydrozoa/Bryozoa	101003	X
20	*Magallana gigas*	107915	X
21	*Metridium senile*	1354	X
22	*Modiolus* sp.	106979	x
23	*Mytilus edulis*	140003	x
24	*Necora puber*	100999	x
25	*Ophiothrix fragilis*	138220	
26	Ophiura	140480	

	Taxa	WORMS Aphia ID	Present inside monopile F1
27	Polybius	103731	
28	Porifera	107285	X (*Halichondria panicea*)
29	*Psammechinus miliaris*	124988	x
30	*Sagartia undata*	123789	x
31	Serpulidae	164	x
32	*Spirobranchus* sp.	124087	x
33	*Taurulus bubalis*	101001	
34	*Ulva* sp.	1045	
35	*Urticina felina*	131097	x

For the species found in F1, literature was reviewed to determine relevant ecophysiological parameters to be utilized as input for the modelling, namely oxygen consumption rates (in µmol O_2 g AFDW^{-1} h^{-1}) and carbon assimilation (µg C uptake µg C biomass^{-1} day^{-1}). Oxygen consumption rates that were provided in different units were converted. Where rates were presented in units other than Ash Free Dry Weight (AFWD) conversion was undertaken using Riccardi & Bourget 1998 conversation factors. The video analysis did not provide biomass data. Estimates of mean biomass per frame (g AFDW m-^{2}) were derived based on expert judgement of the video footage (see chapter 3).

To be able to utilize the biomass estimates for carbon assimilation assessments, the carbon content of the biomass (g AFDW m-^{2}) needed to be determined. To this end, a conversion factor of 0.5 (Kindeberg, et al. 2024) was applied to estimate the carbon assimilation rates of relevant species (µg C assimilation µg C^{-1} of biomass m-^{2} day $^{-1}$) as input for the model. There is very limited literature available on converting biomass to organic carbon content, in particular for relevant individual species. Ranges commonly used in literature are between 40-50% (Mackinson and Daskalov 2007, Rueda, Smaal and Scholten 2005, Wijsman, Herman and Gomoiu 1999).

Where species referred to higher taxonomic groups, a representative species for the group was identified, as indicated in Table 4-1 in brackets.

There is limited literature available for the Oxygen Consumption Rate (OCR) and of individual species. The literature search found the OCR for 10 out of the listed 25 taxa found inside the monopile F1. For four out of these 10 species POC values could be sourced from literature. The data points used are shown in Table 4-2.

Table 4-2 - Oxygen Consumption Rates for taxonomic groups found on the inside of F1 monopile with proxy species in brackets.

Taxa	WORMS Aphia ID	OCR (µmol O_2 h^{-1} g $AFDW^{-1}$)	Source	POC (µg C uptake µg C biomass−1 day −1)	Source
Actiniaria (*Actinia equina*)	103731	22.6287	(Ortega, de Pariza en Navarro 1988)		
Amphipoda (*Jassa herdmani*)	106979	12.2778	(Voet, van Colen and Vanaverbeke 2022)	0.00060	(Mavraki, Degraer, et al. 2020a)
Crepidula fornicata	124988	34.5	(Noisette, et al. 2016)	0.00186	(Mavraki, Degraer, et al. 2020a)
Didemnum vexillum	131097	3.0859375	(Harrington 2010)		
Magallana gigas	107915	0.009882813	(Pack, Rius and Mieszkowska 2021)		
Metridium senile	1354	18.8964	(Voet, van Colen and Vanaverbeke 2022)	0.00010	(Mavraki, Degraer, et al. 2020a)
Mytilus edulis	140003	1.69556	(Voet, van Colen and Vanaverbeke 2022)	0.02950	(Mavraki, Degraer, et al. 2020a)
Porifera (*Halichondria panicea*)	107285	1.995	(Kumala, Thomsen and Canfield 2023)		
Psammechinus miliaris	124988	21.6	(Souster, Morley en Peck 2018)		
Urticina felina	131097	4.0625	(Migné and Davoult 1997)		

Subsequently, the OCR and POC values were used to arrive at a mean consumption and assimilation rate per mean biomass of carbon estimated per frame of the video analysis. Averages were derived from the available rates and assumed to represent the frame's species composition OCR and POC, in the absence of information of rates for every species present per frame. An example of the conversion is given in Table 4-3 and Table 4-4.

Table 4-3 - Example calculation for mean OCR and POCs per video frame

Frame	Taxa	Depth (m)	g AFDW m^{-2} (estimated)	OCR (µmol O_2 h^{-1} g $AFDW^{-1}$)	µg C uptake (µg C $biomass^{-1}$)
363	Amphipoda (*Jassa herdmani*)	0.14	21.66534499	12.2778	0.0006
363	Ascidiidae (*Actinia equina*)			n/a	n/a
363	*Metridium senile*			18.8964	0.0001
Means				15.5871	0.00035

Table 4-4 - Example conversion of OCR and POC per biomass for modelling use

Frame		Oxygen Consumption Rate (OCR)			Particulate Organic Carbon (POC)		
#	Depth (m)	g AFDW $m^{2\ -1}$ (estimated)	Mean OCR (µmol O_2 g $AFDW^{-1}$ h^{-1})	Mean OCR (mol O_2 h^{-1} m^{2-1})	µg C g $AFDW^{-1}$ $m^{2\ -1}$ estimated (factor 0.4)	Mean C uptake (µg C µg C $biomass^{-1}$ day^{-1})	Mean carbon uptake (µg C µg C $biomass^{-1}$ m^{2-1} day^{-1})
363	0.14	21.66534499	15.5871	0.0003377	8.666137997	0.00035	0.003033148

These data points were subsequently used for the water quality modelling efforts, described in the next section (Water quality inputs and conditions 4.3.2).

4.3.2 Water quality inputs and conditions

To represent water quality inside the monopile, the model couples the internal flow field, computed from the water replenishment module, with ambient concentrations of the primary water quality variables and data-driven biotic consumption. The sustainability of the interior community depends primarily on two parameters:

- Dissolved oxygen concentration
- Particulate organic carbon (POC) concentration

Unlike in the earlier approach, oxygen demand and C assimilation are derived directly from the depth-resolved video analysis (Section 3.2) and the literature-based ecophysiology of hard-substrate species (Section 4.2.2.1). Depth-derived biomass (ash-free dry weight per m2) was converted to carbon biomass using a factor of 0.4, and species-specific OCR were applied.

This modelling approach assumes that the resulting oxygen and POC concentrations present in the water column, are dependent on the biomass present inside the monopile, influencing the oxygen demand and C removal.

To use the previously derived mean OCR and mean carbon assimilation rates in the water quality model, for each depth range, these rates were combined with biomass to calculate areal fluxes translating them to g O_2 m^{-2} day^{-1} and g C m^{-2} day^{-1}. A Python workflow interpolated these fluxes to the 61 evenly spaced layers matching the DELWAQ model schematization. The resulting profiles (Figure 4-7) were then implemented as negative extractions per segment, so as oxygen and carbon removal from water, representing the consumption by the fouling community at that depth.

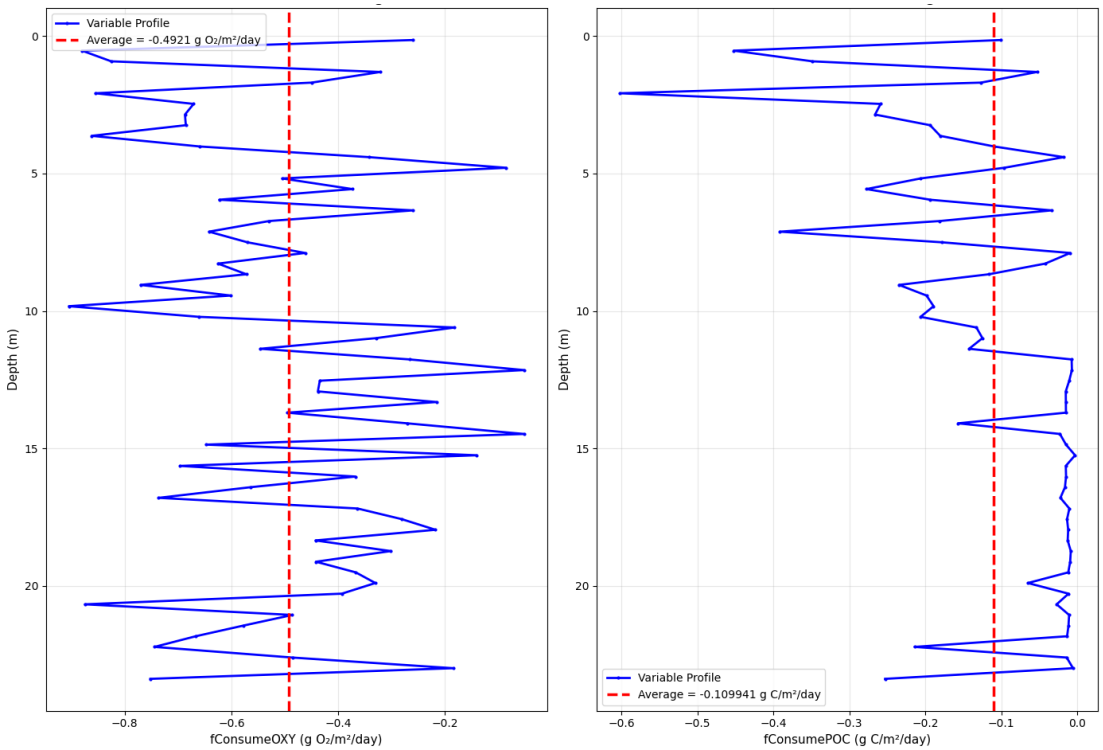

Figure 4-7 Negative waste loads for oxygen (fConsumeOXY) and POC (fConsumePOC) based on biomass-specific consumption rates derived from the video analysis and ecophysiology (Section 4.2.2.1). The red dashed line shows a constant rate over the vertical, derived over an average rate

In addition to the biotic consumption terms, DELWAQ schematization includes a set of physical and biogeochemical processes and parameters that govern the transport and transformation of substances in the water column and sediment:

- The vertical diffusion coefficient is set to 1.0×10^{-5} m^2 s^{-1}, representing weak background mixing. This value is consistent with diffusivities commonly applied in oceanographic modelling under low-turbulence conditions (Itoh, et al. 2021, N. Kusters, et al. 2025). CFD simulations of the water replenishment hole (WRH) exchange further show that velocities and turbulence levels inside the monopile away from the openings are low (order mm s^{-1} to cm s^{-1}), supporting the assumption that background vertical mixing is weak. The vertical diffusion coefficient primarily affects the vertical mixing in the layers below the Lower Water Replenishment Holes (LWRH) and above the Upper Water Replenishment Holes (UWRH). In contrast, vertical exchange between the LWRH and UWRH is dominated by advective flow through the replenishment openings, and the role of background diffusion in this region is secondary. The adopted diffusion coefficient therefore provides a physically consistent representation of vertical mixing processes across the monopile interior.
- POC Sedimentation settles from the water column to the sediment at a set velocity 1 m/day.
- The material that has settled onto the bottom is subject to microbial decay at a rate of 0.3 day^{-1}.
- Biotic consumption processes vary based as shown in Figure 4-7.

These parameters are typically valid for an ambient temperature of 20° C.

The boundary conditions and initial concentrations of OXY and POC were kept the same as in previous schematization. High-frequency measurements of the concentration of chlorophyll outside the monopile are available over a part of the simulation period of interest. These

measurements have been used to estimate the ambient concentration of particulate organic material.

The high-frequency measurements provided by Vattenfall (corrected with a calibration factor of 1.85) show a mean concentration of chlorophyll of 4.2 µg/L in October and 2.0 µg/L in November and the rest of the winter period. These are typical conditions in offshore regions in the North Sea. As the model requires the concentration of POC, representing both living algae and detritus, this concentration was converted to a total concentration of POC:

- 1 gram chlorophyll per litre means a concentration of living algae of roughly 33 gram per litre. (This amount depends on all manner of conditions, such as the type of algae, but is a reasonable “ballpark” figure).
- 1 gram living algae per litre means that the total concentration of POC is roughly 3 grams per litre. (Again, a reasonable ratio).
- Therefore, the observed mean concentration of 4.2 µg/L corresponds to 420 µg POC/L or 0.42 mg/L.

For oxygen the ambient concentration was roughly 8.0 mg/L and that was used throughout the simulation period.

4.3.3 Method limitations

The water quality modelling relies on several simplifying assumptions regarding biomass, ecophysiological parameters, and ambient conditions. These assumptions are necessary because only limited species-specific data are available, but they also constrain how precisely DELWAQ can represent internal ecosystem processes.

Biomass inputs were derived from video based AFDW estimates and converted to carbon biomass using a single factor (0.5) (Kindeberg, et al. 2024) reported for benthic fauna. Because the interior community includes diverse taxa such as ascidians, sponges, amphipods, and anemones, this conversion cannot reflect true species-specific carbon content. As a result, both oxygen demand and carbon assimilation may be systematically over or underestimated, depending on the local community composition. This uncertainty is particularly relevant in depth layers where not shellfish groups dominate, as their tissue composition can differ from the assumed ratio.

The same constraint applies to the metabolic rates used to represent oxygen consumption (OCR) and particulate organic carbon assimilation (POC). Only a subset of the species found inside the monopiles has published OCR or POC values, and these values often originate from experiments under different temperatures, food conditions, or life stages. In many cases, organisms could only be identified to higher taxonomic groups, requiring the use of representative species as proxies. Consequently, consumption rates used in the model reflect averaged, literature-based values rather than taxon, or context specific behaviour.

Unit conversions also introduce uncertainty. OCR and POC values occurring in different units were normalised to AFDW and then averaged per video frame, after which these averages were applied uniformly across the corresponding vertical segment. This simplification assumes homogeneous species composition and metabolic activity within each depth band, while in reality, biomass is patchy and often dominated by a few functional groups. The model therefore provides a first-order description of biological demand rather than a detailed ecological budget.

The constant boundary conditions further affect predicted concentrations. Ambient POC was estimated from chlorophyll using fixed ratios, and ambient oxygen was kept constant throughout the simulation period. This approach does not capture short term or seasonal variability in offshore North Sea conditions, which can substantially alter both food and oxygen supply to the monopile interior. Because these ambient values are used directly as

replenishment inputs, the model tends to produce stable background concentrations, unable to replicate potential seasonal variability that would occur under fluctuating environmental conditions.

Together, these limitations mean that the DELWAQ results should be interpreted primarily in a relative sense. The model captures how water quality conditions respond to differences in WRH area, layout, elevation, and forcing, and it provides credible insight into which configurations strengthen or weaken internal replenishment. However, absolute concentration levels, species-specific suitability, and fine scale vertical patterns remain uncertain. The modelling therefore supports design sensitivity analysis and identification of limiting zones within the monopile, but does not provide species resolved ecological thresholds.

4.4 Modelling scenarios

The modelling scenarios are designed to (i) quantify internal exchange and resulting abiotic conditions for the monitoring period and (ii) assess how sensitive these internal conditions are to WRH design choices under a consistent external forcing. The scenario set consist of a base case for monopile F1 and a WRH design sensitivity analysis in which key WRH parameters are varied relative to the F1 configuration.

4.4.1 Base case scenario

The base-case simulation uses the as-built geometry and WRH configuration of monopile F1 (Section 1.5.2) and forms the main reference for interpretation of internal exchange and water-quality conditions during the monitoring period. The base case is simulated for calendar year 2024 and is forced with the corresponding metocean conditions (Section 4.2.3).

4.4.2 WRH design sensitivity scenarios

To identify which WRH design parameters most strongly influence internal exchange and the resulting water-quality indicators, a sensitivity analysis was performed for the main adjustable WRH parameters:

- WRH size / total open area
- Horizontal layout / orientation (angular position)
- Vertical position
- Wave & current forcing direction relative to the WRHs

In the sensitivity analysis, the F1 monopile geometry is used as the reference (Section 1.5.2), from which WRH parameters are altered. All sensitivity scenarios are simulated for November 2024 using the corresponding metocean forcing, to enable consistent comparison across design variants. The evaluated cases are summarised in Table 4-5 and described in the subsequent sections..

Table 4-5 Overview of modelling scenarios

Group	Scenarios	Period	Forcing	Notes
Base case	F1-BASE	2024	Waves + WL + current	Reference for monitoring-period interpretation
WRH size sensitivity	A75, A50, A25	Nov 2024	Waves + WL + current	Total WRH open area = 75%, 50%, 25% of F1 (A25 used as base for groups below)
Layout sensitivity *(25% area)*	L-F1, L-E5, L-CROSS, L-6HOLE	Nov 2024	Waves + WL + current	Layout = F1 / E5 angular positions / cross / 6 holes (3 upper + 3 lower); total area fixed (25% of F1); for L-6HOLE area equally divided

Group	Scenarios	Period	Forcing	Notes
Vertical sensitivity *(25% & 100% area)*	V-U-2, V-U-5, V-L-2, V-L+2	Nov 2024	Waves + WL + current	Upper WRH shifted −2 m or −5 m (lower fixed), or lower WRH shifted −2 m or +2 m (upper fixed)
Orientation vs waves *(cross, 25% area)*	OW-00, OW-22.5, OW-45, OW-67.5, OW-90	Nov 2024	WL + Waves only (current = 0)	Wave direction prescribed constant for full month: 0–90°N in 22.5° steps; H_{m0}, T_p from Nov 2024
Orientation vs current *(cross, 25% area)*	OC-0, OC-22.5, OC-45, OC-67.5, OC-90	Nov 2024	WL + Current only (waves = 0)	Current direction prescribed constant for full month: 0–90°N in 22.5° steps; Nov 2024 current magnitudes applied

4.4.2.1 Size of the WRHs (A-cases)

Three variations in WRH size were modelled by reducing the total open area to 75% (A75), 50% (A50), and 25% (A25) of the original F1 WRH open area. Only reductions were considered, since the HKZ WRHs were designed to provide substantial replenishment; reducing the opening area provides clearer insight into the performance limits under reduced exchange capacity.

4.4.2.2 Layout of the WRHs (L-cases)

To evaluate the effect of horizontal layout, four cases were considered. Here, *layout* refers to the angular position of the openings in plan view. For this analysis, the reference configuration is L-F1, which uses the F1 layout with WRH size reduced to 25% (i.e., the A25 case). This reduced-area reference is used because layout effects are more distinguishable when the effective opening area is smaller.

Relative to L-F1, three layout variants were tested:

- L-E5: WRH angular positions set equal to those of monopile E5 (Figure 4-8).
- L-CROSS: four WRHs arranged in an idealised cross pattern.
- L-6HOLE: six WRHs (three at the upper elevation and three at the lower elevation).

For all layout variants, the total WRH open area is kept constant at 25% of the original F1 total area. For the six-hole layout, this total open area is equally distributed across the six openings. A top-view overview of the evaluated layouts is provided in Figure 4-8.

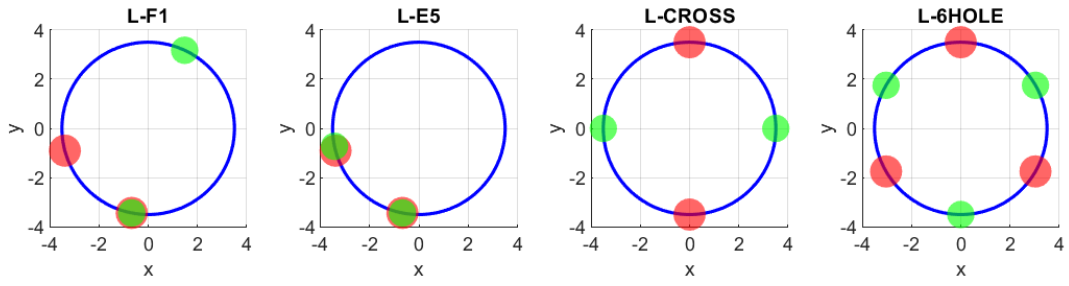

Figure 4-8 Top view of WRH layouts. Red and green dots indicate the upper and lower WRHs, respectively.

4.4.2.3 Vertical placement of the WRHs (V-cases)

To assess sensitivity to vertical WRH placement, four elevation-variation cases were set up:

- Upper WRH variations: upper WRHs shifted by −2 m (V-U-2) and −5 m (V-U-5) relative to the reference upper elevation, with the lower WRHs fixed.

- Lower WRH variations: lower WRHs shifted by −2 m (V-L-2) and +2 m (V-L+2) relative to the reference lower elevation, with the upper WRHs fixed.

These four cases were performed for the 25% area configuration (A25) and repeated for the 100% area configuration (i.e., original F1 area), resulting in two comparable sets that isolate the effect of vertical placement under both reduced and full opening areas.

4.4.2.4 Forcing direction relative to the WRHs orientations (OW/OC-cases)

To evaluate the influence of forcing direction relative to the WRH configuration, the cross-layout case (Figure 4-8) was used, with WRH area fixed at 25% of the original F1 area. Wave-direction and current-direction effects were evaluated separately using the November 2024 forcing.

Wave direction (OW-cases). Current was set to 0 m/s. The hourly H_{m0} and T_p from November 2024 were applied, while the wave direction was prescribed as constant over the full month and varied from 0°N to 90°N in steps of 22.5° (five cases; Figure 4-9).

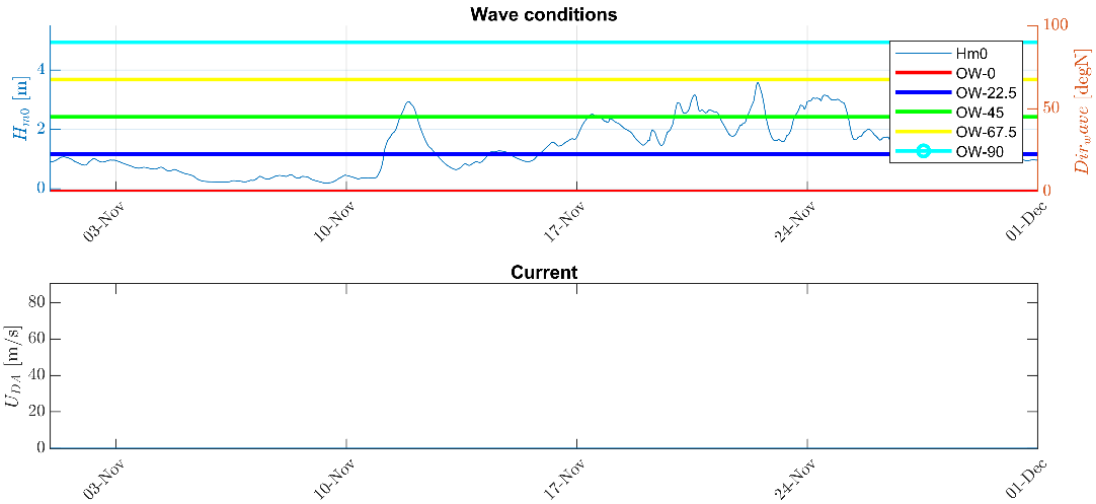

Figure 4-9 Hydrodynamic forcing for the OW-cases: waves from prescribed constant directions (0–90°N).

Current direction (OC-cases). Wave forcing was set to zero, while the November 2024 current magnitudes were applied. Current direction was prescribed as constant over the full month and varied from 0°N to 90°N in steps of 22.5° (five cases; Figure 4-10).

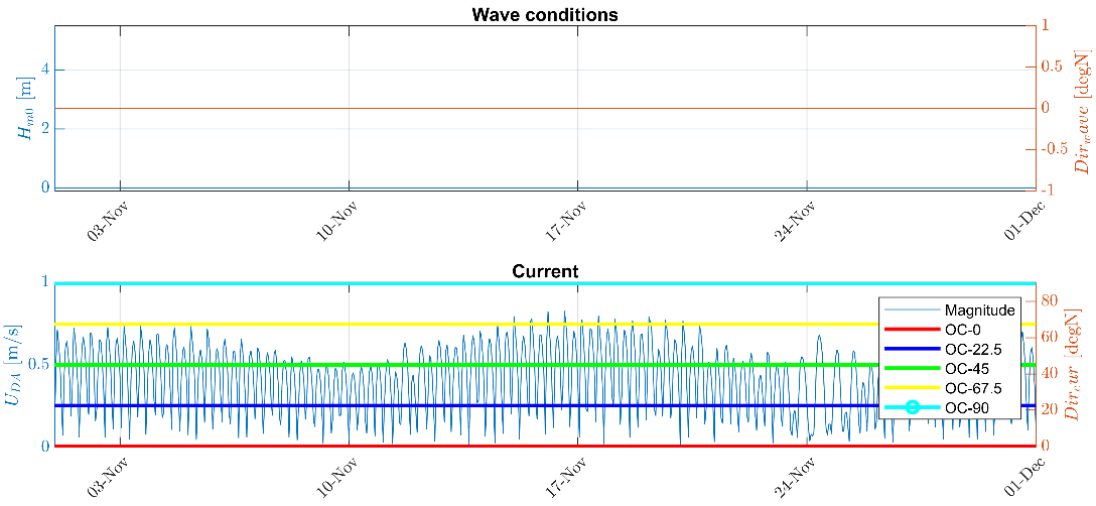

Figure 4-10 Hydrodynamic forcing for the OC-cases: current from prescribed constant directions (0–90°N).

4.5 Modelling results

This section presents the results of the numerical simulations described in Section 4.4. First, the base-case scenario is used to illustrate the simulated internal exchange and resulting concentration patterns within monopile F1 during the monitoring period, and to compare these with the available observations. Subsequently, the WRH design sensitivity scenarios are evaluated to assess the relative influence of WRH size, layout, vertical placement, and orientation with respect to hydrodynamic forcing. The interpretation focuses on scenario-to-scenario differences and spatial patterns, rather than absolute concentration levels.

4.5.1 Base case WRH scenario

The result of the model consists of hourly modelled oxygen and POC1 concentrations per cell in the vertical. The results for the 2024 base case scenario for F1 are included in Figure 4-11. The figure contains the concentrations in colour, for the various cells in the vertical (y-axis), over time (x-axis). The bottom panel contains the calculated average concentrations in the full water column for the two substances.

Figure 4-11 indicates that the internal concentrations remain broadly stable at the water-column average over 2024, while strong vertical gradients persist within the monopile. Concentrations are highest near the elevations of the WRHs, where exchange with ambient seawater is strongest. Below the LWRH and above the UWRH, concentrations occasionally decrease, consistent with reduced replenishment and weaker mixing away from the openings.

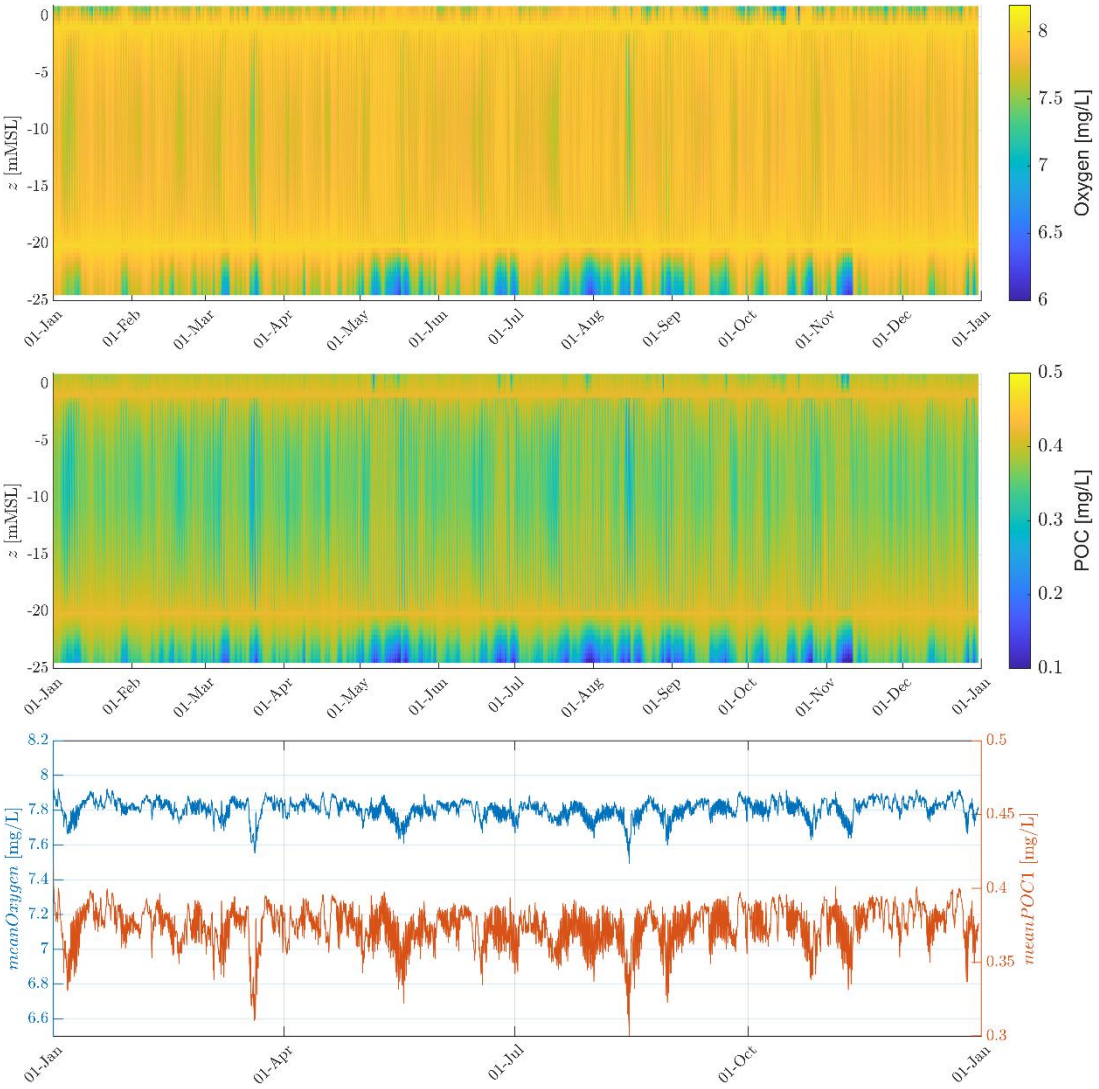

Figure 4-11 Hourly modelled dissolved oxygen (top), POC1 (middle), and volume-averaged concentrations over the full internal water column (bottom) for the F1-BASE (2024) scenario.

The model output was compared with monitoring data. Figure 4-12 presents measured raw oxygen and chlorophyll concentrations as a function of depth and time (left-hand panels). The right-hand panels show vertical concentration profiles, obtained by averaging the spot-monitoring measurements at each fixed elevation (typically approximately 15 minutes per elevation). Because the probe was stationary during each interval, these averaged values are taken as the most representative estimate of the local concentration at that elevation.

For comparison, the corresponding model results are included in the profiles. Modelled POC1 concentrations were converted to chlorophyll using the linear relationship described in Section 4.3.2. The results show that the model reproduces the order of magnitude and overall vertical trend of chlorophyll reasonably well, although differences are observed in the vertical distribution. Both measurements and model indicate lower concentrations near the top of the monopile and higher concentrations closer to the LWRHs. However, the pronounced decrease below the LWRH is only predicted by the model and is not evident in the measurements.

The lower panels of Figure 4-12 show that the modelled oxygen concentrations are substantially higher than the measured values. Nevertheless, a broadly comparable vertical pattern is visible, with lower concentrations in the central section and higher concentrations

near the UWRH. Similar as for chlorophyll, the modelled decrease below the LWRH is not reflected in the monitoring data.

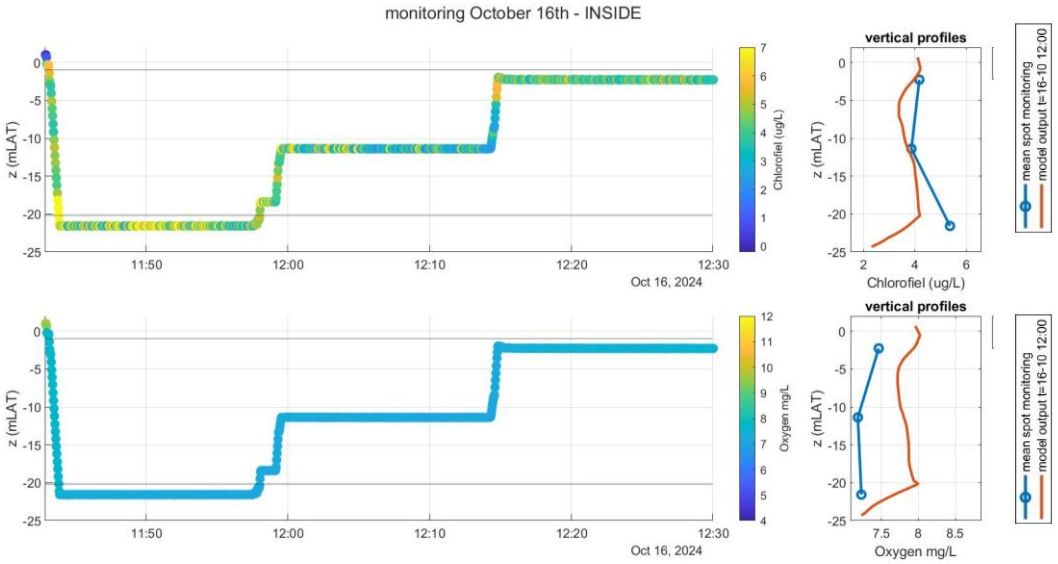

Figure 4-12 Measured dissolved oxygen and chlorophyll concentrations over time (left panels). The right panels present the average concentrations obtained from spot monitoring (blue) together with the corresponding modelled concentrations (where chlorophyll is modelled via a POC1 conversion) (orange) during the monitoring campaign on 16 October 2024.

Figure 4-13 presents a similar comparison for the monitoring campaign conducted on the 4th of November 2024. In this case, the measured and modelled concentrations differ substantially. The measured oxygen concentrations are significantly higher than the modelled values and also exceed the assumed ambient oxygen concentration applied in the model (8.0 mg/L). A similar discrepancy is observed for chlorophyll concentrations, where measured concentrations in the lower part of the monopile exceed the ambient concentrations prescribed in the model.

A possible explanation for the higher oxygen concentrations measured in November when compared to Octobre is the influence of the water temperature. The measured water temperatures are included in Figure 4-13. This effect is not included in the model, where the ambient concentration is assumed constant.

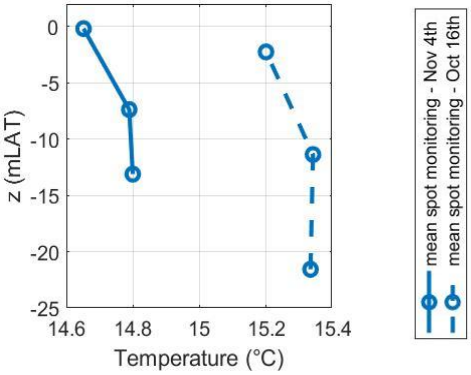

Figure 4-13 Measured temperatures during the monitoring campaign on October 16th and November 4th, 2024.

Given these differences, the lack of agreement between model results and measurements is not unexpected (as the modelled concentrations inside the monopile cannot exceed the concentrations of the ambient sea water). Despite these discrepancies, the model results for both oxygen and chlorophyll indicate concentrations that are close to ambient conditions throughout most of the monopile, with the exception of the region below the LWRH. This does agree with the overall high observed concentrations within the monopile. The differences highlight the need for caution when interpreting the model results. The imposed boundary conditions, particularly the assumption of temporally constant ambient concentrations, represent a considerable simplification of the real system and are likely to contribute to deviations from observed conditions. Moreover, the drop in concentrations below the LWRH cannot be verified with the measured data, because spot monitoring was only performed at the LWRH and not below that elevation. However, low oxygen concentrations are expected in this area since signs of anoxic conditions were observed in the monitoring campaign, see also Section 3.2.2. It is therefore expected that the drop in concentrations, due to reduced replenishment is a correct representation of the system. Within the limitation of not including temporally changing ambient conditions, the model is considered suitable for providing a first-order indication of concentration levels within the monopile.

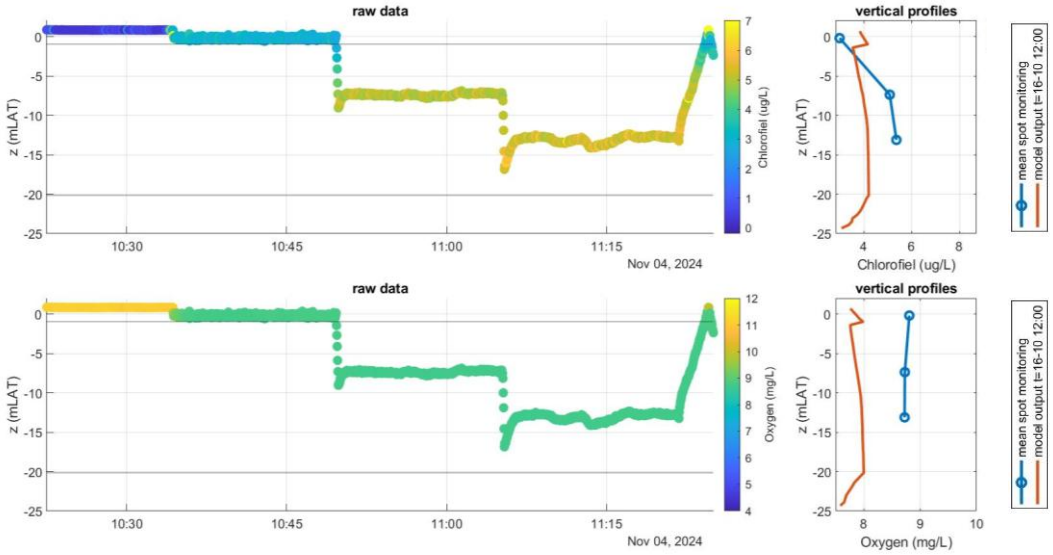

Figure 4-14 On the right measured (blue) and modelled (orange) dissolved oxygen and chlorophyll concentrations (chlorophyll measured; chlorophyll modelled via POC1 conversion) during the monitoring campaign on 4 November 2024.

4.5.2 WRH design sensitivity scenarios

This section presents the results of the WRH design sensitivity analysis. For clarity, the scenarios are compared using two compact oxygen metrics: (i) the volume-averaged mean concentration and (ii) the minimum concentration in the monopile, shown as time series for November 2024. This summary approach avoids the complexity of full spatiotemporal concentration fields (Figure 4-11) while retaining sensitivity to both overall conditions and locally depleted regions. The metrics are computed as volume-weighted values to account for the variable cell volumes associated with the tapered monopile geometry. For most design variations, the scenario curves separate mainly during the initial adjustment period and remain approximately parallel thereafter, indicating that WRH design primarily sets the baseline exchange regime while temporal variability is driven by the external forcing.

4.5.2.1 Size of the WRHs (A-cases)

Figure 4-15 compares the simulated oxygen concentrations for three WRH open-area cases (A75, A50 and A25). Both the volume-averaged mean (left) and the minimum concentration (right) show a clear and consistent dependence on WRH open area: reducing the total opening area lowers internal oxygen levels, reflecting reduced replenishment with ambient seawater. The separation between scenarios is visible throughout the month and is most pronounced for the minimum concentrations, indicating that reduced WRH area primarily increases the extent and persistence of locally depleted conditions. Superimposed on these scenario differences, all cases exhibit coherent temporal variability that follows the November hydrodynamic forcing (Figure 4-3), with short-term fluctuations and event-scale changes affecting the concentrations in all scenarios.

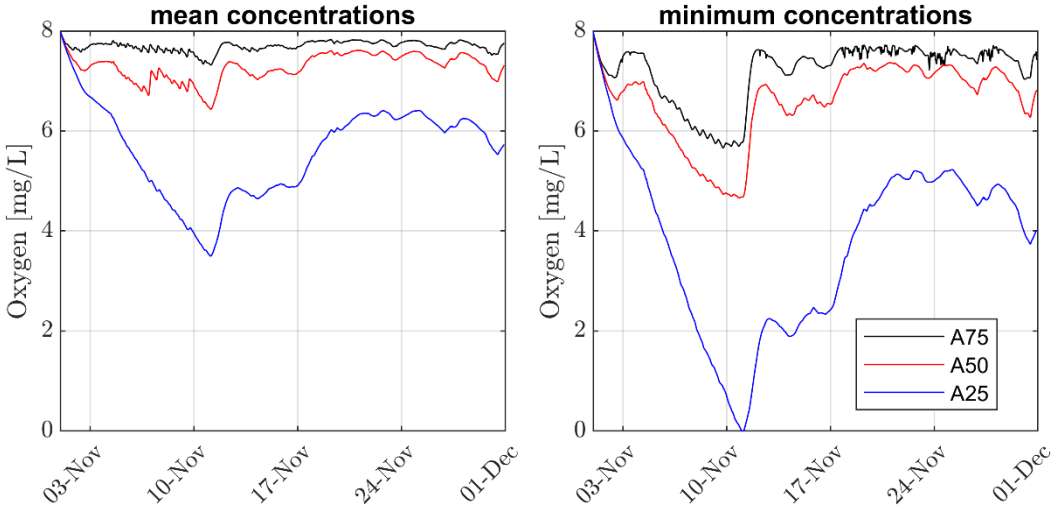

Figure 4-15 Volume-averaged mean (left panel) and minimum (right panel) oxygen concentrations inside the monopile for three cases with varying WRH open area (A75, A50, A25).

4.5.2.2 Layout of the WRHs (L-cases)

Figure 4-15 compares oxygen concentrations for the four WRH layout cases (L-F1, L-E5, L-CROSS and L-6HOLE), all with the total WRH open area fixed at 25%. The figure shows that F1 and subsequently E5 configuration perform least well in terms of mean and minimum oxygen concentrations. The cross layout consistently produces higher mean oxygen concentrations throughout most of the month, indicating more effective replenishment under the applied forcing. The six-hole layout improves mean oxygen levels relative to the F1/E5 layouts, but remains below the cross layout, suggesting that distributing the same total area over more openings does not automatically enhance exchange. This is attributed to the combined effect of a less favourable effective orientation and increased hydraulic losses (higher loss coefficient) in the six-hole configuration.

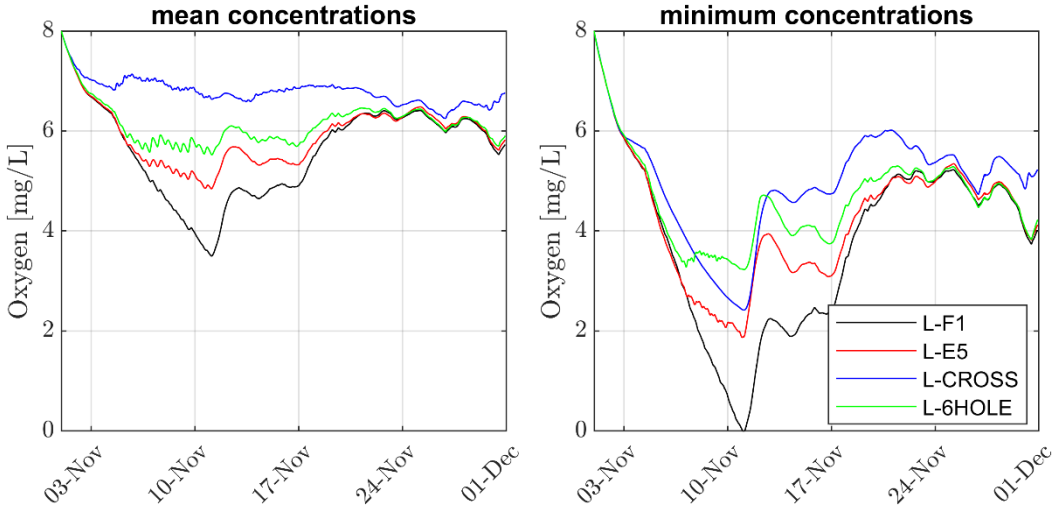

Figure 4-16 Volume-averaged mean (left) and minimum (right) oxygen concentrations inside the monopile for WRH layout cases in plan view (L-F1, L-E5, L-CROSS, L-6HOLE; total WRH open area fixed at 25% of F1).

4.5.2.3 Vertical placement of the WRHs (V-cases)

Figure 4-16 shows the volume-averaged mean and minimum oxygen concentrations inside the monopile for the four scenarios with varying vertical positions of the WRHs, using the 25% open area reference case. Overall, the figure shows that moving the UWRHs towards the vertical centre of the water column (cases V-U-2 and V-U-5) results in higher mean oxygen concentrations compared to V-0, indicating more effective replenishment of the interior water column under reduced opening area. The effect of moving the LWRH more to the centre (case V-L+2), is most clearly visible in the minimum concentrations, while the mean concentrations appear hardly affected.

To better interpret where these changes occur, Figure 4-17 decomposes the monopile into three vertical sections: (i) above the UWRH, (ii) between the UWRH and LWRH, and (iii) below the LWRH. Lowering the UWRH (V-U-2 and V-U-5) reduces oxygen concentrations in the section above the UWRH, because a larger part of this upper section becomes weakly replenished. Similarly, raising the LWRH (V-L+2) reduces oxygen concentrations below the LWRH relative to V-0. However, the local reductions are balanced by the increased mean concentrations between the WRH's. Lowering of the LWRH (V-L-2), results in higher concentrations in the layer below the WRH's, but this effect is outweighed by the decrease in concentration in the larger section between the WRH's.

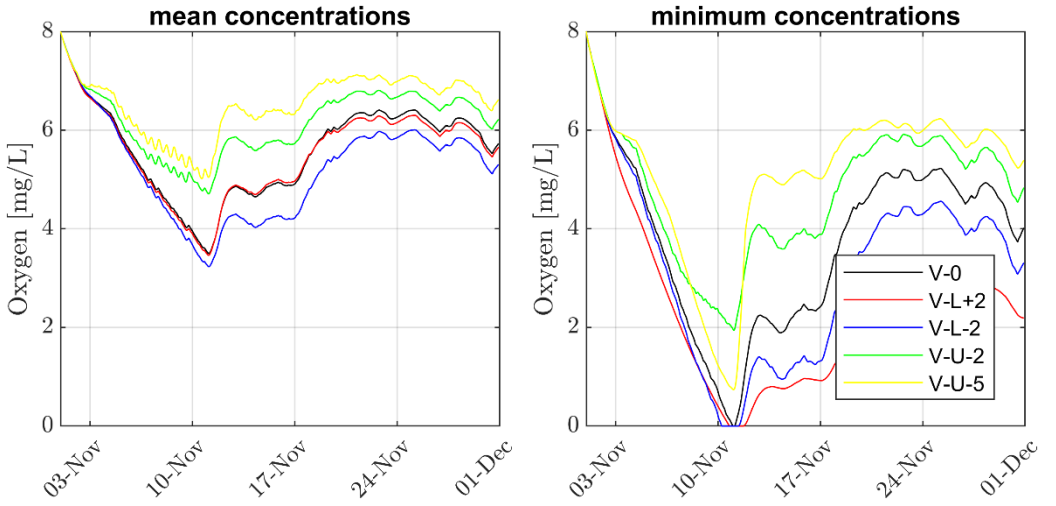

Figure 4-17 Time series of volume-averaged mean (left) and minimum (right) oxygen concentrations inside the monopile for vertical WRH-placement cases (25% WRH open-area reference).

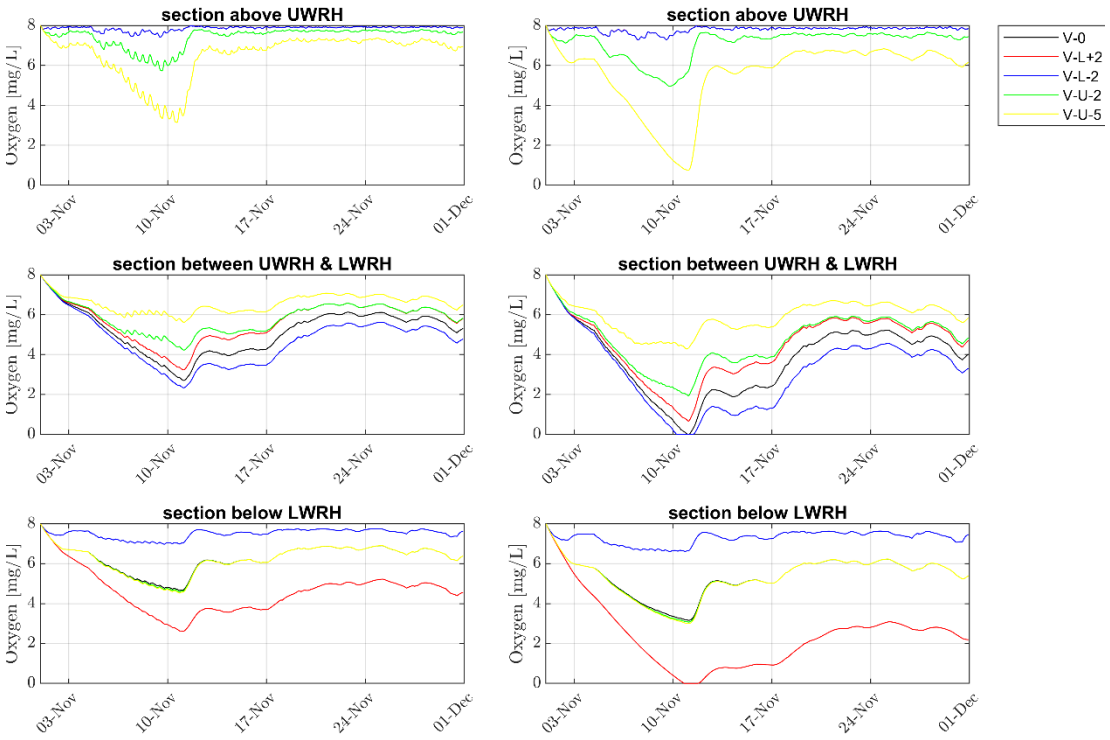

Figure 4-18 Volume-averaged mean (left column) and minimum (right column) oxygen concentrations in three monopile sections (rows): above the UWRH, between the UWRH and LWRH, and below the LWRH, for vertical WRH-placement cases (25% WRH open-area reference).

Figure 4-18 and Figure 4-19 show the corresponding results for the 100% (F1) WRH open-area cases. Under these conditions, the overall mean oxygen concentration is close to ambient and is only weakly affected by WRH elevation. The largest sensitivity appears in the minimum concentrations in the sections above the UWRH and below the LWRH, where replenishment remains weakest compared to the region between the openings.

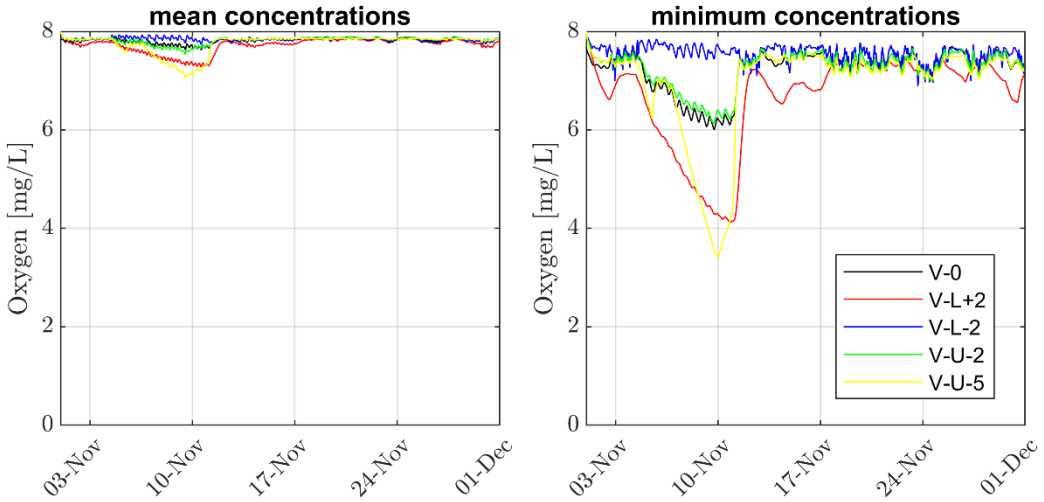

Figure 4-19 Time series of volume-averaged mean (left) and minimum (right) oxygen concentrations inside the monopile for vertical WRH-placement cases (100% WRH open area).

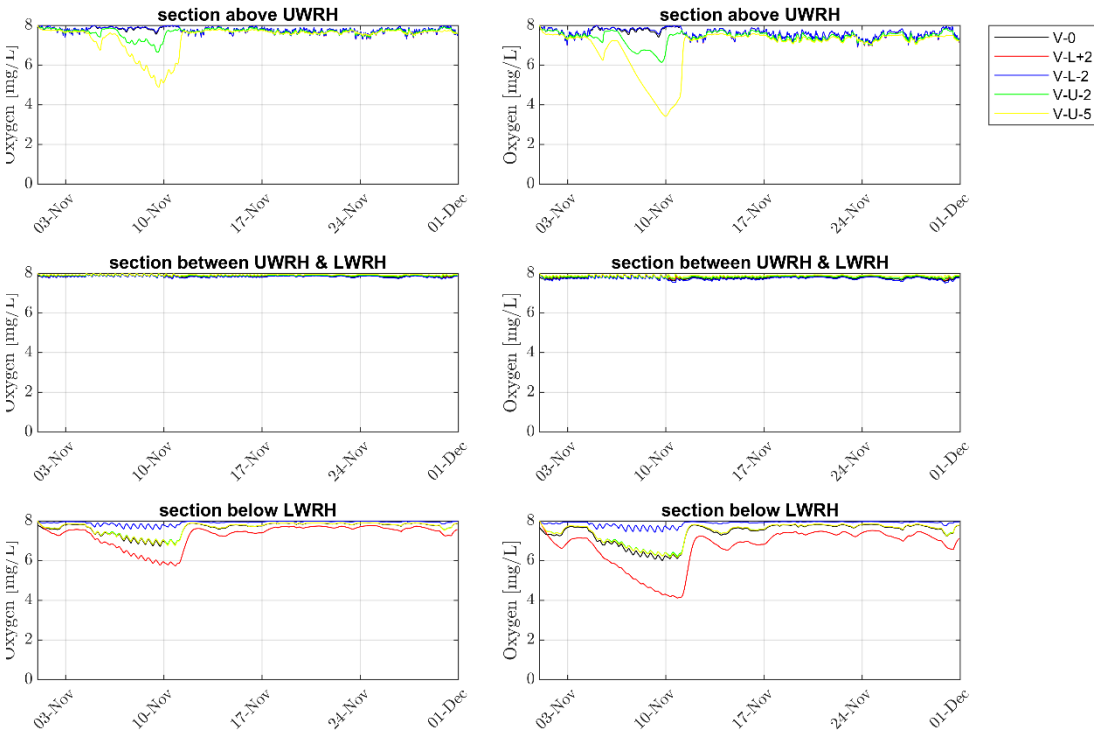

Figure 4-20 Volume-averaged mean (left column) and minimum (right column) oxygen concentrations in three monopile sections (rows): above the UWRH, between the UWRH and LWRH, and below the LWRH, for vertical WRH-placement cases (100% WRH open area).

4.5.2.4 Forcing direction relative to WRHs orientation (OW/OC-cases)

Figure 4-20 shows the volume-averaged mean and minimum oxygen concentrations for the wave-only cases, for five prescribed wave incidence angles relative to the WRH configuration. The results indicate that the modelled oxygen concentrations are largely insensitive to wave direction, with both mean and minimum concentrations showing almost complete overlap between the different angles throughout the month.

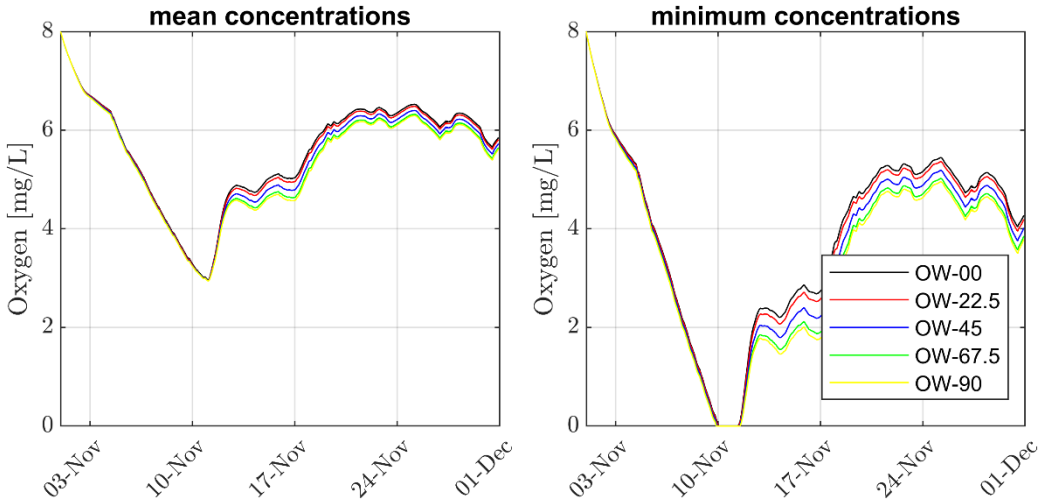

Figure 4-21 Time series of volume-averaged mean (left) and minimum (right) oxygen concentrations inside the monopile for different wave incidence angles relative to the WRH configuration (wave-only forcing).

Figure 4-21 presents the corresponding results for the current-only cases. In contrast to the wave-only simulations, a modest directional dependence is observed in the mean concentrations. Differences in volume-averaged mean concentrations remain small, whereas

the minimum concentrations exhibit clearer separation between incidence angles, indicating that current direction primarily affects the extent of locally depleted conditions. The most favourable oxygen levels occur when the current direction is most aligned with the UWRH configuration, promoting more effective exchange through the openings. When aligned with the LWRH configuration, there is little to no mixing with the lower layers, resulting in a steep drop in local concentrations.

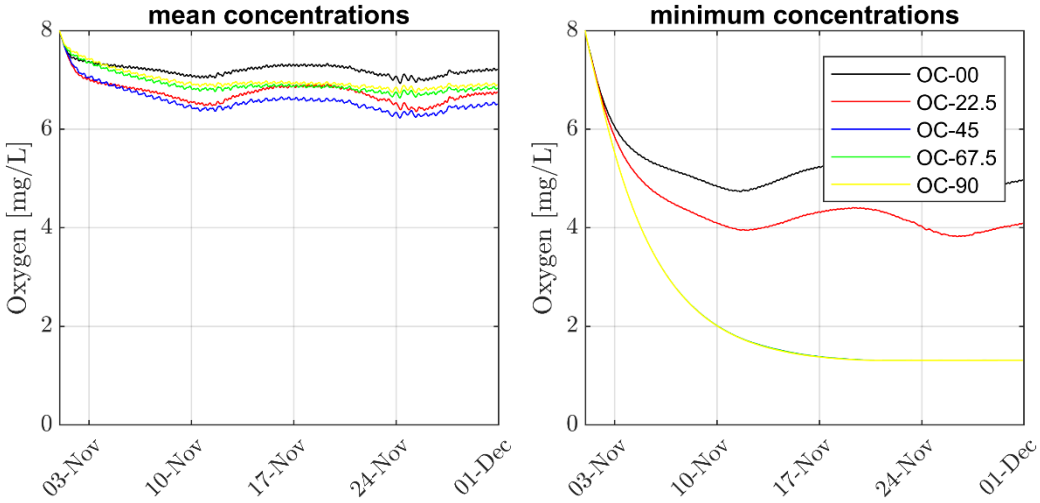

Figure 4-22 Time series of volume-averaged mean (left) and minimum (right) oxygen concentrations inside the monopile for different current incidence angles relative to the WRH configuration (current-only forcing).

4.6 Recommendations

The sensitivity study was performed to derive recommendations that can support the design of a water replenishment system. In practice, the design is the result of multiple considerations (e.g. structural integrity, constructability, corrosion protection, and operational constraints). This section focuses specifically on recommendations from a water quality perspective, using the coupled hydrodynamic replenishment model and the 1DV DELWAQ water quality model.

From a water quality perspective, the objective of a WRH system is to maintain internal conditions as close as possible to ambient conditions, i.e. to maximise renewal and avoid persistent local deficits in dissolved oxygen and food availability. The modelling indicates that internal concentrations are governed by the interaction between (i) the exchange capacity of the WRH system (set by design and forcing) and (ii) internal sinks (consumption and settling/decay processes). Based on these findings, the following integrated recommendations are formulated.

- **Prioritise total open area.** The total open area of the WRHs is the most influential design parameter for water quality inside the monopile. Increasing total open area increases replenishment rates and drives concentrations towards ambient values in DELWAQ. *Recommendation:* maximise total open area within design constraints and evaluate performance under representative low-energy conditions, as these govern the most limiting internal states.
- **Apply hydraulically efficient layouts (avoid unnecessary losses).** Besides total open area, exchange is controlled by hydraulic efficiency. The sensitivity analysis shows that symmetric cross-shaped layouts provide the highest replenishment rates and most favourable concentrations, whereas splitting the same area into more holes can reduce net exchange due to increased losses and reduced effective pressure differences between openings. *Recommendation:* use a symmetric cross-shaped

layout where possible and treat increases in hole number per layer as a trade-off that requires justification in terms of net exchange.

- **Select vertical placement based on target renewal patterns.** Vertical placement affects the vertical distribution of exchange and therefore the internal concentration structure. Under strong replenishment, the effect is mainly local around the WRHs; under weaker replenishment, vertical placement can materially affect the monopile-average concentrations and the location of concentration minima. *Recommendation:* evaluate vertical placement using layer-specific indicators (e.g. minimum DO and POC in lower layers) in addition to average concentrations, and avoid configurations that shift limiting conditions to sensitive zones (typically near the bottom).
- **Orientation: secondary optimisation only.** The orientation of WRHs relative to the dominant tidal current has a modest influence on average concentrations, while wave direction is negligible for the scenarios considered. *Recommendation:* where feasible, align the UWRHs with the dominant tidal current direction, but do not rely on orientation to compensate for insufficient area or suboptimal layout.
- **Use the water quality model as a feasibility check on internal demand.** DELWAQ results show that internal sinks (consumption and settling/decay) can dominate locally if replenishment is insufficient, particularly in deeper sections. Model outcomes indicating persistent local depletion should be interpreted as a signal that the assumed internal demand cannot be supported by the replenishment regime. *Recommendation:* use coupled modelling to verify that the selected WRH design maintains non-limiting DO/POC throughout the vertical water column for the assumed biomass and process settings, and use “worst-case” periods (low replenishment, low ambient food) as design checks.

Based on the sensitivity analysis, the relative importance of the investigated design parameters from a water quality perspective is: total open area (dominant), followed by layout, vertical placement (particularly under low replenishment), and orientation.

Finally, it is recommended that WRH design would be supported by a site-specific coupled sensitivity study, as the results depend on monopile geometry, water depth, hydrodynamic forcing, and ambient water quality boundary conditions. The results presented in this chapter are representative for the applied assumptions and typical North Sea conditions; site-specific variations may change both absolute performance and the relative influence of individual design variables.

5 Overall/summary Conclusion & recommendations

The JIP LIFE project set out to assess whether water replenishment holes (WRHs) in offshore wind monopiles can support the development of epifaunal communities inside the monopiles. Through an integrated programme of offshore monitoring, ecological analysis, and coupled hydrodynamic–water quality modelling, the project has delivered the first detailed evidence base describing the internal physical and biological environment of monopiles equipped with WRHs in the North Sea.

5.1 Conclusions

5.1.1 Ecological development inside monopiles

The monitoring results demonstrate that the interior of monopiles hosts an ecological community that is fundamentally distinct from the exterior. Exterior communities showed the expected vertical zonation patterns known from offshore hard substrates, with high biomass of mussels, amphipods, anemones, and other typical North Sea fouling taxa. In contrast, interior communities were more heterogeneous, had substantially lower biomass, and showed no clear vertical zonation. Taxa such as sponges, ascidians, tube-building polychaetes, and brittle stars were more prominent internally. Signs of low-oxic conditions were found on the seabed of the interior of all four surveyed monopiles. The development thereof should be monitored closely and considered in future WRH design. Additional monitoring efforts should also be made to assess the presence of non-indigenous species, which may benefit from this new type of habitat.

The videos confirm that mobile species such as small gadoids actively use the interior. DNA from small gadoids, rocklings, and other shelter-associated fish was detected inside the monopile. However, the eDNA results also show that genetic material likely circulates through the interior via water exchange, so the detection of the species' genetic material does not proof their presence.

5.1.2 Abiotic conditions and water replenishment

The monopile interior is dark, enclosed, and reliant on WRHs for the supply of oxygen and particulate organic carbon (POC). Monitoring showed that dissolved oxygen concentrations were generally high inside the monopiles, though with vertical gradients. Nutrient measurements suggested accumulation of ammonium, phosphate, and silicate inside, especially near the seabed, likely linked to mineralisation of organic matter and absence of phytoplankton uptake in low-light conditions.

The modelling confirms that water replenishment is sufficient to prevent largescale oxygen depletion under typical North Sea conditions but also highlights that areas above the upper WRH and below the lower WRH receive markedly less exchange, making these zones the most vulnerable to oxygen decline. This is consistent with field observations of patchy microbial mats at the seabed, indicating local oxygen stress and organic matter accumulation. The analysis however did not consider seasonal or extreme events (e.g. heat wave) as information on the effects across all present species differs significantly. Scale oxygen depletion under typical North Sea conditions but also highlights that areas above the upper WRH and below the lower WRH receive markedly less exchange, making these zones the most vulnerable to oxygen decline. This is consistent with field observations of patchy microbial mats at the seabed, indicating local oxygen stress and organic matter accumulation.

5.1.3 Sensitivity of internal conditions to WRH design

The modelling shows that internal water quality is governed by various design parameters, and primarily by:

- **Total WRH area.** The dominant parameter controlling exchange. Larger areas strongly increase replenishment and bring oxygen and POC levels closer to ambient conditions.
- **Horizontal layout.** A cross-shaped symmetric arrangement yields the most efficient exchange. Increasing the number of holes per layer without increasing total area reduces efficiency due to higher hydraulic losses. -shaped symmetric arrangement yields the most efficient exchange.
- **Vertical placement.** This mostly affects local conditions above and below the WRHs. Reducing the vertical distance between the holes improves the average interior conditions under low-exchange conditions.
- **Orientation to forcing.** Although some influence is there, this has relatively limited effect. Alignment with dominant currents slightly improves exchange; wave direction has negligible influence.

A robust conclusion is that WRHs can effectively maintain abiotic conditions compatible with diverse fouling communities, provided that the WRH system is appropriately designed.

5.1.4 Synthesis across monitoring, ecological analysis and modelling

Integrating findings from the measurements and modelling leads to the following overarching insights:

- The interior ecosystem is resource limited, but not inhospitable. Oxygen and food availability depend strongly on replenishment, which for the current design and derived communities, the system of WRHs can provide at adequate levels.
- The interior habitat is distinct from the exterior hard substrate habitat, increasing overall biodiversity at turbine scale.
- While the interior environment is suitable for some fauna, high biomass communities typical of exterior surfaces do not develop internally, likely due to reduced food supply and flow.
- Areas below the lower WRH are most prone to oxygen depletion and accumulation of fine organic matter, visible as microbial mat formation.
- Appropriate WRH design is important: suboptimal WRH sizing or placement can create zones of low oxygen, even while other parts of the monopile remain well replenished.
- Model–measurement comparison shows general consistency in vertical gradients but also underscores the need for more detailed temporal measurements of ambient concentrations to improve model accuracy.

Together, these findings confirm that when well designed, WRHs are capable of supporting ecological communities in monopile interiors.

5.2 Final reflection

JIP LIFE demonstrates that WRH systems, originally driven by engineering and operational considerations, can also support ecological communities within monopile interiors. While these habitats differ strongly from exterior communities, they enrich the overall habitat diversity of offshore wind farms. These interior habitats differ markedly from exterior hard-substrate communities and contribute to habitat heterogeneity at the turbine scale.

While the project does not allow for direct comparison with monopiles lacking WRHs or with alternative WRH designs, it provides a robust basis for understanding the ecological

implications of internal water replenishment. The combined monitoring and modelling framework offers practical guidance for future offshore wind projects that may wish to explicitly integrate ecological objectives into WRH design and optimisation. Continued monitoring will be valuable to understand long-term successional trajectories and investigate if WRH systems remain effective as ecological features throughout the operational life of the turbines.

Future research is also required to investigate if this will substantially contribute to biodiversity enhancement goals as well as assessing the risk for non-natives or invasive species' occurrence.

6 References

Akaike, H. “Information Theory and an Extension of the Maximum Likelihood Principle.” *International Symposium on Information Theory,.* 1973. 267-281.

Avant, P. “Common eel (Anguilla anguilla).” In *Marine Life Information Network: Biology and Sensitivity Key Information Reviews*, by In Tyler-Walters H. and Hiscock K. Plymouth: Marine Biological Association of the United Kingdom., 2007.

Bolam, S.G., et al. “Functional traits in benthic ecology: definitions and applications.” *Marine Ecology Progress Series, 516*, 2014: 283–302.

Borja, A., J. Franco, and V. Pérez. “A marine biotic index to establish the ecological quality of soft-bottom benthos within European estuarine and coastal environments.” *Marine pollution bulletin, 40(12)*, 2000: pp.1100-1114.

Boutin, Kevin, Sylvie Marylene Gaudron, Jérémy Denis, and Frida Ben Rais Lasram. “Potential Marine Benthic Colonisers of Offshore Wind Farms in the English Channel: A Functional Trait-Based Approach.” *Marine Environmental Research 190* 190 (2023): 106061.

Bremner, J., S.I. Rogers, and C.L.J. Frid. “Assessing functional diversity in marine benthic systems.” *Marine Ecology Progress Series, 311*, 2006: 23–41.

Chust, G., et al. “Dispersal similarly shapes both population genetics and community patterns in the marine realm.” *Scientific reports, 6(1)*, 2016: p.28730.

Coolen, J.W., et al. “Benthic biodiversity on old platforms, young wind farms, and rocky reefs.” *ICES Journal of Marine Science, 77(3)*, 2020: pp.1250-1265.

Coolen, J.W., et al. *Marine growth sampling tool evaluation.* Den Helder: Wageningen Marine Research, 2025.

de Juan, S., et al. “Biological Traits Approaches in Benthic Marine Ecology: Dead Ends and New Paths.” *Ecology and Evolution, 12(6)* 12, no. 6 (2022): e9001.

De Mesel, I., F. Kerckhof, A. Norro, B. Rumes, and S Degraer. “Succession and seasonal dynamics of the epifauna community on offshore wind farm foundations and their role as stepping stones for non-indigenous species.” *Hydrobiologia 756:1* (Springer) 756, no. 1 (1 2015): 37-50.

Degen, Renate, and Sarah Faulwetter. “The Arctic Traits Database – A Repository of Arctic Benthic Invertebrate Traits.” *Earth System Science Data 11* 11 (2019): 301-322.

Degraer, Steven, et al. “Offshore Wind Farm Artificial Reefs Affect Ecosystem Structure and Functioning: A Synthesis.” *Oceanography, 33(4)* 33, no. 4 (2020): 48-57.

Deltares. “D-Flow Flexible Mesh: Computational Core and user Interface – User Manual Version 2022.02.” 2022.

DNV. “Environmental Conditions and Loads, DNV-RP-C205.” 2021.

Dye, B., I. Tulp, A. van Leeuwen, E. Blom, and E. Schram. “A rockling’s choice: The trade-off between thermal preference and physical structure in the five bearded rockling, Ciliata mustela.” *Journal of Experimental Marine Biology and Ecology, 570*, 2024: 151959.

Gili, J. M., and R. Coma. “Benthic Suspension Feeders: Their Paramount Role in Littoral Marine Food Webs.” *Trends in Ecology & Evolution* 13, no. 8 (1998): 316-321.

Gogina, Mayya, Anja Zettler, and Michael L Zettler. “Weight-to-Weight Conversion Factors for Benthic Macrofauna: Recent Measurements from the Baltic and the North Seas.” *Earth System Science Data 14 (1)* 14 (2022): 1-4.

Gutiérrez, J.L., C.G. Jones, D.L. Strayer, and O.O. Iribarne. “Mollusks as ecosystem engineers: the role of shell production in aquatic habitats.” *Oikos, 101(1)*, 2003: pp.79-90.

Harrington, Carlene Theresa. *The Invasion of the Colonial Ascidian Didemnum vexillum into South Shore Bays of Long Island, New York—Feeding and Metabolic Characteristics.* Stony Brook, NY: State University of New York at Stony Brook, 2010.

Idelchik, I E. *Handbook of Hydraulic Resistance.* Begell House, 2008.

Itoh, S., et al. “Vertical eddy diffusivity in the subsurface pycnocline across the Pacific.” *Oceanography, 77(2)*, 2021: 185-197.

Jones, Clive G, John H Lawton, and Moshe Shachak. “Organisms as Ecosystem Engineers.” *Oikos 69* 69, no. 3 (1994): 373-386.

Kerckhof, F.; Rumes, B.; Degraer, S. “A closer look at the fish fauna of artificial hard substrata of offshore renewables in Belgian waters.” In *Environmental Impacts of Offshore Wind Farms in the Belgian Part of the North Sea: Assessing and Managing Effect Spheres of Influence*, by S. Degraer, R. Brabant, B. Rumes and L. Vigin, 79-89. 2018.

Kerckhof, Francis, Bob Rumes, Alain Norro, T G Jacques, and Steven Degraer. “Seasonal Variation and Vertical Zonation of the Marine Biofouling on a Concrete Offshore Windmill Foundation on the Thornton Bank (Southern North Sea).” Edited by Steven Degraer, R Brabant and B Rumes. *Offshore Wind Farms in the Belgian Part of the North Sea: Early Environmental Impact Assessment and Spatio-temporal Variability* (Royal Belgian Institute of Natural Sciences), 2010: 53-68.

Kerckhof, Francis, Bob Rumes, T Jacques, Steven Degraer, and Alain Norro. “Early Development of the Subtidal Marine Biofouling on a Concrete Offshore Windmill Foundation on the Thornton Bank (Southern North Sea): First Monitoring Results.” *Underwater Technology* 29, no. 3 (2010): 137-149.

Kindeberg, T., K.M. Attard, J. Hüller, J. Müller, C.O. Quintana, and E. Infantes. “Structural complexity and benthic metabolism: resolving the links between carbon cycling and biodiversity in restored seagrass meadows.” *Biogeosciences, 21(7)*, 2024: pp.1685-1705.

Korhonen, P, F K C Hui, J Niku, S Taskinen, and B van der Veen. “A comparison of joint species distribution models for percent cover data.” *Methods in Ecology and EvolutionVolume 15 (12)*, 2024.

Korhonen, P., J. Niku, F. K. C. Hui, S. Taskinen, and B. van der Veen. *Analysing Sparse Ecological Percent Cover Data Using gllvm.* 2025. https://cran.r-project.org/web/packages/gllvm/vignettes/vignette8.html.

Korhonen, Pekka, Francis K C Hui, Jenni Niku, and Sara Taskinen. “Fast and Universal Estimation of Latent Variable Models Using Extended Variational Approximations.” *Statistics and Computing 33(1)* 33 (2023): 26.

Krone, R, L Gutow, T J Joschko, and A Schroder. “Epifauna dynamics at an offshore foundation–implications of future wind power farming in the North Sea.” *Marine environmental research, 85*, 2013: pp.1-12.

Kulinski, K, G Rehder, E Asmala, A Bartosova, J Carstensen, and others. “Biogeochemical functioning of the Baltic Sea.” *Earth System Dynamics, 13(1)*, 2022: pp.633-685.

Kumala, Lars, Malte Thomsen, and Donald E Canfield. “Respiration Kinetics and Allometric Scaling in the Demosponge Halichondria panicea.” *BMC Ecology and Evolution 23(1)* 23 (2023): 53.

Kusters, N, S Groeskamp, B Fernandez Castro, and H van Haren. “Microstructure Observations and Mixing Parameterizations along an Atlantic Transect in Very Weak Turbulence.” *Ocean Science, 21(6)*, 2025: 3397–3426.

Kusters, N., S. Groeskamp, B. Fernandez Castro, and H. van Haren. “Microstructure observations and mixing parameterizations along an Atlantic transect in very weak turbulence.” *Ocean Science*, 2025: 1125–1140.

Lewin, L. A., H. Caswell, K. D. De Pedra, and E. L. Creed. “Demographic Consequences of Larval Development Mode: Planktotrophy vs. Lecithotrophy in Streblospio Benedicti.” *Ecology, 68(6)*, 1987: 1877-1886.

Lipsewers, Y A, E C Hopmans, F J R Meysman, J S S Damste, and L Villanueva. "Abundance and diversity of denitrifying and anammox bacteria in seasonally hypoxic and sulfidic sediments of the saline lake Grevelingen." *Frontiers in Microbiology*, 2016.

Loebl, M., et al. "Recent patterns in potential phytoplankton limitation along the Northwest European continental coast." *Journal of Sea Research, 61(1-2*, 2009: pp.34-43.

MacCamy, R., and R.A. Fuchs. *Wave forces on piles: a diffraction theory - Technical Memo, No. 69.* Technical Memo, No. 69, U.S. Army Corps of Engineers, Beach Erosion Board, 1954.

Mackinson, S., and G. Daskalov. *An ecosystem model of the North Sea to support an ecosystem approach to fisheries management: description and parameterisation Science Series Technical Report no.142.* Cefas (Centre for Environment, Fisheries and Aquaculture Science, 2007.

Mavraki, N., et al. "Ecological Functioning of Macrofaunal Assemblages: Contrasting Natural and Artificial Hard Substrates (under review)." *Ices Journal of Marine Science.*, 2026 under review.

Mavraki, N., S. Degraer, J. Vanaverbeke, and U. Braeckman. "Organic matter assimilation by hard substrate fauna in an offshore wind farm area: a pulse-chase study." *ICES Journal of Marine Science, 77(7-8)*, 2020a: pp.2681-2693.

Mavraki, Ninon. *On the food-web ecology of offshore wind farms, the kingdom of suspension feeders.* PhD Thesis, Ghent: Ghent University, 2020b.

Migné, A, and D Davoult. "Oxygen Consumption in Two Benthic Cnidarians: Alcyonium digitatum and Urticina felina." *Proceedings of the 6th International Conference on Coelenterate Biology, 1995*, 1997: 321-328.

Migne, A., and Davoult. "Experimental nutrition in the soft coral Alcyonium digitatum (Cnidaria: Octocorallia): removal rate of phytoplankton and zooplankton." *Cahiers de Biologie Marine, 43(1)*, 2002: pp.9-16.

Miya, M., et al. "MiFish, a set of universal PCR primers for metabarcoding environmental DNA from fishes: Detection of more than 230 subtropical marine species." *Royal Society Open Science, 2(7)* (Royal Society Publishing) 2, no. 7 (7 2015): 150088.

Niku, J., F. K. C. Hui, S., Taskinen, and D. I. Warton. "gllvm: Fast analysis of multivariate abundance data with generalized linear latent variable models in R." *Methods in Ecology and Evolution, 10(12)* 10, no. 12 (2019): 2173-2182.

Noisette, F., F. Bordeyne, D. Davoult, and S. Martin. "Assessing the physiological responses of the gastropod Crepidula fornicata to predicted ocean acidification and warming." *Limnology and Oceanography, 61(2)*, 2016: pp.430-444.

Omstedt, A, et al. "Future changes in the Baltic Sea acid–base (pH) and oxygen balances." *Tellus Series B Chemical and Physical Meteorology, 64(1)*, 2012: p..19586.

Oosterbroek, S. *Decona pipeline v1.5.* 2024.

Ortega, M M, J M de Pariza, and E Navarro. "Seasonal Changes in the Biochemical Composition and Oxygen Consumption of the Sea Anemone Actinia equina as Related to Body Size and Shore Level." *Marine Biology 97(1)* 97 (1988): 137-143.

Pack, Kathryn E, Marc Rius, and Nova Mieszkowska. "Long-Term Environmental Tolerance of the Non-Indigenous Pacific Oyster to Expected Contemporary Climate Change Conditions." *Marine Environmental Research, 164* 164 (2021): 105226.

Pearson, T. H., and R. Rosenberg. "Macrobenthic succession in relation to organic enrichment and pollution of the marine environment." *Annual Review of Oceanography and Marine Biology, 16*, 1978: 229-311.

Pianka, E. R. "On R- and K-selection." *The American Naturalist 104(940)*, 1970: 592-597.

Postma, L., P. Boderie, J. van Gils, and J. van Beek. "Component Software System for Surface Water Simulations." *Lecture Notes in Computer Science, 2657*, 2003: 649–658.

Queirós, A.M., and et al. "A bioturbation potential index for marine benthic fauna." *Ecological Indicators, 30*, 2013: 65–76.

Reeve, A. *Conger conger Conger eel.* 2007. https://www.marlin.ac.uk/species/detail/2126.
Ricciardi, A, and E Bourget. “Weight-to-weight conversion factors for marine benthic macroinvertebrates.” *Marine ecology progress series, 163* (Inter-Research Science Center) 171 (1998): 245-251.
Rueda, J.L., A.C. Smaal, and H., Scholten. “A growth model of the cockle (Cerastoderma edule L.) tested in the Oosterschelde estuary (The Netherlands).” *Journal of Sea Research* (Elsevier) 54, no. 4 (11 2005): 276-298.
Salt, L A, H Thomas, F Prowe, A V Borges, Y Bozec, and H J W De Baar. “Variability of North Sea pH and CO2 in response to North Atlantic Oscillation forcing.” *Journal of Geophysical Research: Biogeosciences, 118(4)*, 2013: pp.1584-1592.
Siems, A., T. Zimmermann, T. Sanders, and D., Pröfrock. “Dissolved trace elements and nutrients in the North Sea—a current baseline.” *Environmental Monitoring and Assessment, 196(6)*, 2024: 539.
Solis, J., and J. Genesca. “Effect of calcareous deposit formation on galvanic anode cathodic protection of steel in seawater.” *NACE – International Corrosion Conference Series. Paper no. 09520.* 2009. 1-10.
Souster, T.A., S.A. Morley, and L.S. Peck. “Seasonality of oxygen consumption in five common Antarctic benthic marine invertebrates.” *Polar Biology, 41(5)*, 2018: pp.897-908.
Strong, J.A., et al. “Marine biodiversity and ecosystem function relationships: the potential for practical monitoring applications.” *Estuarine, Coastal and Shelf Science, 161*, 2015: pp.46-64.
Sumer, B M, and J Fredsoe. *Hydrodynamics around cylindrical structures.* World Scientific, 1999.
Takahashi, S, K Tanimoto, and S Miyanaga. “Uplift wave forces due to compression of enclosed air layer and their similitude law.” *Coastal Engineering in Japan 28, no. 1* , 1985: 191-206.
van der Veen, B. *BertvanderVeen.GLLVM-workshop:Physialia workshop on Generalized Linear Latent Variable Models.* 2025.
Voet, H.E.E., C. van Colen, and J., Vanaverbeke. “Climate Change Effects on the Ecophysiology and Ecological Functioning of an Offshore Wind Farm Artificial Hard Substrate Community.” *Science of the Total Environment, 810* 810 (2022): 152194.
White, F M. *Viscous Fluid Flow.* McGraw-Hill, 1991.
Wickham, H. *ggplot2: Elegant Graphics for Data Analysis.* Springer, 2016.
Wijsman, J. W., P. M. Herman, and M. T. Gomoiu. “Spatial distribution in sediment characteristics and benthic activity on the northwestern Black Sea shelf.” *Marine Ecology Progress Series 181* 181 (1999): 25-39.
Yan, J.-F., T Nguyen, R White, and R Griffin. “Mathematical modelling of the formation of calcareous deposits on cathodically protected steel in seawater.” *Journal of the Electrochemical Society 140(3)*, 1993: 733–742.
Yan, J.-F., T. Nguyen, R. White, and R. Griffin. “Mathematical modelling of the formation of calcareous deposits on cathodically protected steel in seawater.” *Journal of the Electrochemical Society, 140(3)*, 1993: 733-742.
Zuur, A.F., and E.N. Ieno. *The World of Zero-Inflated Models: Using GLLVM.* Highland Statistics Ltd., 2025.

A Species Traits Definitions

Trait Category	Abbreviation	Definition	Source
Body Shape	PmErfle	erect and flexible	(Mavraki, Want, et al. 2026 under review)
	PmErNfle	erect and non-flexible	
	PmTube	tube-building	
	PmEnfle	encrusting and flexible	
	PmEnNfle	encrusting and non-flexible	
	PmNone	other/none of the above	
Feeding Traits	fSuspension	Suspension feeders capture particles from the water column.	
	fDeposit	Deposit feeders ingest sediment and extract organic matter	
	fScavenger/Opp	Scavengers or opportunistic feeders consume dead organic material or varied food sources.	
	fPredator	Predators feed on living organisms.	
	fParasite	Parasites derive nutrition from a host organism	
Larval Development Traits	ldPla	Planktotrophic – Larvae that feed in the plankton and therefore have a relatively long pelagic larval duration, resulting in high dispersal potential	
	ldLec	Lecithotrophic – Larvae that do not feed in the plankton but rely on yolk reserves; they have a shorter pelagic larval duration and therefore lower dispersal potential than planktotrophic larvae.	
	ldDir	Direct development – Species that do not have a pelagic larval stage; juveniles develop directly within the egg or brood pouch, resulting in very limited dispersal potential.	
Living Habitat Traits	lhTube	Lives in a tube constructed in sediment or attached to substrate	
	lhBurrow	Lives in a burrow within sediment.	
	lhFree	Free-living on sediment surface.	
	lhCrevice	Occupies crevices in hard substrates	
	lhEpi	Epifaunal: lives on the surface of the seabed or attached to objects.	
	lhAttach	Attached to substrate (e.g., rocks, shells).	
Longevity	l<1	Less than 1 year	
	l1-3	between 1–3 years	
	l3-10	between 3-10 years	
	l>10	more than 10 years	
Productivity	pb1	Slow-turnover, likely long-lived species	
	pb2	Moderate turnover	
	pb3	Intermediate turnover	
	pb4	Fast turnover, usually small fast-growing species	
	pb5	Extremely rapid turnover	

B Modelling framework

B.1 Water replenishment model

The water and air exchange through the water replenishment holes is computed based on the following sub-modules:

- A wave model describing the pressure on the surface of the monopile for irregular waves.
- A tidal model describing the pressure on the surface of the monopile for a given tidal current (direction and magnitude) and water level.
- An optional module for the excess pressure due to compressible air between the internal free surface and the airtight platform.
- A volume integrated conservation model for the internal wave response due to the external wave pressure. The internal free surface is assumed constant over the monopile (no sloshing).

Each of these components are described below.

B.1.1 Wave model

The water exchange per replenishment hole due to waves is driven by the difference in internal pressure and the external pressure due to waves. Considering a single forward propagating wave around a circular monopile the following effects are present:

- The pressure due to the incident wave.
- A pressure contribution due to the scattered wave.
- The Bernoulli effect around the perimeter of the monopile due to the monopile itself.

These effects are described by applying linear diffraction wave theory following (MacCamy and Fuchs 1954). The diffraction theory by MacCamy and Fuchs (1954) was derived for a single wave frequency after which linear superposition over all frequencies in the wave spectrum is adopted. The wave spectrum is described by a JONSWAP spectrum with a peak enhancement factor of 3.3. Note that nonlinear effects are neglected, which results in a conservative estimate for the mean flux through the monopile. This is the case, because the nonlinear (second order) terms would give rise to a mean pressure difference between two water replenishment holes and thereby drive a mean flow.

The wave direction relative to the position of the water replenishment holes is accounted for. The evaluation of MacCamy and Fuchs (1954) gives rise to the external pressure p_{wave}.

The external wave pressure, p_{wave}, is set to zero, if the local external wave level (accounting for diffraction effects) is below the mean hole position. This means that the water will simply drain under gravity and not be sucked out during the wave trough.

B.1.2 Tidal model

A tidal current gives rise to an external pressure on the surface of the monopile. The total pressure, p_{tide}, reads:

$$p_{tide} = \rho g(\eta_{tide} - z_{SWL}) + \frac{1}{2}\rho C_p U^2 \quad \text{(B.1)}$$

Here, η_{tide} is the surface elevation over the tidal cycle, z_{SWL} is the still water level, C_p is the pressure coefficient and U is the tidal current magnitude. C_p was schematised according to the experimental results presented in FigureApx B.1 for a Reynold's number of $3.6 \cdot 10^6$.

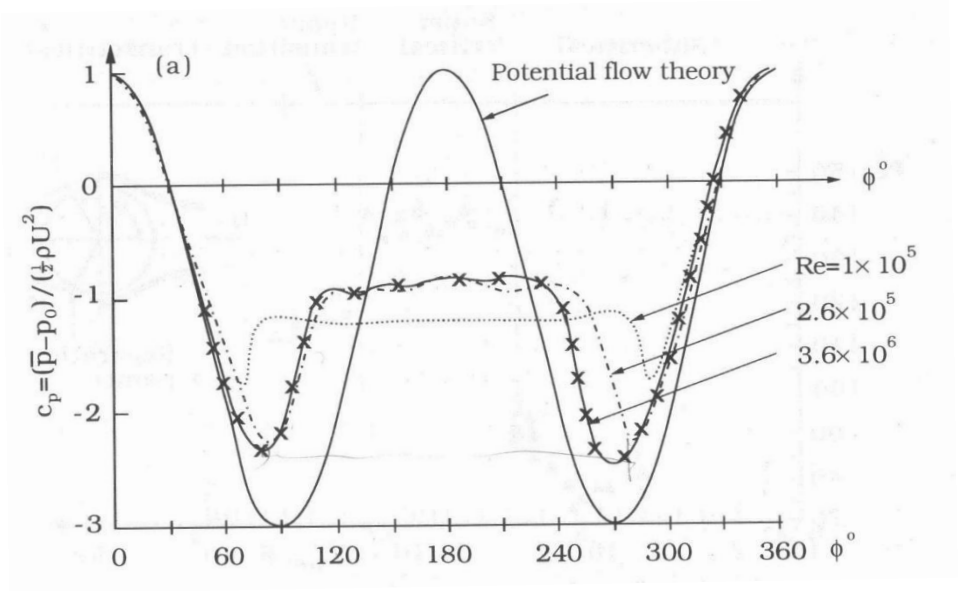

FigureApx B.1 The pressure distribution around a circular structure in a steady current. Taken from (Sumer en Fredsoe 1999). $\phi = 0°$ is the location of the upstream stagnation pressure.

The inclusion of C_p in the evaluation of p_{tide} means that there will be a tidal-averaged offset in the pressure at two water replenishment holes, if they are not placed at the same angle relative to the current direction. The mean pressure differential will thus drive a mean volume flux between the two water replenishment holes. A physical interpretation is that one of the holes will experience an 'undershoot' of the internal water surface, while the other hole will experience an 'overshoot' of the internal water surface. Thus, locally around the holes there will be a mean pressure gradient driving the water replenishment (see below for details on the hydrodynamic model).

The value of C_p depends on the direction of the tidal current relative to the orientation of the water replenishment holes. This is accounted for in the model. In FigureApx B.1, $\phi = 0°$ is the location of the upstream stagnation pressure.

B.1.3 Compressible air phase

The volume of air between the internal free surface and the airtight platform will behave as a compressible system, when the internal surface moves up and down. Generally, there is a pressure equalisation system for the air volume, such that the internal free surface moves freely with the tidal model. Compressibility effects can be completely ignored for tidal motions, since the movement of the free surface is slow.

In the case of extreme waves, the internal free surface can easily move 10-20 cm per wave period. For a monopile with a diameter of 6.0 m at the upper vertical part (transition piece), this corresponds to 2.8-5.6 m^3 of air, which should be removed from the monopile every half wave period (in and out). Since the typical air ventilation system (pressure equalisation) has a small diameter, the volume change is a combination of an actual flux of air in and out of the monopile and compression of the remaining air volume. This gives rise to in internal excess air pressure relative to atmospheric pressure:

$$p_{air} \tag{B.2}$$

The inclusion of the air-phase, the leakage and the compressibility effects follow from the paper by Takahashi et al. (1985). If this effect is omitted, the pressure is set to $p_{air} = 0$ Pa.

The effect of the air pressure introduces oscillatory forces on the airtight platform under wave loading that are calculated as:

$$F_{z,air} = p_{air} \frac{D_{top}^2 \pi}{4} \tag{B.3}$$

B.1.4 Model for the internal wave motion

In this section, the combined model for all water replenishment holes is established. The model describes the variation of the internal free surface, ξ, as a function of time, see FigureApx B.2 for a sketch of the control volume. In the figure, A_{hole} is the area of the individual water replenishment holes and A_{pile} is the cross-sectional area at the instantaneous, internal water surface. The temporal variation in ξ depends on the flux of water through any opening, thus the continuity equation for the control volume reads:

$$A_{pile} \frac{\partial \xi}{\partial t} = \sum_{n=1}^{N} u_n A_{hole,n} \tag{B.4}$$

Here, u_n is the velocity through each of the holes, where the velocity is positive into the monopile. The continuity equation in eq. (B.4) is sufficient in the vertical direction, because there is no wave forcing acting on the water column inside the pile in the vertical direction, so the continuity equation can replace the vertical momentum equation under an assumption of hydrostatic pressure. The area of the individual water replenishment holes can be different. A_{pile} varies in time for a tapered monopile design.

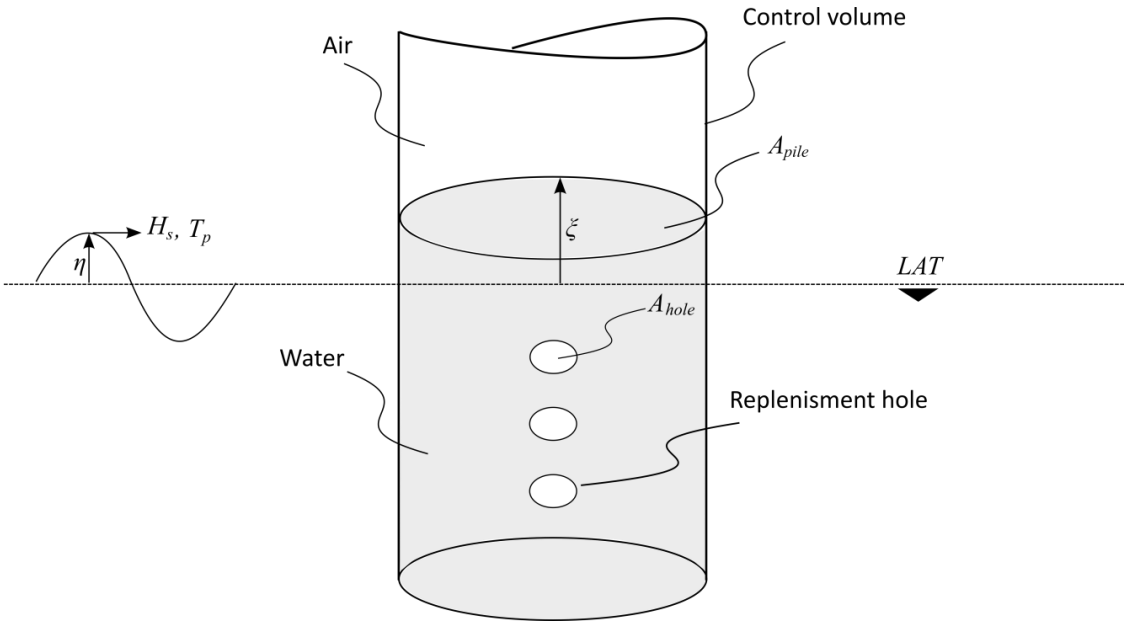

FigureApx B.2 Sketch of the control volume for the conceptual model for the internal wave motion.

The evaluation of the velocity in the holes is based on the following considerations:

- The water replenishment holes are placed sufficiently far from each other in the vertical, such that each layer of water replenishment holes in the vertical can be treated individually.
- If there are more holes in the same layer, there is a risk of interacting jets within the monopile. However, the velocity would decrease sufficiently fast for the over-pressure due to interacting jets to be important.
- The second assumption means that the velocity over all holes, even those in the same vertical layer, can be evaluated independently.

Each hole is described by the unsteady energy equation (Bernoulli's equation with loss terms) that takes the following form:

$$\frac{p_{out}}{\rho g}+\frac{u_{out}^2}{2g}+\frac{1}{g}\frac{\partial \phi_{out}}{\partial t}=\frac{p_{in}}{\rho g}+\frac{u_{in}^2}{2g}+\frac{1}{g}\frac{\partial \phi_{in}}{\partial t}+\frac{\zeta_{hole}}{2g}u_{hole}^2 \tag{B.5}$$

Here, subscript '*out*' refers to the outside of the monopile and '*in*' refers to the inside of the monopile. The boundaries for the energy equation are taken far enough away from the hole for u_{out} and u_{in} to be significantly smaller than u_{hole}, therefore they are neglected hereafter. The two pressures are $p_{out}=p_{wave}$ and $p_{in}=\rho g\xi+p_{air}$, respectively. The former states that the pressure adjacent to the outer surface of the monopile is given by linear wave theory. The latter gives that the internal pressure is the sum of hydrostatic pressure from the excess height ξ and the excess pressure due to compressibility of the air volume. The hydrostatic pressure due to the mean water level cancels out.

The variable ϕ is the velocity potential, where the velocity field is given as $\boldsymbol{u}=(u,v,w)=\nabla\phi$. Consequently, the inner and outer velocity potentials are related as follows:

$$\phi_{in}=\phi_{out}+\int_{\text{path}}\boldsymbol{u}(s)\,ds \tag{B.6}$$

Collecting the values above yields the following reduced energy equation for the replenishment of water through each of the holes:

$$\rho \frac{\partial}{\partial t} \int_{path} \mathbf{u}(s) \mathrm{d}s = p_{wave} - \rho g \xi - p_{air} - \rho \frac{\zeta_{hole}}{2} u_{hole} \left| u_{hole} \right| \tag{B.7}$$

Two properties require evaluation and calibration, namely the increase in the velocity potential along the path of the water particles and the loss coefficient, ζ_{hole}.

B.1.4.1 Increase in velocity potential

The increase in the velocity potential along the path of the water particles is schematised as:

$$\frac{\partial}{\partial t} \int_{path} \mathbf{u}(s) \mathrm{d}s = \int_{path} \frac{\mathbf{u}(s)}{u_{hole}} \mathrm{d}s \frac{\partial u_{hole}}{\partial t} = C_m D_{hole} \frac{\partial u_{hole}}{\partial t} \tag{B.8}$$

The integral of the increase in velocity potential relative to the velocity in the hole is independent of time, because the velocity field of a jet is self-similar (White 1991) when normalised by u_{hole}. Hence the integral can be placed outside of the time differentiation. It is realised that the integral can be schematised as an added mass coefficient times a length scale, the latter taken equal to D_{hole}.

C_m depends on the acceleration of the water through the hole (on the upstream side of the hole), the development of the jet and subsequent breakdown of the jet on the downstream side of the hole. All within half a wave cycle after which the process repeats in the other direction. The value for C_m requires calibration, see Appendix B.1.6.

B.1.4.2 Loss coefficients

The loss coefficient is sometimes written as $\zeta_{hole} = 1/K^2$. Both values are mentioned below, where the choice of coefficients are provided in Appendix B.1.6.

B.1.5 Risk of resonance

The combined system of ordinary differential equations described in Section B.1.4 is a mass-spring type system, thus there is a possibility of resonance at some frequencies. This was investigated for a range of realistic A_{hole}/A_{pile} ratios and a single hole. The hydrodynamic loss term was found to be so large that the response amplitude operator (RAO) was always less than 1. Consequently, resonance issues – as otherwise seen in the related problem of moonpools – are not expected.

B.1.6 Default loss coefficients

The case specific model coefficients for the hydrodynamic model are described in the following paragraphs.

B.1.6.1 Hydrodynamic loss coefficients – Tide

The tidal motion can be considered a steady state case and loss coefficients from the literature are adopted. In the case of replenishment holes in a monopile, the hole diameter is large relative to the wall thickness. This is accounted for by choosing loss coefficients as a function of the ratio t_s/D_h', where t_s is the thickness of the steel and D_h' is the effective hole diameter (accounting for marine growth). The loss coefficients ζ and K are tabulated in TableApx B.1 following (Idelchik 2008).

TableApx B.1 Loss coefficient for steady state flow as a function of the length-to-diameter ratio of the opening (Idelchik 2008)

t_s/D_h'	0.00	0.20	0.40	0.60	0.80	1.00	1.20	1.40	1.60	1.80	2.00	4.00
ζ	2.85	2.72	2.60	2.34	1.95	1.76	1.67	1.62	1.60	1.58	1.55	1.55
K	0.59	0.61	0.62	0.65	0.72	0.75	0.77	0.79	0.79	0.80	0.80	0.80

B.1.6.2 Hydrodynamic loss coefficients – Waves

The hydrodynamic loss coefficients in the case of waves have been validated against in-house experimental data of the internal wave motion in a monopile with a single hole for irregular waves. The loss coefficients are found as $C_m = 0.9$ and $K = 1.1$. The latter corresponds to a loss coefficient of $\zeta = 0.83$, which is smaller than the loss coefficients for steady state flow typically encountered (see above).

The smaller loss coefficient is attributed to the dynamics of the system and that the separated flow is not fully developed within half a wave period.

B.2 DELWAQ model

DELWAQ is an open-source model for simulating the reactions and transport of water quality substances that is developed and maintained by Deltares. Here the model concept is described and the introduction into the water quality model is given.

B.2.1 Advection-diffusion equation

The reaction and transport of water quality substances within the monopile are calculated with a combined advection-diffusion-reaction solver (DELWAQ) on a discrete 1DV computational grid. The individual components related to the advection-diffusion-reaction solver are specified in the following subsection.

B.2.1.1 Vertical water exchange in the DELWAQ model

Vertical mixing of the enclosed water and the water quality substances will take place due to (i) diffusion and (ii) forced convection caused by the inflow of water through the water replenishment holes. Due to the slenderness of the monopile, the water exchange is approximated by the 1D (vertical) continuity equation. This section describes the vertical advective water exchange in the monopile based on two layers of replenishment holes, see Figure Apx B.3. The volume fluxes calculated with the hydrodynamic model (Section B.1) are used directly in DELWAQ.

The inflow per replenishment layer is denoted Q_0, Q_1, etc., see Figure Apx B.3. All layers above the lowermost replenishment hole will experience an advection of substances based on the sum of volume flux from holes below this layer, e.g. the volume flux is Q_0 between the first and second hole and $Q_0 + Q_1$ above the second hole, etc.

The recirculation below the lowermost water replenishment is described separately in Appendix C.1.

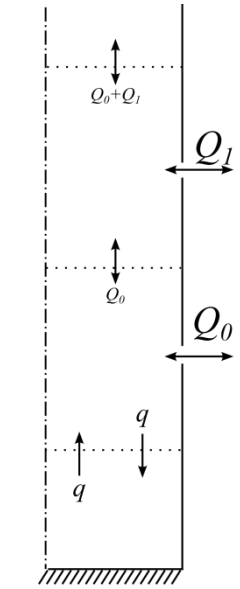

Figure Apx B.3 Schematization of the vertical exchange inside the monopile for the two lowermost replenishment holes.

B.2.1.2 Vertical diffusion

In addition to the advective processes, described in Section B.2.1.1 and Appendix B, vertical diffusion of substances is represented in the model. Additional mixing due to turbulent fluctuations is judged to be small in comparison to the advective exchange through the WRHs. Accordingly, a small background vertical turbulent diffusion coefficient of 10^{-5} m^2/s is applied throughout this work. Typically, the average velocities within the monopile (away from the WRHs) are in the order of centimetres per second, indicating low turbulence levels. Published literature providing representative vertical diffusion coefficients for systems of this specific type is limited; however, diffusivities of this order are commonly applied in oceanographic modelling under low-turbulence conditions (Itoh, et al. 2021, N. Kusters, et al. 2025). CFD simulations of the WRH exchange further show that energetic mixing is localised near the openings, while background mixing in the interior remains weak, supporting the adopted diffusion coefficient. The vertical diffusion coefficient primarily influences mixing in the layers below the LWRH and above the UWRH. In the region between the LWRH and the UWRH, vertical exchange is dominated by advective flow through the replenishment openings, and the contribution of background vertical diffusion is secondary. The chosen diffusion coefficient therefore provides a physically consistent representation of vertical mixing processes within the monopile interior.

B.2.1.3 Discrete model

The discrete model for the combined advection-diffusion-reaction equations consists of a number of segments (volumes) which are stacked in a 1DV column. The top layers (all the layers above the uppermost water replenishment hole) can breathe along with the internal surface elevation. The volume of the individual layers reflects the tapered design of the monopile.

B.2.1.4 Processes regarding dissolved oxygen and particulate organic material

For the purpose of determining the suitability of the interior of the monopile as a habitat for the typical species that are found in and around such structures, the dissolved oxygen concentration is one important parameter: if the oxygen concentration inside the monopile is too low, immobile organisms like mussels and anemones will die, whereas shrimps (and fish) will probably migrate to other areas. The second important parameter is particulate organic material, as that is the primary source of food. While normally organic material will consist of

living algae and detritus (or dead organic material), the circumstances inside the monopile prevent any photosynthesis, so the only processes that govern the transport and transformation of substances in the water column and sediment are:

- Vertical dispersion (VertDisper): Vertical dispersion represents turbulent mixing in the vertical direction, expressed as a diffusion coefficient (m^2/s). This parameter ensures that dissolved substances such as oxygen and POC are redistributed between layers, counteracting sharp gradients caused by biological consumption or settling. The switch ACTIVE_VERTDISP activates this process, and ACTIVE_TOTDEPTH and ACTIVE_DYNDEPTH ensure that dispersion accounts for the full water column depth and dynamic layer thickness. The vertical diffusion coefficient in this work is set to 1.0×10^{-5} m^2 s^{-1}.
- Sedimentation of particulate organic carbon (POC): Particulate organic matter (POC) settles from the water column to the sediment at a prescribed velocity (default 1 m/day). This process transfers organic carbon from the pelagic environment to the benthic compartment, where it becomes subject to slower mineralization. Sedimentation is crucial for representing benthic oxygen demand and long-term carbon burial. The switches ACTIVE_SED_POC1 and related constants activate this settling flux.
- Decomposition of detritus (xxRcDECFAST): Organic matter in the water column and sediment undergoes microbial decay, reducing POC and consuming oxygen. DELWAQ uses first-order kinetics for this process, with rate constants that depend on the detritus fraction. The parameter xxRcDECFAST controls the decomposition rate of the fast-decaying detritus pool (POC1). In this model, it is currently set to 0.3 day^{-1}, which means that approximately 30% of the fast detritus pool is mineralized per day under optimal conditions. This process is temperature-dependent and can be modified by oxygen availability. The switch ACTIVE_DecFast ensures that this process is active.
- Dynamic depth and numerical options: Constants such as ACTIVE_TOTDEPTH, ACTIVE_DYNDEPTH, and ScaleVDisp ensure that vertical mixing and process rates scale correctly with the actual water column depth. Numerical options like MaxIter and Tolerance control convergence of the iterative solver for mass balances.
- Biotic consumption processes: In addition to these abiotic processes, the model applies negative waste loads for oxygen and POC based on biomass-specific consumption rates derived from this study. These loads are implemented as:
    - fConsumeOXY (g O_2/m^2/day) for oxygen demand
    - fConsumePOC (g C/m^2/day) for carbon assimilation

  Both are interpolated to 61 layers and applied per segment (accounting for the segment surface area).

C Distribution of water within the monopile

The hydrodynamic model is a 1DV model, where the water enters through the water replenishment holes. The mixing processes, especially above the uppermost water replenishment holes and below the lowermost water replenishment holes cannot be described by a simple advection. This particularly holds below the lowermost water replenishment, where the volume of water is constant, so a 1DV advection velocity must vanish due to continuity.

The present section presents a parameterisation of the volume fluxes over the vertical as they are applied in the DELWAQ model.

It is noted that there has not been found literature on oscillating jet into confined spaces, so the parameterisation is based on the literature on steady jets.

C.1 1DV water quality model

C.1.1 Flow into the monopile

The flow into the monopile is essentially a jet. It follows from (White 1991) that a jet starts to expand in a self-similar fashion after a distance of approximately 20 hole diameters, meaning that the jet is quite focussed up to that point and will start to disperse more radially after that. Since the diameter of the water replenishment holes are typically a 0.2-0.4 m, the jet becomes self-similar after 4.0-8.0 m. This is a larger distance than the radius of most monopile foundations, so the jet is likely fairly confined in vertical dimensions. Consequently, the jet is contained in a single vertical cell in the parameterisation of the inflow.

The continuity equation is applied as follows: When water flows into the monopile at the same time as the internal water surface rises, the flux of water towards the top of the monopile equals $A\,\partial\xi/\partial t$, where A is the area of the internal free surface and ξ is the vertical position of the free surface. The remaining volume of water will flow out of the remaining water replenishment holes.

C.1.2 Flow out of the monopile

The flow out of the monopile is described by a symmetric, converging flow towards the water replenishment hole, see FigureApx C.1. This means that the local flow field will be normal to concentric half-spheres with an origin at the centre of the water replenishment hole. The incompressibility of water means that the total volume flux over each of the concentric half-spheres and the velocity normal to the concentric circles, u_n, are given as

$$u_n = \frac{Q}{2\pi r^2} \tag{C.1}$$

Where Q is the volume flux and $2\pi r^2$ is the area of a half-sphere with radius r. Due to the confined space within the monopile, the analogy of the concentric surfaces breaks down at some distance from the hole. The radius of the largest concentric surface is set to 50% of the monopile diameter. The radius of the largest surface is termed R.

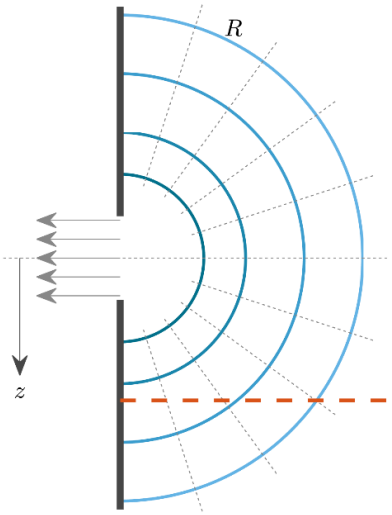

FigureApx C.1 Sketch of the symmetric, converging flow towards the water replenishment hole. The blue concentric circles are normal to the outflow, the dashed grey lines represent the flow direction and the dashed red line the volume flux over a horizontal line.

The volume flux through a horizontal plane that intersects the largest concentric surface can be explicitly calculated (the red 'plane' FigureApx C.1). The volume between the red plane and the surface with radius R is constant, so the flux over the red line is identical to the flux over the cap of the surface below the red plane. Since u_n is assumed constant over the surface, the flux through a horizontal plane, Q_p, is given as:

$$Q_p = Q\frac{2\pi R(R-z)}{4\pi R^2} = \frac{Q}{2}\left(1-\frac{z}{R}\right) \tag{C.2}$$

The nominator is the area of the cap and the denominator the area of a sphere. Hence, the change in volume flux with z is:

$$\frac{dQ_p}{dz} = -\frac{Q}{2}\frac{1}{R} \tag{C.3}$$

The variation in Q_p in eq. (C.2) only holds close to the hole, because it vanishes at the distance R from the hole. However, it is expected that there is an exponential decay in the volume flux towards the bed. Therefore, Q_p is described by

$$Q_p = Ae^{-kz} \quad \text{for} \quad \frac{R}{2} < z \tag{C.4}$$

Setting the two expressions in eqs. (C.2) and (C.4) equal to each other and match the slopes at $z = R/2$, it follows that

$$k = \frac{2}{R} \quad \text{and} \quad A = \frac{Q}{4}e^{1} \tag{C.5}$$

The above expressions for the volume flux can be applied below the lowermost hole, where it describes the upward flux of water. The mass conserving flux in the opposite direction is added to the DELWAQ model, whereby an advection-driven diffusion process is modelled. The parameterised vertical variation of Q_p/Q is shown in FigureApx C.2.

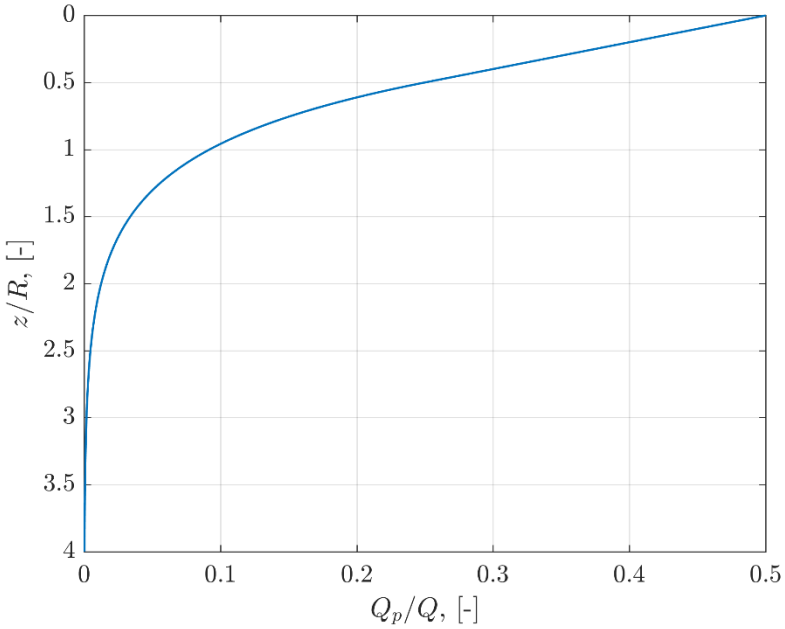

FigureApx C.2 Distribution of the relative flux, Q_p/Q, below the lowermost water replenishment hole.

Above the uppermost hole and above the lowermost hole, it is simply assumed that the fluxes distribute evenly towards the hole. The former because no recirculation is expected and the latter, because the volume flux is driven by the rising and falling free surface.

C.1.3 Distinguishing between tidal and wave-driven flows

A simple simulation of the oscillatory flow through a hole was performed with CFD. While not exhaustive, the simulation provided the following qualitative behaviour:

- A jet is formed every half-period of the oscillation.
- After flow reversal, the jet continues forward and disperses. The continued forward motion is due to the jet momentum that is not instantly deaccelerated by the change in pressure gradient.
- The jet forming on the opposite side is fed by a radial flow as described in Section C.1.2.

Since the jet continues forward, it is deemed acceptable to describe both the tidal and wave-driven water replenishment fluxes as detailed in Section C.1.1 and C.1.2.

C.2 On the parameterisation of the volume fluxes

It is noted that the proposed parameterisation has not been validated with experimental data, since no data is available. The main uncertainty relates to the parameterisation of the volume fluxes below the lowermost water replenishment hole. It is in any case deemed a realistic behaviour, where the volume flux (advection-driven diffusion) is reduced to less than 10% of the volume flux in the hole at a distance of 50% of the diameter below the hole. Similarly, the volume flux is decreased to 1.2% of the volume flux one monopile diameter below the hole.

Nonetheless, validation would be useful, where especially laboratory measurements of the replenishment of a dye or field measurements of the pH variation within a monopile would be useful. No such data sources are presently available to Deltares.

Deltares is an independent institute for applied research in the field of water and subsurface. Throughout the world, we work on smart solutions for people, environment and society.

Deltares

www.deltares.nl